Summer 8-15-2015

Mechanisms Underlying Memory Deficits Following West Nile Virus Neuroinvasive Disease

Michael John Vasek
Washington University in St. Louis

WASHINGTON UNIVERSITY IN ST. LOUIS

Division of Biology and Biomedical Sciences
Neurosciences

Dissertation Examination Committee:
Robyn Klein, Chair
John Cirrito
Michael Diamond
David Gutmann
Keiko Hirose

Mechanisms Underlying Memory Deficits Following West Nile Virus Neuroinvasive Disease

by

Michael John Vasek

A dissertation presented to the
Graduate School of Arts & Sciences
of Washington University in
partial fulfillment of the
requirements for the degree
of Doctor of Philosophy

August 2015

St. Louis, Missouri

Table of Contents

List of Figures

List of Tables

Acknowledgements

I would like to thank my advisor, Dr. Robyn Klein, whose drive and vision simultaneously for the big picture and the mechanistic details have inspired me as a scientific role model. Her insights, scientific flexibility, and vast knowledge of both the immune system and the central nervous system have been invaluable towards the completion of this project.

I thank members of the Klein laboratory past and present for their technical advice, encouraging lab banter, and for being fantastic colleagues and friends. I would like to especially thank Denise Dorsey for her technical help and knowledge of everything pertaining to immunohistochemistry. I also thank Douglas Durrant for his mentorship and moments of laboratory meeting humor. I also thank Charise Garber for her ability to quickly learn new protocols and her assistance in completing my manuscript. I look forward to the future of this project in her hands. Lastly, I thank Tony Sun, who I mentored as an undergraduate – and is now enrolled in an MSTP program, for his unquenchable enthusiasm and thirst for knowledge in so many scholarly fields, including stem cells, Shakespeare, black holes, time travel, virology, and star trek. He was also a technical wizard who greatly sped up my ability to collect and study the neurogenic zones of mice.

I thank my family for their enduring life-long support and especially since I became a scientist. My mother helped connect me with my first position in a research lab and I have been at it ever since. They also provided me with many scholarly conversations and episodes of thoughtful questions which has helped me put my research in perspective and be able to convey my findings to wider audiences.

I thank my wife, Kelsey, for her love and support over the last six years of graduate school. As a fellow scientist, her understanding of the scientific highs and lows has been of great comfort. I cherish our conversations had about all things scientific and political, of which we share many viewpoints.

I also thank the NIH-NINDS for supporting me with a pre-doctoral NRSA fellowship F31 NS077640.

Dedication

This thesis is dedicated to my wife, Kelsey, whose love and support have carried me through this work, and to my son, Deegan, who is in the midst of an exciting developmental stage full of neurogenesis and synaptic pruning.

Abstract of the Dissertation

Mechanisms Underlying Memory Deficits Following West Nile Virus Neuroinvasive Disease

by

Michael John Vasek

Doctor of Philosophy in Biology and Biomedical Sciences

Neurosciences

Washington University in St. Louis, 2015

Professor Robyn Klein, Chair

Neurocognitive sequelae are observed in >50% of patients who survive neuroinvasive infections with encephalitic arboviruses, such as the mosquito-borne West Nile virus (WNV)[1]. Early diagnosis and high survival rates from WNV neuroinvasive disease (WNND) (>90%) have thus led cumulatively to approximately ten thousand patients living with neurocognitive impairments[2,3], with 1-3000 cases accruing yearly, yet underlying mechanisms responsible for these deficits have not been investigated.

Within the last 15 years, studies have begun uncover many pathways which are utilized both by the developing CNS as well as the immune system, including the use of cytokines in the regulation of progenitor cell proliferation[4–6] and synaptic refinement via the classical complement cascade[7]. Under healthy conditions, an intact blood-brain-barrier limits potential crosstalk between these domains. But amidst settings of CNS

infection or damage, invocation of CNS developmental programs could be initiated by proinflammatory factors. With this in mind, the chapters of this thesis are centered around a theme of studying pathways utilized by both the immune system and the developing CNS and determining what the consequences are for cognition and memory during CNS West Nile virus infection.

First we have established a novel murine model of recovery from WNND in which intracranial inoculation of the attenuated mutant WNV-NS5-E218A[8,9] leads to similar CNS viral loads and inflammation as peripheral inoculation of its parent strain, WNV-NY99, with rates of survival and cognitive dysfunction that mirror human WNND. WNV-NS5-E218A-recovered mice exhibit impaired spatial learning without significant alterations in cortical and hippocampal volume or total neuron numbers, but exhibit persistently activated microglia. Whole transcriptome analysis of hippocampi from WNV-NS5-E218A-recovered mice with poor spatial learning revealed increased expression of genes known to drive microglial effects on synaptic pruning, including the classical complement pathway and phagocytosis. Indeed, the classical complement cascade initiation factor, C1qA, was found to be produced primarily by microglia and localized to infected neurons and synapses during WNND. Electron and confocal microscopy revealed a loss of hippocampal mossy fiber synapses while synaptophysin-positive puncta and phagosomes containing synaptic vesicles were observed within microglia. This loss of mossy fiber synapses was also observed in human WNND post-mortem samples. Importantly, mice with fewer microglia (IL34 -/-) or mice deficient in complement (C3 -/-) were protected from WNV-induced synapse loss. This study provides a novel murine model of WNV-induced spatial memory impairment, provides evidence that viral infection

of adult neurons may induce complement-mediated elimination of synapses, and identifies a potential mechanism underlying neurocognitive impairments experienced by patients recovering from WNND.

Next we report that during WNND recovery, significantly fewer new granule cell neurons are born within the hippocampal dentate gyrus, as revealed by BrdU-labeling. And although neuronal progenitor cells (NPCs) are not direct targets of WNV infection, their homeostatic levels of proliferation, differentiation, and migration were significantly altered. Using immunohistochemistry and flow cytometry coupled with *in vivo* BrdU labeling during acute WNV infection, we found NPCs within the subventricular (SVZ) and subgranular (SGZ) neurogenic zones generated fewer new neuroblasts, but greater numbers of astrocytes, an effect which slowly recovers over about 45 days. This effect was dependent upon Interleukin-1 receptor (IL-1R) signaling, which we have previously shown to be necessary for promotion of viral clearance by T lymphocytes[10]. Lastly, mice deficient in IL-1R were resistant to the WNV-mediated impairment in spatial learning and memory via the Barnes maze task at 45 days post infection, suggesting that alterations to neuronal progenitor cell homeostasis could also underlie long term cognitive consequences of WNND.

CHAPTER 1 – Introduction: The effects of neuroinflammation on memory and cognition

Nearly every disease of cognitive dysfunction presents with an underlying pro-inflammatory state within the central nervous system (CNS). Proper cognitive function involves not only the correct assembly, maintenance, and function of existing neural circuits, but also the capacity to generate or enhance new circuits. It involves one to be able to efficiently respond to stimuli, remember past memories and associations, as well as make new memories and associations. Mechanistically, there is an extremely intricate and complex series of events underlying these tasks, of which new details are constantly being discovered. And as is evidenced by the number of diseases of cognitive disability stemming from abnormal CNS development, there are many developmental molecules and pathways which are critical to complex cognitive functions. In this chapter, using West Nile virus Neuroinvasive Disease (WNND) as an example, I will discuss the inflammatory response to CNS infection, cells and molecules involved in this process, and how the homeostatic state of the brain can be altered through invocation of several neural development pathways which share many molecules and receptors with the immune system.

West Nile virus and the host immune response

West Nile virus is a single-stranded, mosquito-borne, arbovirus of the genus, flavivirus. Since WNV arrived in North America in 1999, 18,810 cases of WNV Neuroinvasive Disease (WNND), which include cases of meningitis, encephalitis, and acute flaccid paralysis, plus 22,952 non-neuroinvasive cases, mostly cases of which West

Nile fever (WNF), have been reported within the United States[11]. Symptoms of acute WNND include fatigue, muscle weakness, headache, fever, coma, and about 10% of WNND cases are fatal [12], with an estimated cost of care totaling approximately $800 million over this period [13]. Unfortunately, for the 16,000+ survivors of WNND, about half of patients will experience long term cognitive sequelae including, memory impairments, parkinsonism, word-finding difficulties, confusion, depression, and weakness[12,14–17]. And although the diagnosis of WNF is technically considered to exclude cases of CNS entry, some WNF patients experience symptoms for weeks to months including headaches, neck pain, and difficulties with concentration[18], suggesting that low-level CNS infections may occur in WNF patients as well. To date, there have been no published studies which examine mechanistic causes of cognitive sequealae during WNND.

In studies examining post-mortem tissue from acute WNND patients, WNV has been found within neurons of many different regions of the CNS including the frontal cortex, hippocampus, thalamus, basal ganglia, brainstem, cerebellum, and spinal cord[19]. Fortunately, a well-established murine model of acute WNND exists and many insights into WNV pathogenesis and the host immune response against it have been gained over the last 15 years. WNV primarily infects neurons within the CNS[20] and can induce their apoptosis via Caspase-3[21].

There are several steps between the mosquito bite and CNS invasion by WNV. And though the blood-brain-barrier is an important mechanism in CNS pathogen defense and is able to exclude many pathogens from entry, WNV as well as several other members of the flavivirus genus, including Japanese Encephalitis virus and St. Louis encephalitis virus, are known for their ability cause neuroinvasive disease. First,

mosquito-borne WNV enters the dermis and infects local Langerhans dendritic cells, which then traffic to the lymph nodes[22]. At this stage, the initiation of a successful innate immune response, including upregulation of type I and II interferons, likely prevents further viral spread in asymptomatic or mild WNF cases[23,24]. But if WNV is not controlled within the periphery, viremia develops, followed by potential invasion into the CNS[24]. And although the exact mechanism by which WNV enters the CNS is not known, especially in human pathogenesis, several possible theories have been discussed. In response to WNV and other neurotropic viruses, peripheral-derived cytokines such as Tumor Necrosis Factor-α (TNFα), Interferon-γ, and Interleukin-1β may act to temporarily permeabilize the blood brain barrier, facilitating viral entry[25,26]. Another hypothesis is that WNV gains CNS entry through a "trojan horse" method[27], initially brought in by an infected leukocyte, similar to the mechanism of HIV CNS invasion. Finally, WNV has been observed to travel along peripheral nerve axons and undergo retrograde trans-neuronal trafficking in a sciatic nerve infection model, suggesting that spread from peripheral nerves into the spinal cord may be another possible route of CNS entry[28,29].

The complement system of pathogen defense

The complement system is a well-studied cascade of proteins involved in recognizing and facilitating the opsinization or lysis of foreign material as well as apoptotic cellular debris[30]. This process from recognition to opsinization or lysis can occur within seconds to minutes of an invading pathogen entering the blood and is a very important component of early immune defense. There are three potential initiating pathways, the classical, lectin, and alternative pathways, which all converge and lead to either

opsinization or formation of the membrane attack complex, acting to lyse the cell or pathogen. The classical pathway is initiated by the factor C1q binding to aggregated IgG/IgM antibodies or other moieties such as nucleic acids or amyloids, setting off a series of zymogen activations via recruitment and cleavages of additional factors (C1r, C1s, C4, C2, and C3)[30]. The Lectin pathway is initiated by mannan-binding lectin or ficolins, which recognize carbohydrates and polysaccharides on pathogen surfaces[31]. The alternative pathway relies on the spontaneous hydrolysis and activation of complement, which due to a short half-life, would only continue amplification in the absence of endogenous regulators and inhibitors, such as decay accelerating factor and membrane cofactor protein (MCP)[32]. The alternative pathway can also act as an amplification loop for complement activation derived from the classical and lectin pathways. All three pathways lead to either the eventual cleavage of C3 into iC3b, which causes the particles or cells to be recognized and engulfed by phagocytes such as macrophages and microglia, or formation of the membrane attack complex via sequential activations of C5, C6, C7, C8, and C9, resulting in membrane lysis[33].

All three activation arms of the complement pathway can independently contribute to anti-WNV host defense. Mice deficient in components of either the alternative, classical, or lectin pathways show increased viral loads and enhanced mortality to WNV in a peripheral infection model[34]. Additionally, mice deficient in either the lectin or classical pathways produced lower levels of anti-WNV antibodies and had less reactive T cells[34,35]. Interestingly, WNV and related flaviviruses, antagonize complement C4 activity through binding of the virus' non-structural protein, NS1[36], further suggesting a key antiviral defense role for the complement pathway.

Leukocytes and cytokines in anti-WNV defense

Following WNV neuro-invasion, leukocytes have been shown to play important roles in aiding viral clearance. CD8+ T lymphocytes, especially, are indispensable in mediating viral clearance[37]. CD4+ T lymphocytes[38] and B cells[39] are also important for WNV clearance. Several cytokines including CXCL10[40], Interleukin-1β[10], Tumor Necrosis Factor α (TNFα)[41], CXCL12[42,43], and CCL3-CCL5[44] play important roles in helping to recruit T cells, macrophages, and other leukocytes into the CNS and across the brain endothelium into the infected brain parenchyma.

Microglia as immune cells of the CNS

Microglia, as the resident phagocytes of the brain, are frequently in close proximity to and involved during episodes of CNS damage or infection. They have been shown to phagocytize viruses, bacteria, and apoptotic cellular debris in these settings[45]. Furthermore, they are potent producers of many antimicrobial molecules, such as nitric oxide, as well as cytokines and chemokines such as Interleukin 1β, Interleukin 6, Tumor necrosis factor alpha (TNFα), and CXCL10[46]. While these microglial-derived oxidative molecules and cytokines may be instrumental in microbial defense, several studies have pointed to neurotoxic roles for microglia, especially in neurodegenerative conditions such as Alzheimer's disease[47]. Furthermore, during Japanese Encephalitis Virus, over-activation of microglia could contribute to the observed neurotoxicity in the murine model[48].

Neural development

The (CNS) does not instantly attain the ability to perform complex cognitive tasks from the moment that the neural tube takes shape, but rather must follow an intricate and prolonged series of developmental events. During neurulation, gradients of bone morphogenic proteins, Wnts, transforming growth factor beta (TGFβ), and Homeobox domain genes help to establish asymmetry and the basis for CNS patterning[49]. This allows for formation of ventricles and the ventricular zone immediately adjacent, where multipotent neural stem cells (radial glia) give rise to transit-amplifying progenitors, which in turn proliferate further in order to generate the many millions of neuroblasts, many of which will develop into mature neurons.

Axon guidance, synaptic connections, and synaptic refinement

Following and during developmental neurogenesis, neurons from all the different regions of the CNS begin to establish synapses with target neurons, forming circuits which will eventually serve as the basis for cognition. During this stage and for the rest of life, new neuronal connections can be made, unnecessary connections can be removed, and existing connections can be strengthened or weakened[50].

Proteins of the MHC class I (MHCI) complex, including MHCI, TAP and Beta 2 microglobulin, expressed by nearly all cells, are key to the immune system's ability to distinguish self from non-self[51,52]. Peptide fragments of proteins from the cell's lysosomal pathway are presented by the MHC complex on the cell surface for potential recognition by T lymphocytes. Thus, when a cell is infected with a pathogen, peptide fragments of that pathogen will be able to be presented to T cells, priming the immune system to invoke

a response. Interestingly, within the last 15 years it was discovered that neurons express high levels of MHCI, usually only upregulated during infection[53], during the CNS developmental stages of axon guidance and synapse formation/refinement[54]. It was later discovered that neurons also express an MHCI receptor, Paired Immunoglobulin-like Receptor B (PirB), as well as the CD3ζ chain subunit of the T cell receptor, and that expression of neuronal MHCI and its receptors was required for proper axon targeting, synapse formation, and ocular dominance plasticity within the mammalian visual system[55–57]. It is interesting that T lymphocytes and neurons, two cell types which often undergo long distance migrations and then must identify highly specific targets, have both adapted versions of the MHCI system for target recognition.

Earlier in this chapter, I discussed the critical role of the Complement system in innate immune pathogen defense, which has been discovered over 100 years ago[58]. Recently in 2007, components of the classical complement cascade have been shown to be highly expressed in the period of CNS development during which excess synapses are pruned to promote the maintenance of efficient and synchronous neuronal circuits[7]. Deficiency in the classical complement pathway resulted in mice which were not able to properly refine their visual system into eye-specific layers. Later, it was discovered that microglia, through expression of the complement receptor 3 (CR3) facilitate this synaptic pruning through recognition of C3 and iC3b deposition on neuronal synapses, and that this process is regulated by neuronal activity[59]. Though the expression of CNS classical complement components is reduced following the period of synaptic pruning, there is evidence that the system can be restimulated during adulthood in several neurologic disease states including Alzheimer's Disease[60,61] and Multiple Sclerosis[62]. The intriguing

scenario where the classical complement cascade is activated during adult CNS neurotropic WNV infection will be discussed in detail in Chapter 2 of this thesis.

Several other molecules are utilized during CNS development for axon guidance and synapse refinement which are either expressed by the immune system or are related to immune genes. Neuronal pentraxins, which are highly related to C reactive protein and Serum amyloid P component protein, two pattern recognition receptors of the immune system, have also been shown to play a role in synaptic plasticity and refinement[63]. Finally, the chemokine CXCL12 and its two receptors, CXCR4 and CXCR7 regulate both the trafficking of leukocytes across endothelial barriers[64,65] as well as the proliferation[5] and migration of neuronal progenitors during development[66,67].

Adult neurogenesis

In mammals, the generation of new neurons completely halts in most brain regions within a few weeks of life, but two brain regions continually generate new neurons throughout adulthood: the dentate gyrus (DG) of the hippocampus and the subventricular zone (SVZ), whose progenitors give rise to neuroblasts which migrate into the olfactory bulb, a vestigial organ in humans[68]. Within the DG, adult neural stem cells can give rise to progenitors which will eventually generate either astrocytes or neurons[69], and within the SVZ neural stem cells can additionally give rise to oligodendrocyte precursors[70]. Within both zones, along the neuronal lineage, rapidly dividing transit-amplifying progenitors (also known as “intermediate progenitors”) give rise to neuroblasts, which begin to migrate to their target areas. Once neuroblasts arrive at their correct layers, the olfactory bulb for SVZ-derived neuroblasts, and the granule cell layer for DG-derived

neuroblasts, they either gradually integrate into the neuronal circuit or become apoptotic[71]. And although the extent of the functional contribution of adult-born neurons is not precisely known within this relatively young field, it is known that mice whose adult neurogenesis is severely impacted, for example via radiation, suffer impairments in certain spatial learning and memory tasks[72], as well as fear-associated memory tasks[73]. Furthermore, tasks such as environmental enrichment and voluntary running, which boost cognitive performance also increase rates of adult neurogenesis[71]. Because newborn neurons display a period of enhanced excitability as they integrate into the neuronal network, it is speculated that this could add an additional layer of contextual memory enhancement, especially within the DG[74].

Of interest, neural stem and progenitor cells seem to be particularly affected by cytokines in settings of damage or infection (reviewed in [75]). During CNS development, such conditions can have drastic consequences, but also during adulthood, within the two regions of adult neurogenesis (only the hippocampus in humans), changes to progenitor cell proliferation, migratory patterns, and cell-fate differentiation could affect cognition. How SVZ and DG adult neurogenesis are affected during the immediate acute phase as well as the recovery phase following West Nile neuroinvasive infection will be the focus of chapter 3 of this thesis.

Microglia during development and in healthy conditions

Although roles for microglia within tumor models, CNS damage, and infections have been documented for over a century[76,77], only within the last 5-10 years have we begun to understand microglia's function in the healthy brain. Microglia arise from early

myeloid progenitors during the yolk-sac stage of development, which migrate into the CNS before a blood-brain-barrier has been established and represent a distinct lineage from circulating monocytes[78]. Thus, they are present during the very early stages of CNS development and indeed play critical roles during this time. Microglia act as important sources of growth factors such as basic fibroblast growth factor for neural progenitors and promoting survival of neurons[79]. Microglia also phagocytize ventricular zone neuronal progenitors during the end stages of embryonic cortical neurogenesis[80], presumably to help limit the genesis of new precursors and neurons once enough neurons have been generated. Following neurogenesis, microglia also act to induce apoptosis of excess neurons[81,82]. Within the hippocampus, this process has been shown to require Dap12 and CD11b, which along with CD18, comprises Complement Receptor 3[83]. Interestingly, mutations in either Dap12 or TREM2, two proteins which are only expressed within the CNS by microglia, in humans can cause a loss of function inherited dementia termed nasu-hakola disease[84]. Of interest, both Dap12 and TREM2 are involved in the regulation of phagocytosis by microglia and Dap12 can affect synaptic function[85]. These studies suggest that in order for proper cognitive functioning to occur and be maintained, the phagocytic activity of microglia must remain intact.

As previously discussed, microglia mediate the pruning of synapses via complement during normal CNS development[59]. This process has been shown to be necessary for proper brain development and function[86]. Furthermore, depletion of microglia during development using diphtheria toxin in a CX_3CR1-DTR murine model causes impairments in multiple learning tasks[87]. Microglia are now known to contribute to synapse maintenance during healthy adulthood and have been shown to constantly

monitor and contact nearby synapses, in addition to their roles during development[88]. Aiding in this process, microglia express the receptor, CX_3CR1, which recognizes the ligand, CX_3CL1, which is expressed by neurons[45]. Indeed, murine deficiency in CX_3CR1 lead to impairments in spatial learning and synaptic plasticity[89].

It should not be surprising that microglia, which are responsible both for the maintenance and refinement of synapses under healthy conditions, as well as antimicrobial functions such as cytokine release and phagocytosis during CNS inflammatory conditions, are deeply entwined in studies on the effect of neuroinflammation on cognition. This is especially of interest when groups of molecules like the Complement proteins mediate the opsinization and phagocytosis of both synapses and pathogens, during normal CNS development and inflammatory conditions, respectively. This dual role of microglia will be investigated and discussed in chapter 2.

CHAPTER 2 - A complement-microglial axis is required for synapse elimination during virus-induced memory impairment

This chapter is derived from the following manuscript

A complement-microglial axis is required for synapse elimination during virus-induced memory impairment

Michael J. Vasek[1], Charise Garber[1], Denise Dorsey[1], Tony Sun[1], Bryan Bollman[1], Douglas Durrant[1], Jinsheng Yu[2], Carlos Perez-Torres[3], Arnaud Frouin[4], Daniel Wilton[4], Xiaoping Jiang[5], Steven Mennerick[5], John Robinson[6], Kenneth L. Tyler[8], Joel Garbow[3], Robert E. Schmidt[7], Beth Stevens[5], and Robyn S. Klein[1,7,9]

Departments of [1]Medicine, [2]Genetics, [3]Radiology, [5]Psychiatry, [7]Pathology and Immunology, [8]Anatomy and Neurobiology, Washington University School of Medicine, St Louis MO 63110

Department of [4]Neurology, F.M. Kirby Neurobiology Center, Boston Children's Hospital, Harvard Medical School, Boston, MA 02115

Department of [6]Integrative Neuroscience, Stonybrook University, Stony Brook, NY 11794

Department of [8]Neurology, University of Colorado School of Medicine, Aurora, CO 80045

Abstract

Neurocognitive sequelae are observed in >50% of patients who survive neuroinvasive infections with encephalitic arboviruses, such as the mosquito-borne West Nile virus (WNV)[1]. Early diagnosis and high survival rates from WNV neuroinvasive disease (WNND) (>90%) have thus led cumulatively to approximately ten thousand patients living with neurocognitive impairments[2,3], with 1-3000 cases accruing yearly, yet underlying mechanisms responsible for these deficits have not been investigated. Here, we established a novel murine model of recovery from WNND in which intracranial inoculation of the attenuated mutant WNV-NS5-E218A[8,9] leads to similar CNS viral loads and inflammation as peripheral inoculation of its parent strain, WNV-NY99, with rates of survival and cognitive dysfunction that mirror human WNND. WNV-NS5-E218A-recovered mice exhibit impaired spatial learning without significant alterations in cortical and hippocampal volume or total neuron numbers, but exhibit persistently activated microglia. Whole transcriptome analysis of hippocampi from WNV-NS5-E218A-recovered mice with poor spatial learning revealed increased expression of genes known to drive microglial effects on synaptic pruning, including the classical complement pathway and phagocytosis. Indeed, the classical complement cascade initiation factor, C1qA, was found to be produced primarily by microglia and localized to infected neurons and synapses during WNND. Electron and confocal microscopy revealed a loss of hippocampal mossy fiber synapses while synaptophysin-positive puncta and phagosomes containing synaptic vesicles were observed within microglia. This loss of mossy fiber synapses was also observed in human WNND post-mortem samples. Importantly, mice with fewer microglia (IL34 -/-) or mice deficient in complement (C3 -/-)

were protected from WNV-induced synapse loss. Our study provides a novel murine model of WNV-induced spatial memory impairment, provides evidence that viral infection of adult neurons may induce complement-mediated elimination of synapses, and identifies a potential mechanism underlying neurocognitive impairments experienced by patients recovering from WNND.

Introduction

In 2003, WNV produced the largest encephalitic arbovirus epidemic within the USA on record (9,862 cases) and continually resurges every year[2,90]. Since its emergence in North America in 1999, rodent models have yielded insights into the neuropathogenesis of WNV, demonstrating critical roles for innate and adaptive immune responses in controlling peripheral infection and neuroinvasion[24]. WNV is capable of infecting neurons within several CNS regions including the basal ganglia, brain stem, cerebellum, cortex, hippocampus, and spinal cord[19,23,40,91,92]. In human post-mortem WNND patient samples and in rodent models with low survival rates (<50%), significant neuronal loss, leukocyte infiltration, and microglial activation occur within infected brain regions[10,21,43,93], however, the extent and location of viral burden and neuronal loss may be significantly different within the >90% of patients who survive the acute phase of WNND. Moderate viral burdens, variations in the locations of infection, and differential host-pathogen interactions could explain the diverse array of cognitive sequelae experienced by WNND survivors, which includes memory impairment, parkinsonism, confusion, and ataxia[12,94]. Studies in humans and rodents indicate that cortical structures such as the hippocampus are among the highly targeted areas of infection[19], and patient survivors of both WNND and West

Nile Fever (WNF), a flu-like illness that occurs in 20% of cases[95], often suffer from impairments to visuospatial processing and memory[96,97]. The hippocampus is essential for spatial and contextual memory formation via a trisynaptic circuit between the entorhinal cortex and the dentate gyrus, CA3, and CA1 regions of the hippocampal formation[98]. Damage to hippocampal neurons, their synaptic connections, or alterations in expression of critical gene pathways could restrict proper spatial memory formation or memory recall.

Microglia, the only resident myeloid cell type within the CNS parenchyma, exhibit critical roles in immune defense, antigen presentation, and as phagocytes within the virally infected CNS[99,100]. Recent studies in mice have additionally highlighted important roles for microglia in the development and maintenance of proper neuronal synapses[59,88]. Mice deficient in CX_3CR1 – CX_3CL1 signaling, which are expressed by microglia and neurons within the CNS, respectively, exhibit impaired developmental synaptic pruning[101], impaired spatial learning and memory[89], and reduced hippocampal long term potentiation (LTP)[89]. Recently, studies have shown that the proteins C1q and C3, members of the classical complement cascade which assist in the opsonization of pathogens and apoptotic debris, are necessary for the pruning of weak retinothalamic and cortical synapses during murine CNS development[7,102]. Microglia recognize and phagocytize synaptic elements through their expression of complement receptor CR3, which recognizes C3[59]. The classical complement system is activated and contributes to control of WNV dissemination following peripheral WNV infection[34], but whether complement is induced within the brain during WNND has not been investigated. It is unknown how microglia manage their dual roles in pathogen recognition/clearance and

synaptic modeling and how complex brain processes such as learning and memory may be affected as a result of viral infection of the CNS.

Results

The neuropathogenesis of cognitive impairments in patients recovering from WNND or WNF are unknown, in large part due to lack of good murine recovery models. Current murine models that utilize WNV-99 (NY isolate 1999) yield either 100% death following i.c. WNV infection[41] or 10-70% survival and variable CNS viral burdens following peripheral routes of infection, depending on the age of the mice[103,104]. While hamster models show better survival and are therefore more amenable to spatial learning tasks, they lack the attractive genetic approaches available for murine models[105]. To circumvent this, we utilized a strain of WNV with a point mutation in nonstructural protein 5 (WNV-NS5-E218A), which lacks functional 2′-O methyltransferase, an enzyme which generates a 5' cap on viral RNA to evade type I interferon-mediated restriction of viral translation[8,106] to develop a novel model of recovery from WNND for evaluation of spatial learning. While this mutation does not prevent replication in permissive cells, we previously reported that 90% of 8 week-old mice survive an i.c. inoculation (10^4 pfu) (**Fig. 2.S1a**), resulting in uniform viral brain burdens that peak between 6-8 days post infection (dpi)[9], with near complete viral clearance from the brain at 15 dpi (**Fig. 2.S1b-c**), although positive sense (non-replicating strand) viral RNA may be detected by quantitative PCR in low levels (5-10 copies per 10000 copies of GapDH) for weeks as previously described for WNV-NY00[107], RNA from the replicating, negative sense strand, of WNV was completely absent at 25 and 52 days post-infection, providing evidence against any persistent CNS WNV

infection in our model (**Fig. 2.S2a**). Mice i.c. infected with WNV-NS5-E218A develop a robust CNS inflammatory response within 7 dpi, with numbers of infiltrating leukocytes, lymphocytes, macrophages and microglia not significantly different from those observed during i.c. infection of WNV-NY99 (**Fig. 2.S1d**), consistent with prior data demonstrating early reversion of WNV-NS5-E218A to wild-type virus within the CNS[9]. Acute WNV-NS5-E218A i.c. infection resulted in low, but measurable numbers of apoptotic neurons (0.5 – 1.5%) at 7 dpi (**Fig. 2.S1e**) numbers comparable to that observed in 8 week-old mice after f.p. infection with WNV-NY99[21]. These data indicate that WNV-NS5-E218A may be used as a model to examine behavioral, cellular, and molecular mechanisms of CNS recovery from WNND.

To determine whether WNV-NS5-E218A-recovered mice exhibit neurocognitive disturbances, 8 week-old, infected mice were permitted to recover for over a month p.i. (45 dpi), followed by assessment of their ability to spatially locate and remember the location of a target hole over the course of 5 consecutive days of testing on the Barnes maze behavioral task[108]. On average, mice recovering from WNV encephalitis exhibit a significantly slower learning curve than mock-infected controls, committing more errors (**Fig. 2.1a**; $p = 0.0008$ by two-way repeated measures ANOVA) and requiring significantly more time (**Fig. 2.1b**; $p = 0.016$ by two-way repeated measures ANOVA) before locating the target hole on days 2-5 of testing (data not shown). WNV recovered animals eventually learn the task, although they continue to make more errors than mock-infected controls, even after 5 days of learning. Of note, recovered animals do not exhibit any impairments in activity or exploratory anxiety as assessed through number of lines crossed or center crosses, respectively, in an open field behavioral assessment at 45

days p.i. (**Fig. 2.1c-d**), indicating that impairments in solving the Barnes maze are specific to spatial learning deficits.

Prior studies reported that WNV may trigger caspase-3-dependent apoptosis in infected neurons of animals that succumb to WNND[21]. Quantitative immunohistochemistry did not detect ongoing apoptosis (**Fig. 2.S2b**) or significant loss of NeuN+ neurons within the dentate gyrus, hippocampal CA1, hippocampal CA3, entorhinal/perirhinal cortex, and visual cortex, regions associated with learning and memory (**Fig. 2.S2c**). Similarly, volumetric brain analysis at 52 dpi, as assessed by MRI, revealed no difference in hippocampal or total brain volume in mock- versus WNV-NS5-E218A-recovered animals (**Fig. 2.S2d**). While immunofluorescent studies revealed an increase in reactive astrocytes within the cortex in WNV-NS5-E218A- versus mock-infected animals (data not shown), this was not observed within the hippocampus (**Fig. 2.S3a**). However, microglial nodules within several brain regions, including the hippocampus, were detected via standard histology (arrowhead in **Fig. 2.S3b**) and WNV-recovered animals exhibited significantly increased levels of the microglial and macrophage activation markers, IBA1 (**Fig. 2.1e**) at 7, 25, and 52 dpi, and CD68 (**Fig. 2.1f-g**) at 7 dpi. Colocalization of CD68 staining in CX_3CR1-GFP heterozygous mice shows CD68 upregulation both on microglia (CX_3CR1-GFP-positive; white arrowheads) and on infiltrating macrophages (red arrowheads) at 7 dpi with WNV-NS5-E218A (**Fig. 2.1f**).

Microglia have been shown to exhibit distinct transcriptomic signatures, expressing a unique cluster of transcripts that encode proteins involved in sensing endogenous ligands and microbes (microglial sensome)[109]. To identify molecular mechanisms that

underlie memory dysfunction in our WNV-recovered animals, we performed whole-transcriptome microarray to compare RNA transcripts differentially expressed in mock- versus WNV-NS5-E218A-infected mice at 25 dpi, a time-point at which infectious virus is cleared and animals display spatial learning defects. Profiling total RNA from the hippocampi of mock- versus WNV-NS5-E218A-infected mice revealed differential expression of 1364 transcripts ($p<0.05$, FC > 1.5) between mock versus WNV-NS5-E218A-recovered animals (**Table 2.S1**). Pathway analyses of these genes identified genetic signatures associated with a variety of neural correlates of spatial memory, including the generation and maintenance of synapses and neurogenesis, especially those involving activation of innate immune responses and the microglial sensome (**Table 2.S2**). In the latter category, we identified genes associated with microglial-mediated phagocytosis (CX_3CR1, Dap12, FcγR1G, FcγR2, Rac2, WAS) and the classical complement pathway (C1qA, C2, C3, C4b, Serping1) (**Fig. 2.2a**), which were validated via quantitative (Q)PCR (**Fig. 2.2b**).

To identify gene expression signatures specifically associated with spatial learning defects, we took advantage of individual variability in spatial learning performance displayed by WNV-NS5-E218A-recovered animals, categorizing WNV-NS5-E218A-infected mice into those that perform similar to mock-infected animals (good learners – fewer than 8 errors) and those that exhibit severe learning deficits (poor learners – greater than 10 errors), based on Barnes maze results on the second day of testing (**Fig. 2.2c-e**). Categorization of mice into good versus poor learners revealed 747 genes that were significantly increased in the WNV-poor learners, 45 genes altered in WNV-good learners, and 572 genes altered in both groups compared to mock-infected littermates (**Fig. 2.2f**)

(**Table 2.S3**). Prior studies indicate that intraparenchymal lymphocytes, especially CD8+ T cells, persist in the CNS after recovery from WNND[110]. Consistent with this, many of the genes identified encoded proteins associated with innate and adaptive immunity including interferon-stimulated genes (ISGs), cytokines, chemokines and many immunoglobulin domains. Because lymphocytes have been shown to drive microglial activation[111–113], we examined microglial sensome and synapse genes in additional cohorts of WNV-NS5-E218A-recovered good and poor learners following Barnes maze screening. QPCR evaluation of hippocampi derived from WNV-NS5-E218A-recovered animals revealed that significantly increased levels of CRRY, Dap12, Fc□R2 and Rac2, increased levels of C1qA and decreased levels of Dlg2 and Grm5 are especially associated with poor spatial learning (**Fig. 2.2g**). Prior studies have shown that Dap12, Fc□R2, FcεR1G regulate phagocytosis in myeloid cells, including microglia[114–117]. Serping1 and CRRY, inhibitors of the classical complement cascade, are known to be expressed in the setting of complement-mediated tissue loss in mice[118,119]. C1qA has been shown to be involved in synaptic pruning during development[7] and in certain disease models including multiples sclerosis[62] and spinal cord injury[120]. Dlg2 acts as a synaptic scaffolding protein involved in complex learning[121], whereas Grm5 and Grin1 are components of metabotropic and ionotropic glutamate receptors, respectively – each shown to contribute to hippocampal plasticity[122,123] and have been previously found to be downregulated in mouse brain during acute phases of WNV, Japanese Encephalitis virus, and Reovirus infections[124]. KEGG pathway analyses of genes differentially altered (fold change > 1.5 and $p < 0.05$) between WNV-good vs. WNV-poor mice reveal cytokine signaling, calcium signaling, and B-cell receptor signaling among the top pathways found

to be upregulated in WNV-poor mice **(Table S4)**, whereas downregulated pathways included LTP, axon guidance, and wnt signaling **(Table S5)**. As all WNV-infected mice in our study exhibit inflammation during viral clearance, which is equivalent in good and poor learners (**Fig. 2.2h**), these differentially expressed genes suggest that poor spatial learners exhibit alterations in pathways specifically tied to cognitive function.

Given the alterations in genes relating to synaptic function we evaluated synapse numbers within the hippocampus of WNV-NS5-E218A-infected mice. Quantitation of synaptophysin-positive puncta within the stratum lucidum of the hippocampal CA3 (mossy fiber synapses) detected a 25% reduction in presynaptic terminals during the peak of viral brain titers in WNV-NS5-E218A-infected animals compared to mock-infected, age and sex-matched controls (**Fig. 2.3a**). Importantly, mice i.c. or f.p. inoculated with wild-type WNV (WNV-NY99) showed similar reductions in synapse numbers to the WNV-NS5-E218A mutant strain during peak infection (**Fig. 2.4a**). Of interest, synapses from mice with fewer and less proliferative microglia (IL34 -/-)[125], however, were not significantly altered during WNV-NS5-E218A acute infection (**Fig. 2.3a)**. In wild type animals, evidence of hippocampal synapse loss continued to be detectable out to 25 days post-infection where WNV-NS5-E218A-recovered mice with severe spatial learning impairments (WNV-poor) had significantly fewer VGlut1-positive synapses than their WNV-NS5-E218A-infected littermates with intact spatial learning (WNV-good), which had fewer synapses than mock-infected controls (**Fig. 2.3b**).

Colocalization studies also observe synaptophysin-positive puncta within GFP^+ cells of WNV-NS5-E218A-infected CX_3CR1^{GFP} heterozygous mice (**Fig. 2.3c**), best observed via 3-dimensional reconstruction using confocal microscopy (data not shown),

demonstrating that resident microglia are pruning synapses. Immunohistochemistry and quantification of colocalization between IBA1 and synaptophysin reveal significantly increased numbers of microglia-engulfed presynaptic terminals in the hippocampal CA3 from WNV-NS5-E218A-infected mice at days 7 and 25 post-infection (**Fig. 2.3d)**. By contrast, WNV-NS5-E218A did not induce any increase in astrocyte colocalization with synapses (**Fig 2.S4b**). Electron microscopy of the CA3 and molecular layer of the hippocampus (**Fig 2.3e**) during acute WNND confirm this synapse loss and identify microglia that are greatly enriched in phagosomes, including phagosomes containing 40nm synaptic vesicles (red arrowheads) and those observed extending processes that surround synapses (**Fig. 2.3ei**), which is rarely seen in mock-infected controls. Moreover, quantitation of synaptophysin-positive puncta within acute post-mortem WNND patient specimens showed significantly reduced hippocampal CA3 synapse numbers compared to age-matched patient controls (median age for each cohort = 62.6 years, n = 5 WNV cases and 8 control cases) (**Table 2.6**) (**Fig 2.3e**). Of note, synapse numbers within the CA3 of WNND patients under 60 years old were comparable to levels observed from control patients 20-30 years older (**Fig 2.3e**). In 3 out of 5 WNV cases, West Nile virus antigen could be detected within the hippocampal CA2/CA3 region, but West Nile antigen was mostly absent from other neighboring regions (Dentate Gyrus: 0/5, CA1: 0/5 cases, Entorhinal Cortex: 1/5 cases) (**Table S6** and **Fig 2.S5a).** Quantification of synaptophysin-positive area within the hippocampal CA1 and entorhinal cortex in the human patient samples displayed synapse reduction that was not significant (p = 0.1), (**Fig. 2.S5 b, c**).

As macrophage-mediated phagocytosis is often accompanied by antibody and complement deposition in the periphery in order to enhance opsinization of dying cells

and pathogens, we next sought out to determine if either or both components of this pathway were necessary for WNV-mediated synaptic pruning. Double-label immunohistochemistry for endogenous mouse IgG and the presynaptic marker, VGlut1, revealed no differences in the amount of endogenous mouse IgG coating VGlut1-positive hippocampal CA3 synapses at both 7 and 25 dpi following WNV-NS5-E218A compared to mock-infected controls (**Fig. 2.S6a**). Furthermore, WNV-NS5-E218A-infected B cell-deficient mice ($\mu MT^{-/-}$) exhibited similar levels of synapse loss within the hippocampus as infected wild-type mice (data not shown), confirming that B cells and antibodies are not necessary for WNV-mediated synapse reduction.

Based on our microarray results identifying WNV-induced alterations in the classical complement cascade and prior studies delineating a role for complement in microglial synaptic pruning during development[7,59], we next determined if complement might mediate the microglial phagocytosis of synapses during WNV infection. Hippocampal upregulation of the initiating factor of the classical complement cascade, C1qA, was detected by quantitative RT-PCR at days 7, 25, and 52 p.i. compared to mock-infected age-matched controls (**Fig 2.4a**). To identify cellular sources of C1qA, we performed in situ hybridization using RNA probes for C1qA together with antibodies to neuron specific enolase (NSE) and IBA1. IBA1-positive cells were the main producers of hippocampal C1qA mRNA, both in mock-infected and WNV-NS5-E218A-infected mice, which showed increased levels (**Fig 2.4b**). Within IBA1+ cells, C1qA mRNA expression can commonly be seen within processes adjacent to or surrounding neurons (insets: arrowhead in **Fig 2.4b**). Double-label immunohistochemistry confirmed co-localization of C1qA with IBA1 (**Fig 2.4c,** white arrowheads), however, as C1qA is a secreted protein,

much of the C1qA staining appears in extracellular spaces surrounding IBA1+ cells. Within WNV-NS5-E218A-infected mice at 7dpi, C1qA can be found within the hippocampal CA3 colocalized within WNV antigen-positive infected neurons (**Fig 2.4d**) and with VGlut1-positive presynaptic terminals in greater levels than mock-infected controls (**Fig 2.4e-f**). To determine if complement was necessary for WNV-mediated hippocampal synapse pruning, we examined synapse loss at 7 days post-infection in mock- versus WNV-NS5-E218A-infected $C3^{-/-}$ littermate mice and found equivalent numbers of synaptophysin-positive puncta in both groups (**Fig 2.4g**), indicating that WNV-mediated synapse elimination requires complement C3, the converging point of the complement pathways.

Discussion

Multiple studies, better diagnoses, and greater numbers of survivors of WNND over the last 10 years have begun to highlight the prevalence of cognitive impairments in this population, however there is little cellular and molecular understanding of these impairments[14,15,97,126]. Using a novel murine model to study memory impairments during recovery from WNND, we show that mice exhibit spatial learning and memory deficits during recovery and robust microglial activation during the acute phase that persists for nearly two months post-WNV infection. Using electron and confocal microscopy, we demonstrate that these activated microglia phagocytize synapses during the peak of WNV infection, leading to a significant loss of synapses in the hippocampus and entorhinal cortex. Using whole transcriptome array approaches we identified genes and pathways associated with poor spatial learning, including molecules involved in

microglial- and complement-mediated phagocytosis of synapses. Consistent with these data, we observed upregulation of complement protein C1q within neurons and microglia and showed that CA3 synapse elimination is abolished in mice deficient in either microglia or complement C3. Moreover, we detected significantly reduced numbers of hippocampal CA3 synapses in post-mortem specimens from human cases of WNV encephalitis compared with age- and sex-matched controls, highlighting the relevancy of our murine model for human infections with WNV. Our study is the first to show synapse elimination as a pathological feature of WNV encephalitis and to delineate mechanisms that underlie this elimination.

The ability of WNV to infect and kill neurons has been well-described in human cases of WNV encephalitis[127] and in rodents lethally infected with WNV-NY99[128], however, infection with attenuated WNV-NS5-E218A induces spatial learning and memory deficits, despite lack of neuron loss during peak infection (**Fig. 2.S1e**) or at one month post-clearance (**Fig 2.S2b**). These data suggest that significant neuron loss is not required for deficits in cognitive function. Consistent with this, WNF patients also report cognitive impairments for months following infection[18], suggesting that low levels of CNS viral burden that do not lead to overt encephalitis may be capable of affecting cognition through disruptions in the network of synapses in the absence of neuron loss.

Complement, which has a well-described role in coating apoptotic cells and cellular debris for opsonization, has recently been implicated in synapse elimination by microglia[7,59]. Many pathogens and pathogen-associated molecular patterns have been shown to induce complement activation within the CNS, including WNV[35], HIV[129], amyloid plaques[130], and prion proteins[131]. CNS cell types, including neurons, astrocytes, and

microglia can express complement components, including C1q[130]. Persistence of viral nucleic acid or intraparenchymal migration of macrophages that harbor viral antigen may promote microglial and complement activation via pathogen recognition[132–136]. Microglial-mediated synapse modulation has been observed in mice both during development[7] as well as in adult animal models of Alzheimer's Disease and Parkinson's disease, both shown to be dependent on Complement C3 and its receptor, CR3[137,138]. Our model of WNV-mediated synaptic pruning is similar in this regard to these cases of synaptic pruning, in that it also requires complement C3. Although synapses are labeled by complement C1qA and lost during WNV infection, it is unknown whether these synapses are connected to healthy neurons, infected neurons, or a mixture of the two. *In situ* hybridization identified microglia as the prominent source of complement C1qA (**Fig. 2.4b**), but other cellular sources of C1q as well as the other members (C1qB, C1qC, C1r, C1s, C2, C4, C3) of the classical cascade have not been examined. Of note, animals deficient in complement C3 are more susceptible to WNV-NY99 and show higher CNS viral burdens, however this susceptibility occurs via loss of virologic control in the periphery[35]. Whether complement C3 might also affect other neurobiological processes during CNS viral infections is unknown.

Over the past 5-10 years there has been significant debate over the pathogenicity of microglia[139,140]. Important studies have begun to describe the critical role of microglia and key molecules they express under normal, healthy CNS conditions for proper neuronal circuit formation and memory function[101,89]. But under neuropathologic conditions, as resident phagocytes and major sources of cytokines[141], they are almost always observed within areas of CNS injury and inflammation, and thus often considered

guilty by association. Recent work, however, points to several neuroprotective roles for microglia during neuroinflammation including the displacement of inhibitory synapses to aid in neuronal survival during inflammation[142] and increased monitoring of synapses during ischemic injury[88]. In our model of WNV encephalitis and recovery, microglia are clearly involved in pruning (glutamatergic) mossy fiber synapses, which is linked to the deficits in spatial memory performance as evidenced by transcriptional profiling (**Fig. 2.2g**) and to greater synapse elimination in WNV-infected mice with poor spatial memory (**Fig 2.3b**). However, in the setting of a neurotropic viral infection, elimination of synapses may be advantageous for the prevention of transsynaptic viral spread or to prevent infected neurons from issuing excitotoxic signals. Indeed, retrograde and anterograde spread of WNV has been observed within peripheral neurons[28]. Several other neurotropic viruses, including Rabies virus and Herpes Simplex virus (HSV) types 1 and 2, are well known for their ability to gain CNS access via peripheral nerves and subsequent retrograde, transsynaptic spread into CNS neurons[143,144]. Of interest, HSV-1 produces glycoprotein C, a protein which binds and antagonizes complement C3[145], which may allow it to travel through networks of neurons undetected. In the setting of neurotropic viral infection, loss of synapses, which readily regenerate, may be preferable to significant neuronal loss. Further studies are warranted to determine if the complement-dependent, microglial, synaptic pruning pathway is capable of preventing neuron-to-neuron spread of WNV and other neurotropic viruses.

Acknowledgements

Funding for this research was provided by the NIH. MJV was supported by a Pre-doctoral NRSA fellowship F31 NS077640 from the NIH-NINDS. R01 NS052632 (RSK), and U19 AI083019 (RSK). The authors would like to thank Dr. Michael Diamond for reagents and feedback on this manuscript.

Methods

Animals

8-10 week-old male and female mice were used at the outset of all experiments. C57BL/6J mice were obtained from Jackson Laboratories. *C3 -/-* mice (> 10 generations backcrossed to C57Bl/6) were obtained from Dr. John Atkinson (Washington University), *CX3CR1-GFP +/-* mice (>10 generations backcrossed to C57Bl/6) were obtained from Dr. Richard Ransohoff (Lerner Research Institute, Cleveland Clinic Foundation), μMT -/- mice (C57Bl/6 background) were obtained from Dr. Michael Diamond (Washington University), and IL-34 -/- mice (C57Bl/6 background) were obtained from Dr. Marco Colonna (Washington University). All experimental protocols were performed in compliance with the Washington University School of Medicine Animal Safety Committee (protocol# 20140122).

Mouse models of WNV infection

Footpad: (WNV-NY99) The WNV strain 3000.0259 was isolated in New York in 2000[146] and passaged once in C6/36 *Aedes albopictus* cells to generate an insect cell–derived

stock. 100 plaque forming units (pfu) of WNV-NY99 were delivered in 50 uL to the footpad of anaesthetized mice.

Intracranial: “WNV-NS5-E218A,” which harbors a single point mutation in the 2’O-methyl-transferase gene, was obtained from Dr. Michael Diamond (Washington University) and passaged in vero cells as described previously[8]. Deeply anaesthetized mice were administered 10^4 pfu of WNV-NS5-E218A or 10 pfu of WNV-NY99 in 10 uL into the brain’s third ventricle via a guided 29 gauge needle.

Stock titers of all viruses were determined by using BHK21 cells for viral plaque assay as previously described[39].

Leukocyte isolation and flow cytometry

Cells were isolated from brains of WT mice at day 7 post-infection and stained with fluorescently conjugated antibodies to CD4, CD8, CD11b, and CD45 as previously described[10]. Data collection and analysis were performed with an LSRII flow cytometer using FlowJo software.

Behavioral Testing

Test for anxiety and locomotor behavior

The Open Field Test was used to assess for baseline differences in anxiety or locomotor behavior, prior to Barnes Maze experiments. A standard Open Field arena (21.25”x21.25”, custom built) was used, consisting of a simple square box with a grid (6

squares/side) along the base. Animals were placed in the center of the arena and allowed to explore for 5 minutes. The arena was decontaminated with 70% ethanol between each trial. Locomotor activity was assessed by counting the number of lines the animal crossed during the testing period, and anxiety was assessed by counting the number of times the animal crossed through the center of the field. Behavior was recorded using a camera (Canon PowerShot SD1100 IS), and a blinded experimenter scored the trial.

Test for visual spatial memory

The Barnes Maze was used to assess for visual spatial memory. An elevated Barnes Maze (36" diameter, custom built) containing 19 empty holes and 1 target hole with a hidden escape chamber was used for testing (2" diameter holes were evenly spaced around the table, 2.5" from the edge). Visual cues were placed around the room and remained in the same location during the entire testing period. Mice were tested on the Barnes Maze over the course of 5 consecutive days. Each mouse received two trials per day, spaced exactly 30 minutes apart. For each trial, the mouse was placed in the center of the maze in a covered start box for 10 seconds, and removal of the box signaled the start of a trial. Each mouse was given 3 minutes to explore the maze and find the target hole. Mice that did not enter the target hole within 3 minutes were gently guided into the hole. After each trial, the mouse remained in the target hole for exactly 1 minute, and then was returned to its home cage. The maze was decontaminated with 70% ethanol between each trial. The numbers of errors (nose pokes over non-target holes) and the latency to find the target hole (amount of time elapsed before nose poke over target hole) were measured. Behavior was recorded using a camera (Canon Powershot SD1100IS), and a blinded experimenter scored the trials.

Immunohistochemistry

Following perfusion with ice-cold PBS and 4% PFA, brains were immersion-fixed overnight in 4% PFA, followed by cryoprotection in 2 exchanges of 30% sucrose for 72 hours, then frozen in OCT (Fisher). 9µm-thick fixed-frozen coronal brain sections were washed with PBS and permeabilized with 0.1% Triton X-100 (Sigma-Aldrich), and nonspecific Ab was blocked with 5-10% normal goat serum (Santa Cruz Biotechnology) for 1 h at room temperature. Mouse on Mouse kit (MOM basic kit, Vector) was used per manufacturers protocol when detecting synaptophysin (mouse, DAKO) to reduce endogenous mouse Ab staining. After block, slides were exposed to primary Ab or isotype matched IgG overnight at 4°C, washed with 0.2% FSG in PBS and incubated with secondary Abs for 1 h at room temperature. Nuclei were counterstained with ToPro3 (Invitrogen) and coverslips were applied with vectashield (Vector). Immunofluorescence was analyzed using a Zeiss LSM 510 laser-scanning confocal microscope and accompanying software (Zeiss). Positive immunofluorescent signals were quantified using the public domain NIH Image analysis software, ImageJ.

TUNEL staining was performed using the TMR-red in situ cell death detection kit (Roche) as per manufacturer's instructions. C1qA staining was performed as previously described[147].

For synaptophysin staining, the mouse-on-mouse blocking kit (Vector Labs) was used as per manufacturer's protocol.

Antibodies

C1qa (Undiluted, described previously in[147,148]), WNV (1:100 described previously [10]), GFAP (1:200 Invitrogen), IBA1 (1:100), IBA1 (for immuno-EM), MAP2 (1:100, Millipore), NeuN-biotin (1:100. Millipore), GFP (1:1000 Abcam), Synapsin-1 (1:200, Millipore), Synaptophysin (1:50. DAKO)

Secondary antibodies conjugated to Alexa-488, Alexa-555, or Alexa-633 (Invitrogen) were used at 1:400 dilution.

MRI

Mice were intracardially perfused, first with ice-cold PBS and then with a mixture of 4% PFA and 10% Multihance (gadobenate dimeglumine, Bracco Diagnostics Inc, Princeton, NJ). Heads were further fixed in 4% PFA for 24 hours before being trimmed of extraneous tissue around the skull (to minimize the field of view). Heads were then placed in 1% Multihance in PBS until being imaged several days later. *Ex vivo*, whole-head MR imaging experiments were performed at 4.7 T using an Agilent/Varian (Santa Clara, CA) DirectDrive1 small-animal scanner. Data were collected with a custom-made RF foil coil that fit tightly around the head using a 3D, T1-weighted gradient echo sequence with the following parameters: TR = 105 ms, TE = 6 ms, flip angle = 90º, isotropic resolution = 0.0625 mm, and scan time ~11 hrs. Regions of interest were manually drawn for the whole brain and hippocampus in ITK-SNAP (www.itksnap.org) from which volumes were calculated.

Harvest and purification of hippocampal RNA

Mice were perfused with ice-cold PBS then hippocampi were dissected and snap-frozen in Tri-reagent (Ambion). Hippocampal tissue was then homogenized, and RNA purified as previously described[149] using the RNA Ribopure kit (Ambion). RNA was precipitated with 25 mM Ammonium Acetate in 100% EtOH at -80 °C overnight, resuspended in RNAse-free H_2O, and checked for purity. RNA was then treated with RNAse-out and DNAse I (invitrogen) as per manufacturer's protocol.

Microarray

Hippocampal RNA was isolated as above and submitted to the Washington University Genome Technology Access Center. The total RNA quality and quantity were then determined by Agilent 2100 bioanalyzer (Agilent Technologies, Santa Clara, CA) and NanoDrop ND-1000 Spectrophotometer (Thermo Scientific NanoDrop, Wilmington, DE), according to manufacturer's recommendations, respectively. A total of 400 ng of RNA transcripts from each sample were amplified by T7 linear amplification with the MessageAmp TotalPrep Amplification kit (Life Technologies-Ambion, Austin, TX). Then 1.5 µg of each amplified and biotinylated RNA (aRNA) sample was hybridized onto Illumina MouseWG-6 v2 Expression Beadchips, followed by cy3 steptavidin–based staining, washing, and scanning, according to Illumina standard protocol. The iScan scanner-created image data were loaded into Illumina GenomeStudio (v2011) for generation of expression values and data normalizations. Only those probes that were detected at $p<0.05$ in at least one of the samples were kept in downstream statistical analysis. Background subtracted and quantile normalized data were used in statistical

analysis for identification of differentially expressed genes with one-way ANOVA test using Partek Genomics Suite (v6.6, St. Louis, MO). All original p-values in the ANOVA analysis were adjusted by q-value based multiple test correction[150]. KEGG pathway analysis was performed using DAVID bioinformatics database functional annotation tool v.6.7 [151].

Real-time quantitative RT-PCR

cDNA was synthesized using random hexamers, oligodT15, and MultiScribe reverse transcriptase (Applied Biosystems). A single reverse transcription master mix was used to reverse transcribe all samples in order to minimize differences in reverse transcription efficiency. The following conditions were used for reverse transcription: 25°C for 10 min, 48°C for 30 min, and 95°C for 5 min.

For calculation of WNV-E protein (positive and negative strand), Taqman primer-probes were used and copies were calculated based on a standard curve generated from a WNV-E protein plasmid as previously described[9]. For all other primer sets, PCR reactions were prepared using Power SYBR Green PCR mastermix. Calculated copies were normalized against copies of the housekeeping gene, GAPDH.

Quantification of synapses

ImageJ was used to threshold confocal images, draw region of interest encompassing the CA3 mossy fibers, and quantify either percent area of synaptophysin staining or number of synaptophysin+ puncta between 0.5 and 5 square microns in area.

Electron microscopy

Mice were perfused with 4% PFA, the brain was removed, and immersion fixed for 24 hours at RT. Tissue was washed in PBS, and 100μm sections were cut from regions of interest using a vibratome. Sections were incubated in 0.5% gelatin, 5% horse serum, and 0.01% saponin in PBS for 5 hours on a rotator at RT. Sections were then incubated for 48 hours at 4°C on rotator with rabbit anti-Iba1 (1:600; Wako). After washing in dPBS, sections were incubated overnight at 4°C on rotator with donkey anti-rabbit biotinylated secondary antibody, (1:500; Rockland) in 0.5% gelatin and 5% horse serum in dPBS. Sections were again washed, and then incubated with streptavidin-HRP (1:1000; Rockland, S000-03) for 3 hours at RT, followed by another wash. HRP was visualized using the DAB Substrate Kit (Cell Marque,957D) for 5 minutes, washed and then fixed with 2%PFA, 2.5% glutaraldehyde, in PBS for 30 mins, followed by a wash in PBS. Sections were post-fixed in 1% osmium tetroxide in PBS for 30 minutes at RT, washed in PBS, and then dehydrated in sequential concentrations of ethanol for 30 minutes each. Sections were then infiltrated with 1:1 Spurr's resin and 100% ethanol overnight on a rotator, followed by two changes in pure Spurr's resin over 24 hours. Sections were embedded with Aclar film (EMS, 50425), and polymerized at 60°C for 48 hours. The hippocampus was trimmed from the polymerized section, glued to a previously prepared block of Spurr's resin, and allowed to cure for at least 24 hours. Using a Diatome ultra

45° diamond knife and a LEICA Ultracut UC7, blocks were sectioned at 500nm to confirm location of the tissue and the positivity of antibodies. Once confirmed, 90nm sections were cut and picked up onto 200 hex mesh, formvar-carbon coated copper grids (Ted Pella, 01800-F). Images were digitally captured using a JEOL 1200 EX II Transmission Electron Microscope with AMT digital camera.

Three-dimensional reconstruction of confocal Z-stack images

Confocal Z-stack images taken with a Zeiss LSM 510 META microscope at 63x magnification, consisting of at least 10 images were transformed into 3-D reconstruction movies using Volocity 3D image analysis software (PerkinElmer).

Super-resolution microscopy of presynaptic terminals

9 micron fixed-frozen sections were stained for the glutamatergic presynaptic marker, VGlut1 and complement C1qA. Z-stack images were then taken using a Zeiss super-resolution microscope and projection images were generated using Zeiss Zen analysis software.

Human Tissue

Human autopsy hippocampal tissue embedded in paraffin was obtained from St. Louis University Medical Center (St. Louis, MO) and Presbyterian / St. Luke's Medical Center (Denver, CO). Sections were first deparaffinized and then boiled in sodium citrate buffer for antigen retrieval before staining with anti-synaptophysin antibody (DAKO, 1:50)

In situ Hybridization

Fluorescent *in situ* hybridization was performed on 9um coronal brain sections which were 4% PFA-fixed and frozen. C1qA and NSE was used as double mRNA staining and Iba1 as immune-staining. C1qA and NSE anti-sense RNA was made and labeled with cyanine and fluorescein, respectively, using an RNA labeling kit (Roche). C1qA was synthesized from pCMV SPORT6 C1qA plasmid from Openbiosystem reference # MMM1013-63584 (which was digested with SalI and transcribed with T7 Promoter). The RNA probes were incubated over night at 64 degree Celsius, and then detected with antibodies against fluorescein and cyanine (Roche). The staining reaction was then amplified with a TSA staining Kit (PerkinElmer). A Rabbit anti-Iba1 (Wako) was used to label the microglia and detected with a Donkey anti Rabbit 647 (Life technologies). Stained sections were then imaged and analyzed on a Zeiss AX10 fluorescent microscope.

Statistical analysis

Results from Barnes Maze spatial learning and memory studies were compared by repeated measures two-way ANOVA. Microarray data was analyzed by one-way ANOVA and fold change greater than 1.5, false discovery rate $q < 0.05$ to correct for multiple hypotheses for Mock vs. WNV-all comparison, $p < 0.05$ for WNV-good vs WNV-poor. All other experiments compared by student's two-tailed T-test, with * $p < 0.05$ considered as significant.

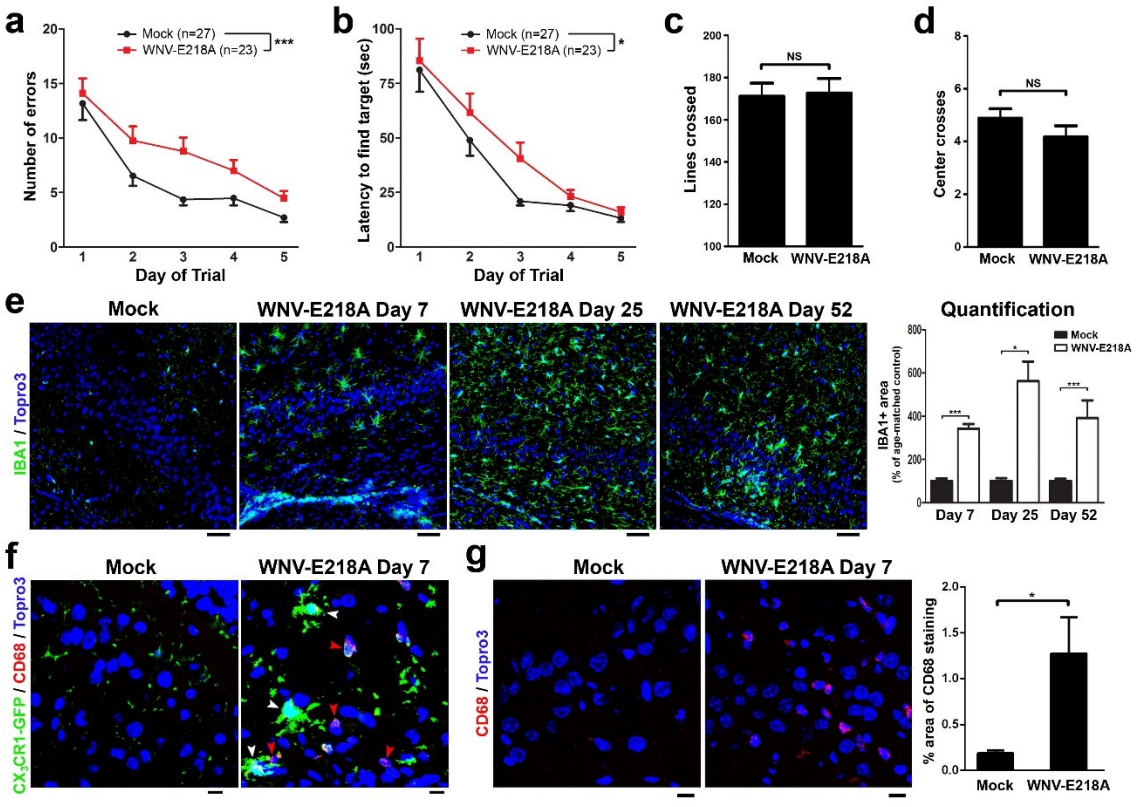

Figure 2.1 Spatial learning and memory impairments and activated microglia persist beyond one month post-infection. (**a**) At days 46-50 post WNV-NS5-E218A or mock-infection, WNV-infected mice commit more errors (nose poke in non-target hole) in the Barnes Maze spatial learning and memory task and take more time (**b**) before finding the target hole as measured in the average of two trials per day for 5 days (*** $p < 0.001$, * $p < 0.05$ by repeated measures two-way ANOVA). At 45 days post-infection (p.i.), mice were observed for 2 minutes on the open-field test and were found to be equivalent to mock-infected controls both in locomotor activity (**c**) and in exploratory anxiety (**d**), as measured by center crosses. (**e**) Immunohistochemistry for IBA1 and Topro3 (nuclear) reveals persistent microglial activation within the hippocampal dentate gyrus and CA3 of WNV-NS5-E218A-infected mice at 7, 25, and 52 days p.i. compared to age-matched mock-infected controls (mean of 2 experiments). Scale bar = 50 μm. (**f**) Representative

images from immunohistochemistry for CD68 within the hippocampal CA3 at 7 days post-mock or WNV-NS5-E218A infection in CX3CR1-GFP heterozygous mice shows increased CD68 staining both within CX3CR1-positive microglia (white arrowheads) as well as in CX3CR1-negative infiltrating macrophages (red arrowheads) (scalebar = 10 μm). (**g**) Representative images and quantification of CD68 staining at day 7 post mock or WNV-NS5-E218A infection in wild type mice (scalebar = 10 μm).*** $p < 0.001$, * $p < 0.05$, by Student's two-tailed T-test

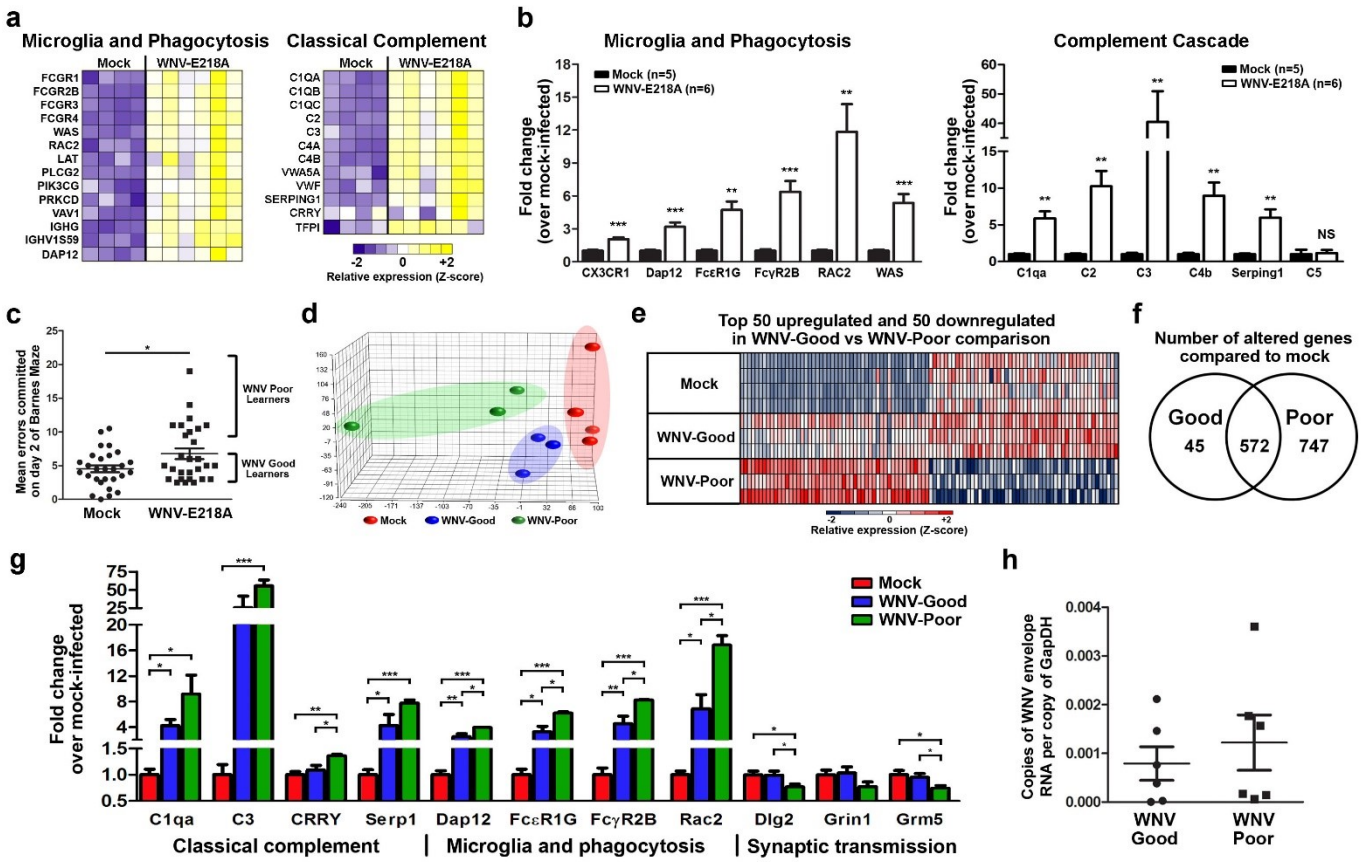

Figure 2.2 Transcriptional expression profile of good and poor spatial learners during WNV recovery. (**a**) Heatmaps showing relative expression of significantly altered genes (FDR q < 0.05, FC > 1.5) generated from a hippocampal microarray analysis of mock vs. WNV-NS5-E218A-recovered mice at 25 days post-infection. (**b**) Validation of select genes and pathways in unique set of mice by quantitative PCR. (**c**) Scatter plot depicting number of errors on day 2 of Barnes Maze testing, the most sensitive learning period, showing good and poor learners among the WNV-NS5-E218A recovery group. (**d**) PCA plots from the microarray analysis shows unique transcriptional expression profiles among mock-infected controls and good and poor learners recovering from WNV-NS5-E218A.(**e**) Relative expression heatmap from microarray of the top 50 upregulated

and 50 downregulated (by fold change) genes comparing WNV-recovery good and poor learners. (**f**) Venn diagram of microarray data showing number of genes significantly altered from mock-infected controls ($p < 0.05$, $FC > 1.5$) which are unique or shared among WNV-recovery good or poor learners. (**g**) Validation by quantitative PCR of select genes significantly altered between WNV-good and WNV-poor learners using a unique set of mice (n = 3-6 mice per group). (**h**) Copies of positive-strand (non-replicating strand) mRNA for the WNV envelope protein present at day 25 post-infection show no difference in amount of persistent positive-strand viral RNA between good and poor learners. *** $p < 0.001$, ** $p < 0.01$, * $p < 0.05$ by Two-tailed student's T-test.

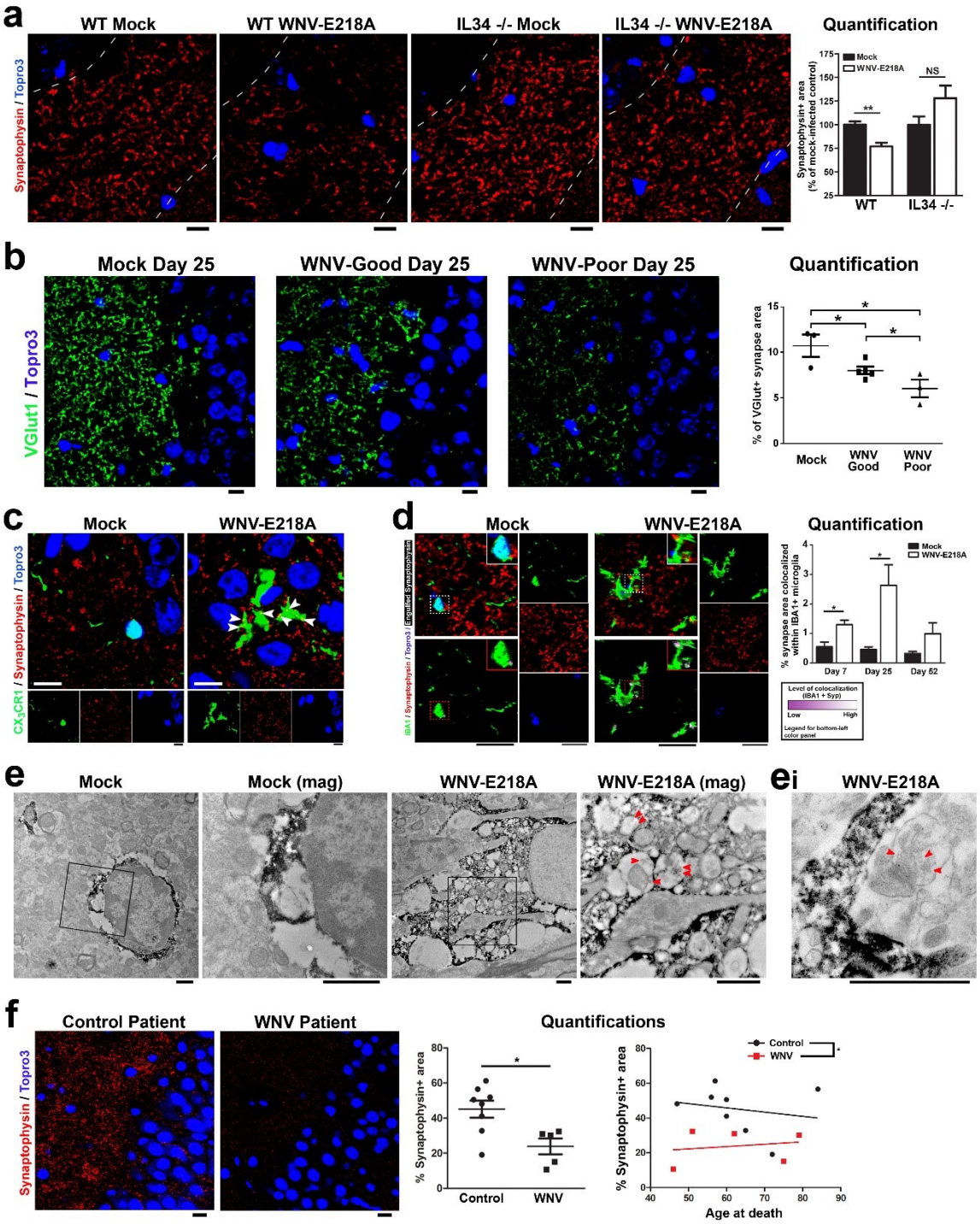

Figure 2.3 WNV causes a loss in hippocampal CA3 synapses in mice and humans.

(**a**) Immunohistochemistry for the presynaptic marker, synaptophysin, reveals a reduction in hippocampal CA3 synapses at 7 days post-infection in wildtype mice infected with

WNV-NS5-E218A compared to age-matched mock-infected controls, but IL34 -/- mice infected with WNV-NS5-E218A do not show any significant loss of synapses compared to mock-infected controls. Scalebar = 10 μm. (**b**) Immunohistochemistry for the glutamatergic presynaptic marker, Vglut1, reveals a reduction in CA3 synapses which persists to 25 days post-infection and is most severe in WNV-infected mice who perform poorly on the Barnes Maze spatial memory task. Scalebar = 10 μm. (**c**) Immunohistochemistry for synaptophysin and GFP within CX3CR1-GFP +/- mice, used as a marker of microglia, show multiple synaptophysin+ puncta localized within microglial cytoplasm. Scalebar = 10 μm. (**d**) Immunohistochemistry for synaptophysin and IBA1 within the hippocampal CA3 reveals a greater percentage of synaptophysin+ area colocalized within IBA1+ microglia in WNV-NS5-E218A-infected WT mice at 7 and 25 days post-infection. Lower-left panel depicts engulfed synapses (magenta to white gradient scale based on colocalization) within IBA1+ cells including a high-power inset. Scalebar = 20 μm. (**e**) At day 7 post WNV-NS5-E218A infection, electron microscopy with immune-DAB staining for the microglia/macrophage marker, IBA1, reveals morphologically distinct IBA1-positive cells often possessing phagosomes which contain 40nm synaptic vesicles (red arrowheads in **e** and **ei**) and which have processes that surround nearby synapses (**ei**). Scalebars = 1 μm.(**f**) Immunohistochemistry for synaptophysin within human autopsy cases shows that acute WNV encephalitis patients show significant reductions in hippocampal CA3 synaptophysin+ area compared to age and sex-matched controls. Scalebar = 10 μm. * $p < 0.05$ by Two-tailed student's T-test.

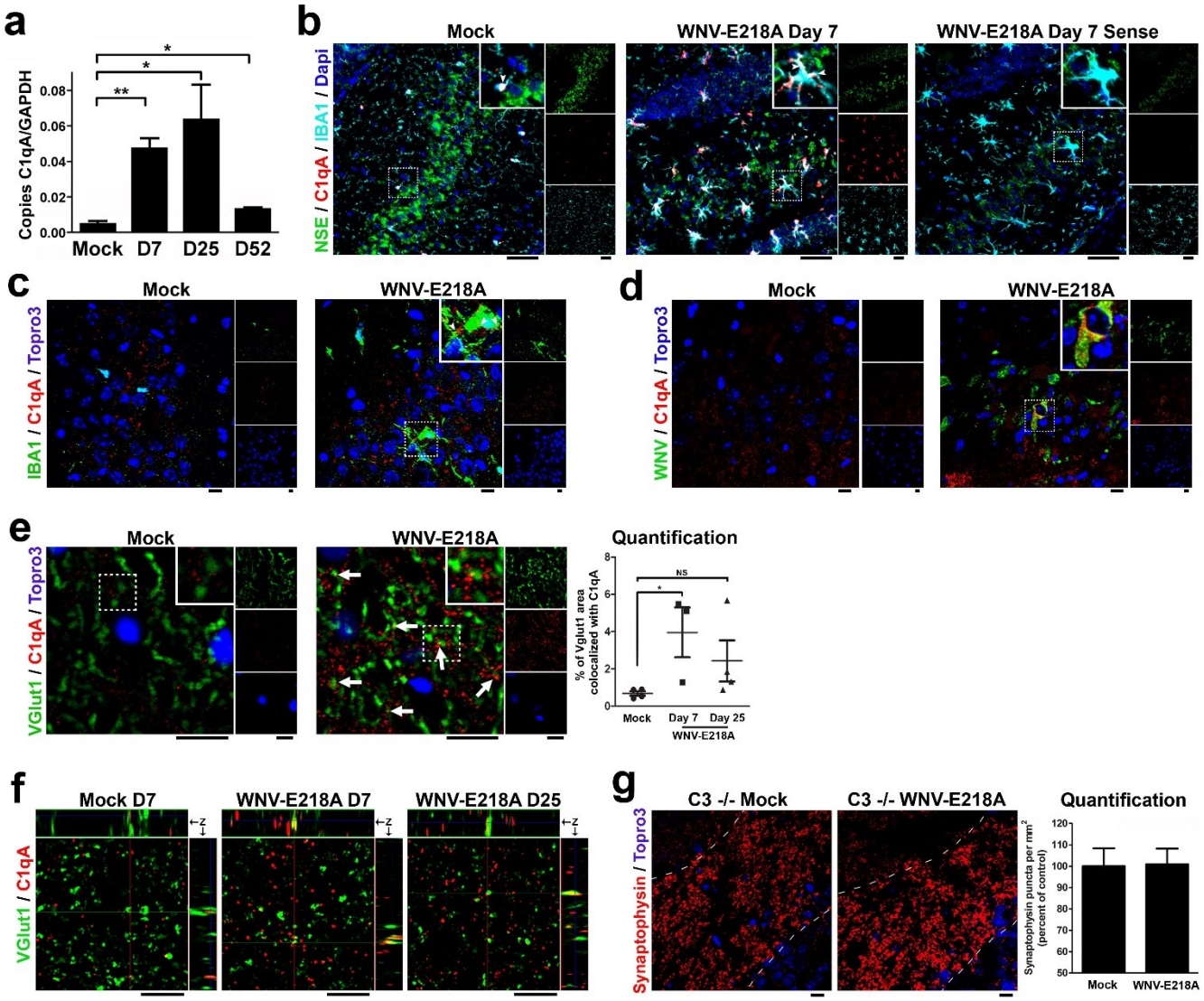

Figure 2.4 Classical complement cascade in neurons and microglia controls WNV-mediated synapse elimination. (**a**) Hippocampal mRNA levels of C1qA are upregulated at days 7, 25, and 52 post WNV-NS5-E218A infection. (**b**) Fluorescent *in situ* hybridization shows upregulation of C1qA mRNA within IBA1-positive cells at 7 days post infection with WNV-NS5-E218A. scalebar = 50 μms (**c**) Immunohistochemistry reveals colocalization (white arrowheads) between C1qA protein and the microglial/macrophage marker, IBA1.

Immunohistochemistry for C1qA protein shows C1qA deposition on WNV antigen-positive (infected) neurons at 7 d.p.i. (**d**) and on VGlut1-positive synapses 7 and 25 d.p.i. (**e**: confocal with quantification & **f:** super-resolution microscopy images). (**g**) Immunohistochemistry for the presynaptic terminal marker, synaptophysin, in complement C3-null mice at 7 days post infection reveals that C3-null mice are resistant to WNV-NS5-E218A-mediated synapse loss within the mossy fiber region of the hippocampal CA3. Synapse numbers quantified as number of 0.5 – 25 sq. μm synaptophysin+ puncta per mm^2, normalized to age-matched mock-infected controls. ** $p < 0.01$, * $p < 0.05$ by student's two-tailed t-test.

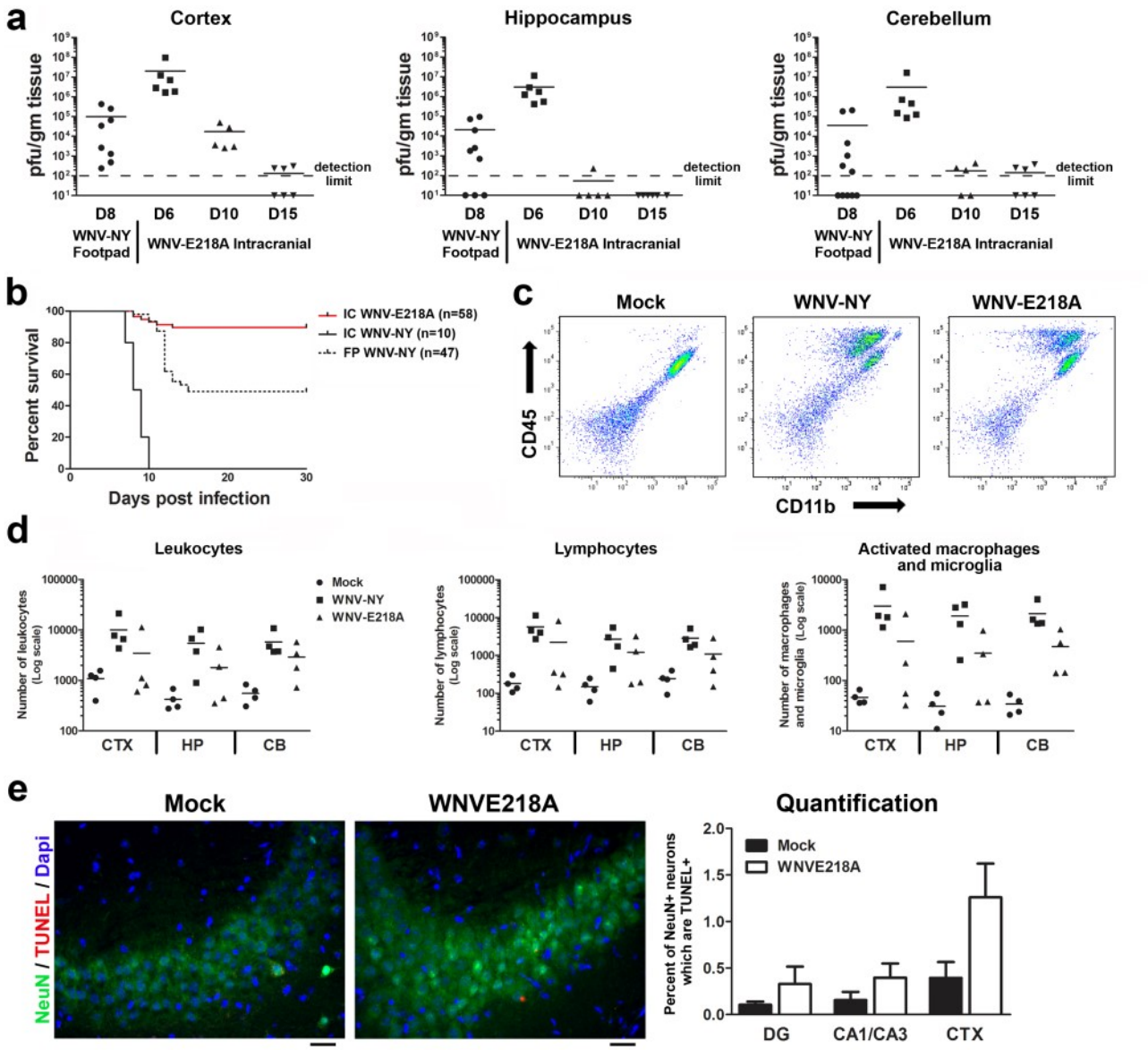

Figure 2.S1. Murine intracranial infection with attenuated WNV-NS5-E218A induces similar viral loads and inflammatory response as wildtype WNV-NY99, but greater overall survival. (**a**) Plaque assay performed on dissected brain tissue at various time points post-infection (p.i.) with either footpad (FP) infection with 10^2 pfu of WNV-NY99 or intracranial (IC) infection with 10^4 pfu WNV-NS5-E218A shows peak titers (plaque forming units per gram of tissue) of WNV-NS5-E218A at 6 days p.i., which are cleared

from the hippocampus by 15 days p.i. (**b**) Survival curve of mice infected at 8 weeks old via the FP with WNV-NY99 or IC with WNV-NY99 or WNV-NS5-E218A. (**c-d**) Flow cytometric analysis of dissected cortex, hippocampus (plots for CD45 and CD11b shown in **c**) and cerebellum at 6 days p.i. with WNV-NY99 and WNV-NS5-E218A show similar increases (**d**) in numbers of leukocytes (CD45-high), lymphocytes (CD45-high, CD11b-low), and activated macrophages and microglia (CD45-high, CD11b-high) compared to mock-infected controls (n = 4 mice per group). (**e**) Immunohistochemistry and counts for TUNEL staining with the neuronal marker, NeuN, during peak infection (day 7) reveals small, but non-significant increases in numbers of TUNEL+ NeuN+ cells in WNV-NS5-E218A (n=5) compared to mock-infected controls (n = 4) (DG = Dentate Gyrus - pictured, CTX = Entorhinal, Perirhinal, and Visual Cortex). Two-tailed student's t-test used to determine significance ($p < 0.05$).

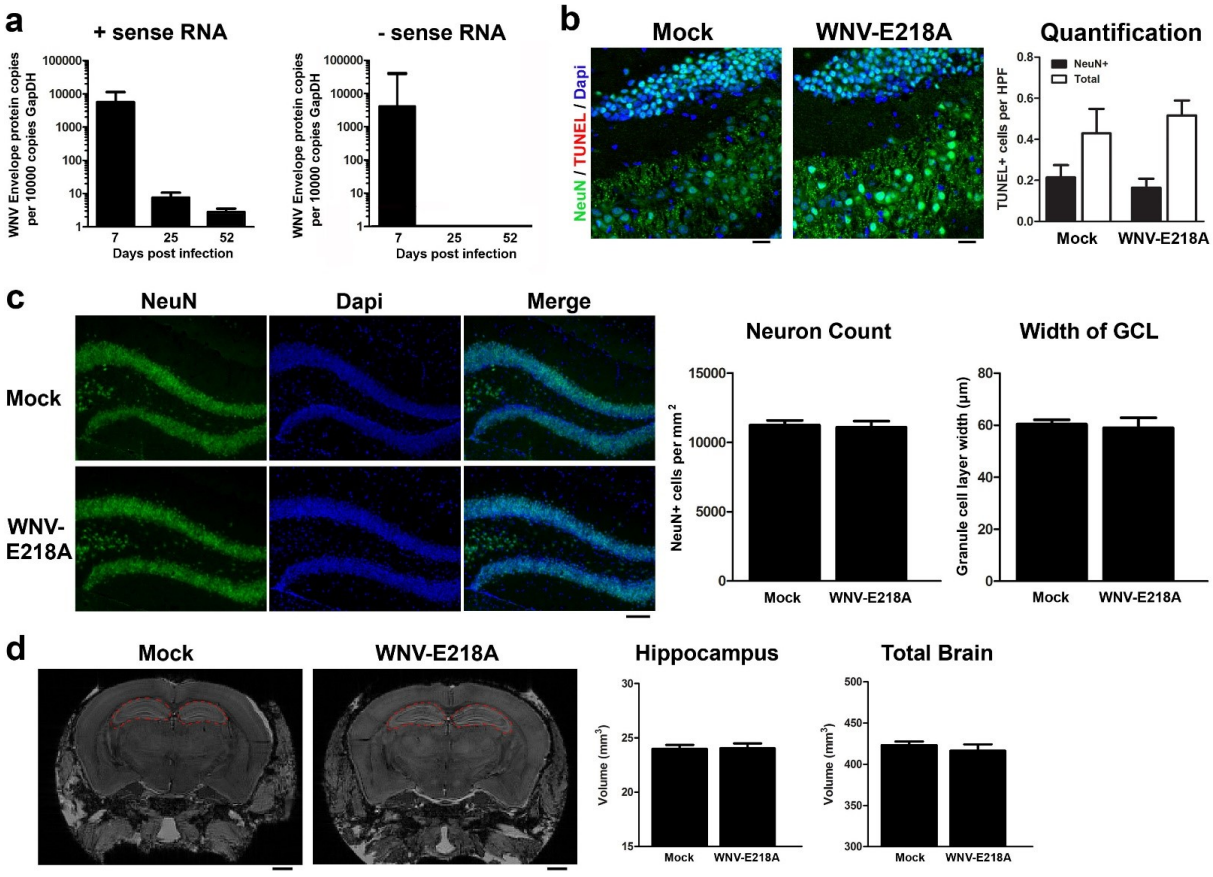

Figure 2.S2. At >50 days post-WNV-NS5-E218A infection, mice do not show any appreciable loss in brain volume or neuron numbers. (**a**) QPCR for positive strand (non-replicating strand) WNV Envelope protein message remaining in hippocampal tissue at 7, 25, and 52 days post-infection (d.p.i) (n = 3-5 mice per group). (**b**) Immunohistochemistry and counts for hippocampal TUNEL staining with the neuronal marker, NeuN, at 52 d.p.i shows that there are equivalent levels of NeuN+ and total apoptotic cells in Mock compared to WNV-NS5-E218A (n=5) compared to mock-infected controls (n = 3) (scalebar = 20 µm). (**c**) Immunohistochemistry and quantification of number of NeuN+ neurons within the Dentate Gyrus and width of the granule cell layer at 52 days post-mock (n=4) or WNV-NS5-E218A (n=5) infection (scalebar = 100 µm). (**d**)

Post-mortem mouse brains were imaged by MRI at 52 days post-infection to determine tissue volume of the hippocampus (outlined in red) and total brain (n = 5 mice per group) (scalebar = 1 mm). Student's two-tailed T-test was used to determine significance of experiments (* $p < 0.05$).

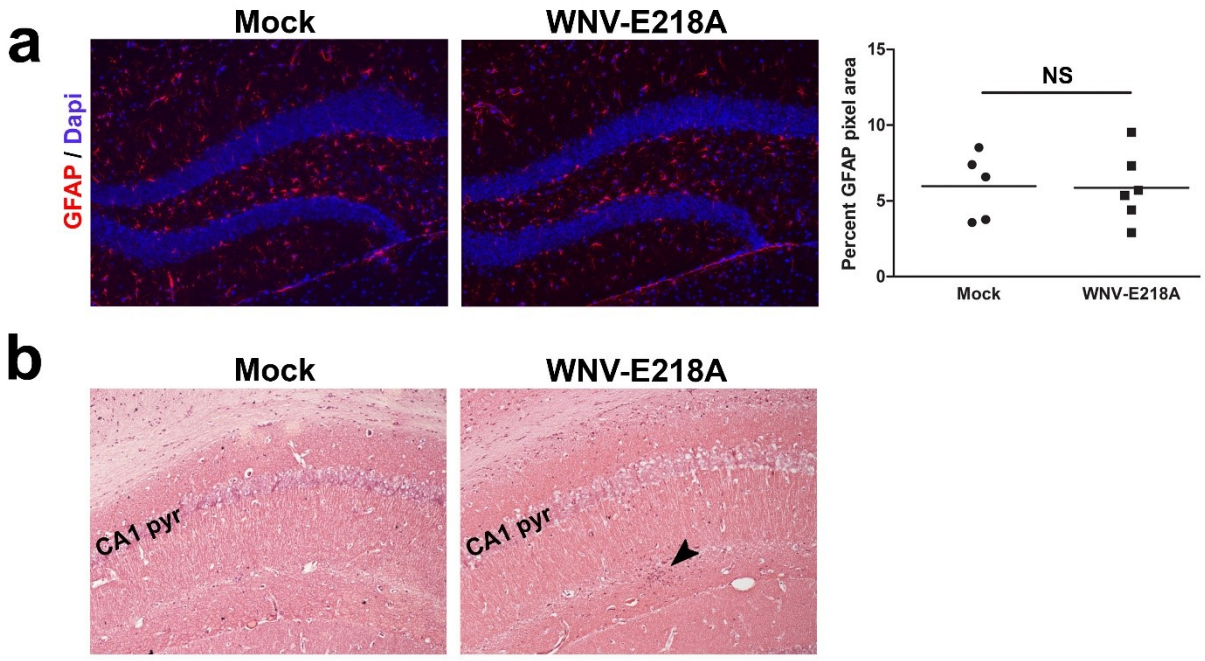

Figure 2.S3. **Following recovery from WNV-NS5-E218A infection, mice do not show gross pathological differences or astrocyte activation.** (**a**) Immunohistochemistry for the reactive astrocyte marker, GFAP, shows that WNV-NS5-E218A-infected mice do not exhibit greater hippocampal astrocyte activation than mock-infected controls at 52 days post-infection. (**b**) H&E staining shows intact hippocampal CA1 pyramidal cell layer, and occasional microglial nodules (arrowhead) surrounded by several lymphocytes at 52 days post-infection in WNV-NS5-E218Arecovered mice. (**c**) During acute WNV-NS5-E218A infection (day 7), there is no increase in engulfment of synaptophysin+ puncta by S100β+ astrocytes as quantified by percent of synapses colabeled with S100β in the hippocampal CA3 (Not significant by student's t-test).

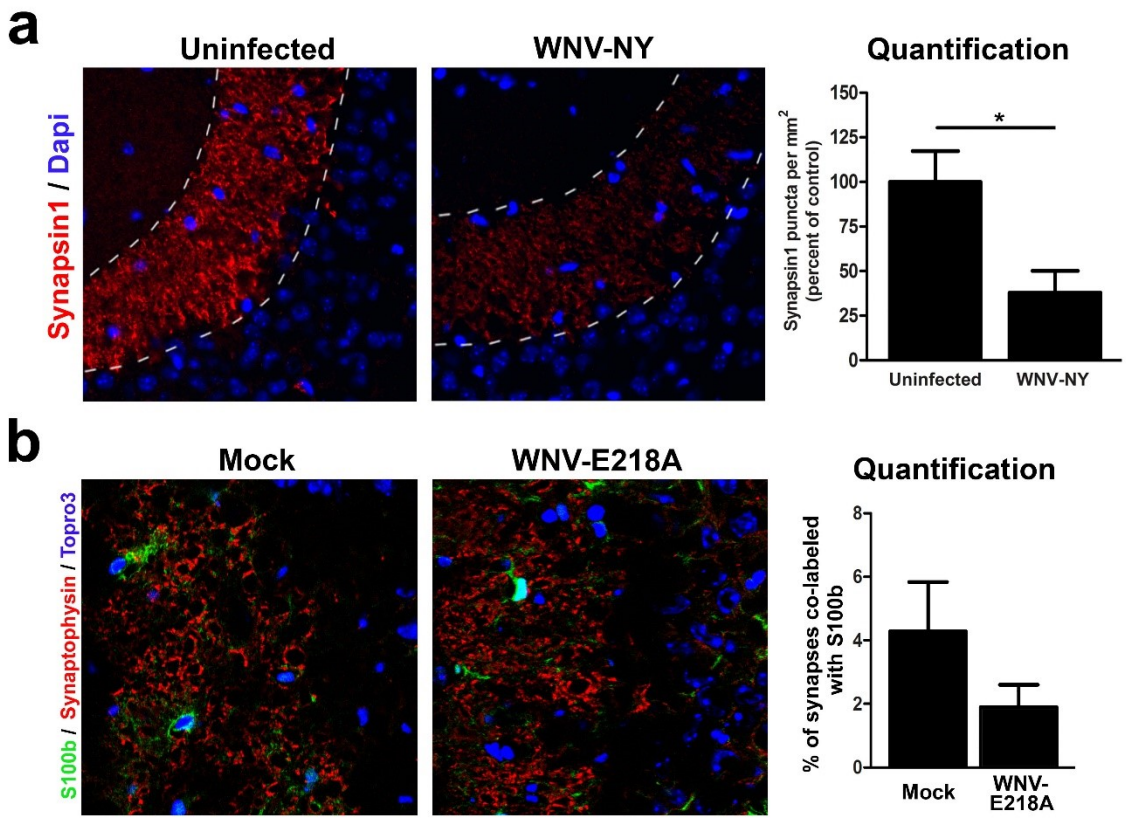

Figure 2.S4. **Acute synapse loss during infection with WNV-NY99** (**a**) Immunohistochemistry for the presynaptic marker, Synapsin1 within the hippocampal CA3 reveals a significant reduction in CA3 synapses during acute wild type (WNV-NY) footpad infection (day 8 post-infection) (**b**) During acute WNV-NS5-E218A infection (day 7), there is no change in hippocampal colocalization of synaptophysin+ puncta with S100β+ astrocytes as quantified by percent of synapses colabeled with S100β (Not significant by student's t-test).

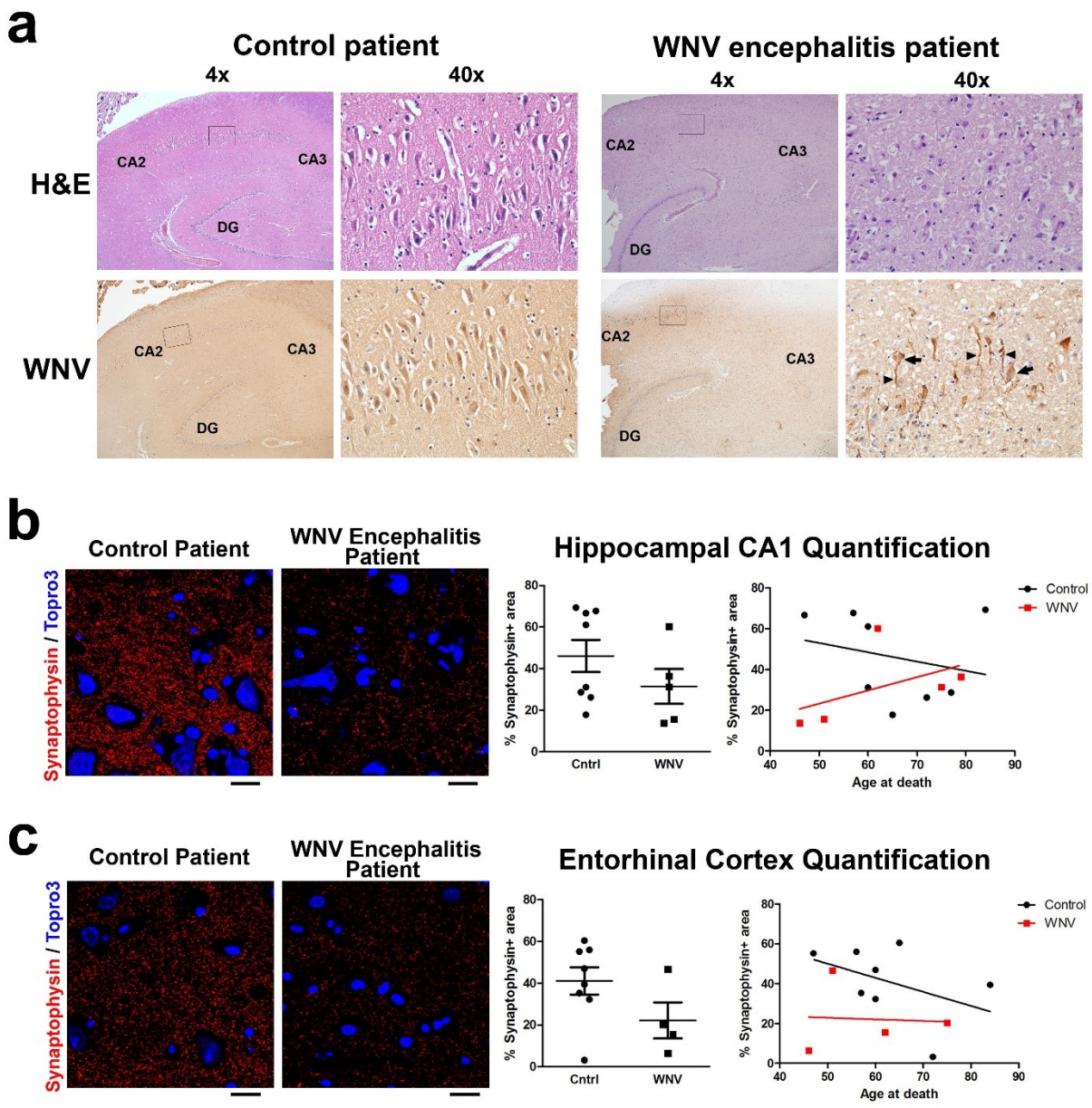

Figure 2.S5. **WNV infection of human hippocampal CA2/CA3 neurons with loss of synapses within the hippocampal CA1 and the Entorhinal Cortex**. (**a**) H&E staining (top) and WNV-antigen immunohistochemistry (bottom) show WNV-antigen located within CA2/CA3 pyramidal cell neuron cell bodies (arrows) and neurites (arrowheads). (**b, c**) Immunohistochemistry for synaptophysin within human autopsy cases shows that acute WNV encephalitis patients show trends towards reductions in synaptophysin+ area

within the hippocampal CA1 (**b**) and entorhinal cortex (**c**) compared to age and sex-matched controls (scalebar = 20 μm). Note: In 1 WNV encephalitis patient sample, the entorhinal cortex was not able to be quantified. Significance determined by two-tailed student's two-tailed t-test (not significant).

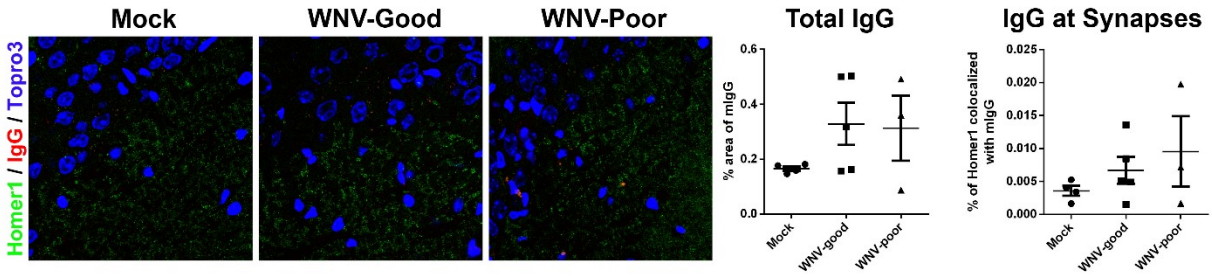

Figure 2.S6. **No differences in endogenous mouse IgG within the hippocampal CA3 region at 25 days post infection with WNV-NS5-E218A.** No significant differences (Student's Two-tailed T-test, all comparisons) were detected between groups (Mock, WNV-good, and WNV-poor learners) from immunohistochemistry and quantifications of total endogenous mouse IgG or mouse IgG colocalization with the post-synaptic marker, Homer1.

Pathway	genes	p- val	Adj p-val	Select Genes within pathway
Systemic lupus erythematosus	23	1.9E-14	0.000	HIST1H4M, HIST1H2AD, GRIN2B, HIST1H4A, C2, HIST1H4I, C4A, C4B, FCGR4, H2-AB1, TRIM21, FCGR3, C1QA, IGHG, CD86, FCGR2B, H2-DMA
Antigen processing and presentation	20	2.0E-12	0.000	H2-K1, CD8B1, H2-M3, H2-D1, IFI30, H2-AB1, CTSS, H2-Q6, H2-Q7, CD74, B2M, TAPBP, H2-OA, PSME1, TAP2, TAP1, H2-EB1, H2-AA, H2-T23,
Allograft rejection	14	2.9E-09	0.000	H2-K1, H2-M3, H2-D1, H2-AB1, H2-Q6, H2-Q7, H2-Q8, IGHG, CD86, H2-OA, H2-EB1, H2-AA, H2-T23, H2-T10, H2-DMA, IGH-VJ558
Cytokine-cytokine receptor interaction	26	6.2E-09	0.000	CCL2, IL21R, CXCL9, CXCR3, CCL5, TNFRSF4, CCL7, CXCL10, IL10RA, TNFRSF18, CSF3R, IL2RG, IFNGR1, CD27, CSF1R, TGFBR2, CCL19
Natural killer cell mediated cytotoxicity	18	2.2E-08	0.000	H2-K1, PIK3CG, PTPN6, CD244, H2-D1, FCGR4, VAV1, HCST, FCGR3, IGHG, RAC2, LCK, PLCG2, FCER1G, H2-T23, IFNGR1, IGH-VJ558, SH3BP2
Viral myocarditis	16	2.4E-08	0.000	H2-K1, H2-M3, H2-D1, H2-AB1, H2-Q6, H2-Q7, H2-Q8, IGHG, CD86, RAC2, H2-OA, CASP8, H2-EB1, H2-AA, H2-T23, H2-T10, H2-DMA
Autoimmune thyroid disease	14	4.8E-08	0.000	H2-K1, H2-M3, H2-D1, H2-AB1, H2-Q6, H2-Q7, H2-Q8, IGHG, CD86, H2-OA, H2-EB1, H2-AA, H2-T23, H2-T10, H2-DMA, IGH-VJ558
Chemokine signaling pathway	21	7.4E-08	0.000	PIK3CG, CCL2, ADCY7, CXCL9, CXCR3, STAT1, CCL5, CCL4, VAV1, PRKCD, WAS, CCL7, STAT2, CXCL10, RAC2, CCR5, CXCL13, CXCL16, CX3CR1
Graft-versus-host disease	12	3.2E-07	0.000	H2-K1, H2-M3, H2-D1, H2-AB1, H2-Q6, H2-Q7, H2-Q8, CD86, H2-OA, H2-EB1, H2-AA, H2-T23, H2-T10, H2-DMA
Primary immunodeficiency	10	3.2E-07	0.000	IGHG, CD8B1, CD3D, CD3E, TAP2, TAP1, TNFRSF13B, LCK, IL2RG, IGH-VJ558
Cell adhesion molecules (CAMs)	18	7.1E-07	0.000	H2-K1, CD8B1, H2-M3, H2-D1, H2-AB1, H2-Q6, H2-Q8, VCAM1, CD86, H2-OA, CD274, H2-EB1, CD2, H2-T10, CD6, H2-DMA, SELPLG
Type I diabetes mellitus	12	7.7E-07	0.000	H2-K1, H2-M3, H2-D1, H2-AB1, H2-Q6, H2-Q7, H2-Q8, CD86, H2-OA, H2-EB1, H2-AA, H2-T23, H2-T10, H2-DMA
B cell receptor signaling pathway	13	1.3E-06	0.000	PIK3CG, PTPN6, IFITM1, CD72, VAV1, IGHG, FCGR2B, RAC2, PLCG2, PIK3AP1, CD79B, INPP5D, IGH-VJ558
Intestinal immune network for IgA production	10	1.2E-05	0.000	IGHG, CD86, TNFSF13B, H2-OA, LOC641240, TNFRSF13B, H2-EB1, H2-AA, H2-AB1, H2-DMA, IGH-VJ558
Toll-like receptor signaling pathway	13	1.3E-05	0.000	PIK3CG, TLR2, CXCL9, CCL5, TLR6, STAT1, CCL4, CXCL10, CD86, MYD88, IRF5, IRF7, CASP8
Hematopoietic cell lineage	12	1.4E-05	0.000	CD3G, CD8B1, CD3D, CD3E, CD9, IGHG, H2-EB1, CD2, CSF3R, H2-AA, IGH-VJ558, CSF1R
Asthma	8	2.3E-05	0.000	IGHG, H2-OA, H2-EB1, H2-AA, FCER1G, H2-AB1, H2-DMA, IGH-VJ558
Cytosolic DNA-sensing pathway	8	6.5E-04	0.004	DDX58, IRF7, TREX1, CCL5, CASP1, CCL4, CXCL10, ADAR
Fc gamma R-mediated phagocytosis	10	1.3E-03	0.007	PIK3CG, IGHG, RAC2, FCGR2B, PLCG2, INPP5D, WAS, PRKCD, VAV1, IGH-VJ558
Fc epsilon RI signaling pathway	9	1.6E-03	0.009	PIK3CG, IGHG, RAC2, PLCG2, FCER1G, INPP5D, PRKCD, VAV1, IGH-VJ558
Complement and coagulation cascades	8	4.0E-03	0.021	C1QA, VWF, C1QB, C4A, C4B, SERPING1, C2, PROS1, C1QC
Jak-STAT signaling pathway	11	8.1E-03	0.040	IRF9, PIK3CG, PTPN6, IL10RA, IL21R, CSF3R, IL2RG, STAT1, CISH, IFNGR1, STAT2

Table 2.S1 – Pathway analysis of genes altered by WNV-NS5-E218A compared to mock-infected controls at 25 days post-infection. KEGG pathway analysis using

DAVID bioinformatics database functional annotation tool v.6.7. Analysis generated with list of genes having greater than 1.5 fold change and false discovery rate q value of less than 0.05 in Mock vs. WNV-all analysis. Adjusted p-values determined by Benjamini false discovery rate.

Rank	Gene	Definition	Fold ch	p
1	**LOC636875**	PREDICTED: similar to Ig kappa chain V-V region L7 precursor (LOC636875)	8.68	0.037
2	**LOC100046552**	PREDICTED: similar to Unknown (protein for MGC:103328) (LOC100046552)	7.81	0.043
3	**IGHG**	PREDICTED: Immunoglobulin heavy chain (gamma polypeptide) (Ighg)	6.91	0.004
4	**IGH-VJ558**		5.99	0.013
5	**LOC381774**		5.79	0.036
6	**IGK-V5**	PREDICTED: immunoglobulin kappa chain variable 5 (V5 family) (Igk-V5)	5.51	0.042
7	**IGK-V5**	PREDICTED: immunoglobulin kappa chain variable 5 (V5 family) (Igk-V5)	5.46	0.010
8	**LOC207685**	PREDICTED: hypothetical protein LOC207685, transcript variant 1 (LOC207685)	4.75	0.018
9	**IGH-VJ558**	PREDICTED: immunoglobulin heavy chain (J558 family) (Igh-VJ558)	4.71	0.016
10	**LOC100047316**	PREDICTED: similar to anti-MOG Z12 variable light chain (LOC100047316)	4.15	0.007
11	**AI324046**		4.00	0.035
12	**AI324046**		3.98	0.041
13	**LOC386520**		3.80	0.006
14	**IGHV1S119_L33961_IG_HEAVY_VARIABLE_1S119_14**		3.78	0.020
15	**AI324046**		3.57	0.019
16	**LOC380801**		3.53	0.011
17	**LOC385109**		3.47	0.018
18	**SAA3**	serum amyloid A 3 (Saa3)	3.46	0.046
19	**LOC100047162**	PREDICTED: similar to immunoglobulin kappa-chain (LOC100047162)	3.33	0.033
20	**LOC640696**	PREDICTED: similar to Ig heavy chain V-I region V35 precursor (LOC640696)	3.29	0.032
21	**LOC636752**	PREDICTED: similar to Ig kappa chain V-VI region NQ2-6.1 (LOC636752)	3.28	0.002
22	**AI324046**		3.26	0.042
23	**IGLC2_J00595_IG_LAMBDA_CONSTANT_2_14**		3.14	0.006
24	**LOC669053**	PREDICTED: similar to Ig kappa chain V-V region MPC11 precursor (LOC669053)	3.04	0.034
25	**LOC630302**	PREDICTED: similar to VH283 protein (LOC630302)	3.00	0.037
26	**IGHG**	PREDICTED: Immunoglobulin heavy chain (gamma polypeptide), transcript variant 1 (Ighg)	2.97	0.030
27	**LOC100048770**	PREDICTED: similar to Ig H-chain V-JH1-region (LOC100048770)	2.96	0.020
28	**IGHV1S133_AF304553_IG_HEAVY_VARIABLE_1S133_89**		2.93	0.001
29	**GBP2**	guanylate binding protein 2 (Gbp2)	2.84	0.037
30	**SLPI**	secretory leukocyte peptidase inhibitor (Slpi)	2.77	0.035
31	**LOC385277**		2.71	0.026
32	**SERPING1**	serine peptidise inhibitor 1 (C1 inhibitor)	2.68	0.043
33	**UBD**	ubiquitin D (Ubd)	2.52	0.046
34	**IGHV1S59_L17134_IG_HEAVY_VARIABLE_1S59_150**		2.46	0.008
35	**LOC383196**	PREDICTED: hypothetical LOC383196 (LOC383196)	2.44	0.002
36	**IGKV4-71_AJ231218_IG_KAPPA_VARIABLE_4-71_20**		2.38	0.017
37	**1110059M19RIK**		2.37	0.040
38	**LOC383196**	PREDICTED: hypothetical LOC383196 (LOC383196)	2.37	0.001
39	**LOC100042270**	PREDICTED: similar to Unknown (protein for MGC:41421) (LOC100042270)	2.30	0.001
40	**DISP2**	dispatched homolog 2 (Drosophila) (Disp2)	2.27	0.008
41	**TSPO**	translocator protein (Tspo)	2.26	0.026
42	**IFITM1**	interferon induced transmembrane protein 1 (Ifitm1)	2.25	0.013
43	**PSMB8**		2.25	0.036
44	**CD274**	CD274 antigen (Cd274)	2.20	0.039
45	**TUBA6**		2.17	0.041
46	**IGHV1S30_X02462_IG_HEAVY_VARIABLE_1S30_12**		2.16	0.046
47	**IGKV4-91_AJ231229_IG_KAPPA_VARIABLE_4-91_29**		2.13	0.033
48	**CXCL10**	chemokine (C-X-C motif) ligand 10 (Cxcl10)	2.12	0.045
49	**PIK3AP1**	phosphoinositide-3-kinase adaptor protein 1 (Pik3ap1)	2.10	0.044
50	**H2-T10**	histocompatibility 2, T region locus 10 (H2-T10)	2.10	0.039
51	**IGHV1S34_X02467_IG_HEAVY_VARIABLE_1S34_71**		2.10	0.050
52	**MVP**	major vault protein (Mvp)	2.09	0.039
53	**CYTIP**	cytohesin 1 interacting protein (Cytip)	2.09	0.025
54	**PRG4**		2.06	0.033

55	**LOC434609**	PREDICTED: similar to Ig heavy chain V region VH558 A1/A4 precursor (LOC434609)	2.05	0.001
56	**CD52**		2.04	0.030
57	**EGR2**		2.03	0.025
58	**IGHA_J00475$V00785_IG_HEAVY_CONSTANT_ALPHA_135**		2.02	0.001
59	**TSPO**	translocator protein (Tspo)	1.99	0.030
60	**SULF1**	sulfatase 1 (Sulf1)	1.96	0.037
61	**4930533K18RIK**		1.93	0.006
62	**2810046M22RIK**		1.91	0.041
63	**LY6C1**	lymphocyte antigen 6 complex, locus C1 (Ly6c1)	1.89	0.037
64	**CDKN1A**	cyclin-dependent kinase inhibitor 1A (P21) (Cdkn1a)	1.89	0.046
65	**HDC**	histidine decarboxylase (Hdc)	1.88	0.013
66	**GIMAP6**	GTPase, IMAP family member 6 (Gimap6)	1.86	0.013
67	**VAMP8**	vesicle-associated membrane protein 8 (Vamp8)	1.85	0.022
68	**TCEA3**		1.83	0.015
69	**LCK**	lymphocyte protein tyrosine kinase (Lck)	1.83	0.031
70	**MIA1**		1.82	0.044
71	**GM1276**	PREDICTED: gene model 1276, (NCBI) (Gm1276)	1.82	0.047
72	**IFITM1**	interferon induced transmembrane protein 1 (Ifitm1)	1.81	0.038
73	**TRAF1**		1.81	0.021
74	**IGHV1S12_J00507_IG_HEAVY_VARIABLE_1S12_239**		1.81	0.001
75	**H2-DMA**	histocompatibility 2, class II, locus DMa (H2-DMa)	1.81	0.047
76	**LOC100048556**	PREDICTED: similar to monocyte chemoattractant protein-5, (LOC100048556)	1.80	0.039
77	**SYNPO**		1.80	0.030
78	**TNF**	tumor necrosis factor (Tnf)	1.78	0.037
79	**LOC100048556**	PREDICTED: similar to monocyte chemoattractant protein-5, (LOC100048556)	1.78	0.023
80	**TAPBP**		1.78	0.005
81	**LOC223672**		1.77	0.041
82	**SELL**	selectin, lymphocyte (Sell)	1.75	0.043
83	**1700024G13RIK**		1.73	0.003
84	**LBP**	lipopolysaccharide binding protein (Lbp)	1.73	0.040
85	**NFKBIA**	nuclear factor of kappa light polypeptide gene enhancer in B-cells inhibitor, alpha (Nfkbia)	1.72	0.042
86	**LOC100038882**	PREDICTED: hypothetical protein LOC100038882 (LOC100038882)	1.72	0.031
87	**IL1A**	interleukin 1 alpha (Il1a)	1.72	0.015
88	**ECM1**	extracellular matrix protein 1 (Ecm1)	1.69	0.048
89	**MIA1**	melanoma inhibitory activity 1 (Mia1)	1.69	0.031
90	**ONECUT3**	one cut domain, family member 3 (Onecut3)	1.69	0.040
91	**TRIOBP**		1.68	0.045
92	**CPT1A**		1.68	0.014
93	**INPP5D**	inositol polyphosphate-5-phosphatase D (Inpp5d)	1.68	0.047
94	**LOC100040402**	PREDICTED: hypothetical protein LOC100040402 (LOC100040402)	1.67	0.039
95	**TAP2**	transporter 2, ATP-binding cassette, sub-family B (MDR/TAP) (Tap2)	1.67	0.028
96	**2600011C06RIK**		1.65	0.044
97	**TNFSF13B**	tumor necrosis factor (ligand) superfamily, member 13b (Tnfsf13b)	1.65	0.044
98	**B930097J01RIK**		1.64	0.027
99	**TNFRSF12A**	tumor necrosis factor receptor superfamily, member 12a (Tnfrsf12a)	1.64	0.040
100	**LASS2**	LAG1 homolog, ceramide synthase 2 (Lass2)	1.64	0.004

Table 2.S2 – Transcriptionally altered genes by microarray, WNV-poor higher than WNV-Good. Genes higher in WNV-poor than in WNV-good (top 100 genes by fold change and p value <0.05)

Rank	Gene	Definition	Fold ch	p
1	**LOC232065**		2.49	0.019
2	**CYFIP2**	cytoplasmic FMR1 interacting protein 2 (Cyfip2)	1.97	0.000
3	**PHF14**	PHD finger protein 14 (Phf14)	1.95	0.009
4	**5430417J04RIK**		1.86	0.009
5	**AU021092**	expressed sequence AU021092 (AU021092)	1.82	0.002
6	**PPAP2A**	phosphatidic acid phosphatase 2a (Ppap2a), transcript variant 2	1.78	0.013
7	**ROCK2**	Rho-associated coiled-coil containing protein kinase 2 (Rock2)	1.78	0.002
8	**TRMT2B**	TRM2 tRNA methyltransferase 2 homolog B (S. cerevisiae) (Trmt2b)	1.74	0.006
9	**CHRNA1**	cholinergic receptor, nicotinic, alpha polypeptide 1 (muscle) (Chrna1)	1.73	0.000
10	**SQLE**	squalene epoxidase (Sqle)	1.73	0.021
11	**TTC30A1**	tetratricopeptide repeat domain 30A1 (Ttc30a1)	1.72	0.004
12	**SC4MOL**	sterol-C4-methyl oxidase-like (Sc4mol)	1.69	0.046
13	**2610044O15RIK**	RIKEN cDNA 2610044O15 gene (2610044O15Rik)	1.68	0.013
14	**GPR155**	G protein-coupled receptor 155 (Gpr155) XM_921852 XM_921857	1.65	0.019
15	**CCDC25**	coiled-coil domain containing 25 (Ccdc25)	1.65	0.001
16	**WDR17**	WD repeat domain 17 (Wdr17)	1.65	0.042
17	**PDGFRL**	platelet-derived growth factor receptor-like (Pdgfrl)	1.65	0.023
18	**RLBP1L1**	retinaldehyde binding protein 1-like 1 (Rlbp1l1)	1.65	0.000
19	**B230107J06RIK**		1.63	0.003
20	**LOC382964**		1.63	0.020
21	**STX3**	syntaxin 3 (Stx3), transcript variant B	1.63	0.005
22	**CYB561D2**	cytochrome b-561 domain containing 2 (Cyb561d2)	1.63	0.012
23	**PDIK1L**	PDLIM1 interacting kinase 1 like (Pdik1l)	1.63	0.001
24	**RASL12**	RAS-like, family 12 (Rasl12)	1.63	0.004
25	**LOC100046855**	PREDICTED: similar to BKLF (LOC100046855)	1.63	0.001
26	**6430531H12RIK**		1.63	0.003
27	**TESC**		1.62	0.018
28	**4631422C13RIK**	PREDICTED: RIKEN cDNA 4631422C13 gene (4631422C13Rik)	1.62	0.015
29	**UBE3A**	ubiquitin protein ligase E3A (Ube3a), transcript variant 2	1.61	0.030
30	**GUCY2E**		1.61	0.005
31	**DOC2B**	double C2, beta (Doc2b)	1.60	0.035
32	**ARHGEF9**	CDC42 guanine nucleotide exchange factor (GEF) 9 (Arhgef9)	1.60	0.016
33	**CCNJL**	cyclin J-like (Ccnjl)	1.58	0.001
34	**SEMA6C**	sema domain, transmembrane domain (TM), and cytoplasmic domain, (semaphorin) 6C (Sema6c)	1.58	0.029
35	**TPPP**	tubulin polymerization promoting protein (Tppp)	1.58	0.005
36	**DOCK9**	dedicator of cytokinesis 9 (Dock9), transcript variant 1	1.58	0.012
37	**4921521J11RIK**		1.58	0.026
38	**GRIN1**	glutamate receptor, ionotropic, NMDA1 (zeta 1) (Grin1)	1.57	0.025
39	**SIAH1B**	seven in absentia 1B (Siah1b)	1.57	0.043
40	**ALDH3A2**		1.57	0.010
41	**A430010E21RIK**		1.56	0.007
42	**DOC2B**	double C2, beta (Doc2b)	1.56	0.014
43	**TERF2IP**	telomeric repeat binding factor 2, interacting protein (Terf2ip)	1.56	0.029
44	**TCF20**	transcription factor 20 (Tcf20)	1.56	0.022
45	**KLRB1B**	killer cell lectin-like receptor subfamily B member 1B (Klrb1b)	1.56	0.020
46	**VTI1A**		1.56	0.001
47	**CHST7**	carbohydrate (N-acetylglucosamino) sulfotransferase 7 (Chst7)	1.56	0.019
48	**2010011I20RIK**	RIKEN cDNA 2010011I20 gene (2010011I20Rik)	1.56	0.039
49	**PCDHAC1**	protocadherin alpha subfamily C, 1 (Pcdhac1)	1.55	0.025
50	**4930503L19RIK**	RIKEN cDNA 4930503L19 gene (4930503L19Rik) XM_001001515	1.55	0.046
51	**HSPA12A**	heat shock protein 12A (Hspa12a)	1.55	0.045
52	**LOC100047052**	PREDICTED: similar to Aptx protein (LOC100047052)	1.55	0.006
53	**GALNT3**		1.55	0.010
54	**ALG8**	asparagine-linked glycosylation 8 homolog (yeast, alpha-1,3-glucosyltransferase) (Alg8)	1.54	0.012

55	**LOC235086**		1.54	0.014
56	**TTLL9**	tubulin tyrosine ligase-like family, member 9 (Ttll9), transcript variant 1	1.54	0.043
57	**PPP2R2C**	protein phosphatase 2 (formerly 2A), regulatory subunit B (PR 52), gamma isoform (Ppp2r2c)	1.54	0.018
58	**ROBO1**	roundabout homolog 1 (Drosophila) (Robo1)	1.53	0.048
59	**ELFN2**	leucine rich repeat and fibronectin type III, extracellular 2 (Elfn2)	1.53	0.020
60	**EG406223**	predicted gene, EG406223 (EG406223)	1.53	0.012
61	**2210008F06RIK**	PREDICTED: RIKEN cDNA 2210008F06 gene (2210008F06Rik)	1.53	0.039
62	**PVRL3**	poliovirus receptor-related 3 (Pvrl3), transcript variant alpha	1.53	0.044
63	**RNF123**	ring finger protein 123 (Rnf123)	1.53	0.000
64	**5830435K17RIK**		1.52	0.025
65	**RTN4**	reticulon 4 (Rtn4), transcript variant 1	1.52	0.016
66	**SEMA3E**	sema domain, immunoglobulin domain (Ig), short basic domain, secreted, (semaphorin) 3E (Sema3e)	1.52	0.018
67	**PPP4R4**	protein phosphatase 4, regulatory subunit 4 (Ppp4r4)	1.52	0.030
68	**COVA1**	cytosolic ovarian carcinoma antigen 1 (Cova1)	1.51	0.016
69	**6030419L17RIK**		1.51	0.003
70	**POPDC3**	popeye domain containing 3 (Popdc3)	1.51	0.049
71	**XKR7**	X Kell blood group precursor related family member 7 homolog (Xkr7)	1.51	0.031
72	**CCDC94**	coiled-coil domain containing 94 (Ccdc94)	1.51	0.024
73	**E130309D02RIK**	RIKEN cDNA E130309D02 gene (E130309D02Rik)	1.51	0.004
74	**1700020L24RIK**	RIKEN cDNA 1700020L24 gene (1700020L24Rik)	1.51	0.006
75	**SGTB**	small glutamine-rich tetratricopeptide repeat (TPR)-containing, beta (Sgtb)	1.50	0.003
76	**CHD5**	chromodomain helicase DNA binding protein 5 (Chd5), transcript variant 1	1.50	0.012
77	**RIC3**	resistance to inhibitors of cholinesterase 3 homolog (C. elegans) (Ric3), transcript variant 2	1.50	0.019
78	**KCNIP2**	Kv channel-interacting protein 2 (Kcnip2), transcript variant a	1.50	0.008
79	**NCKAP1**	NCK-associated protein 1 (Nckap1)	1.50	0.017
80	**GRHL1**	grainyhead-like 1 (Drosophila) (Grhl1)	1.50	0.044
81	**D030013I16RIK**	RIKEN cDNA D030013I16 gene (D030013I16Rik)	1.49	0.005
82	**ARL3**	ADP-ribosylation factor-like 3 (Arl3)	1.49	0.032
83	**PI15**	peptidase inhibitor 15 (Pi15)	1.49	0.012
84	**SNAP91**	synaptosomal-associated protein 91 (Snap91)	1.49	0.017
85	**SEZ6L2**	seizure related 6 homolog like 2 (Sez6l2)	1.49	0.018
86	**BC030500**	cDNA sequence BC030500 (BC030500)	1.48	0.042
87	**6030405A18**		1.48	0.028
88	**MCRS1**	microspherule protein 1 (Mcrs1)	1.48	0.011
89	**LAMA4**	laminin, alpha 4 (Lama4)	1.48	0.026
90	**GDA**	guanine deaminase (Gda)	1.48	0.018
91	**PARP1**	poly (ADP-ribose) polymerase family, member 1 (Parp1)	1.48	0.004
92	**MAPK8IP1**	mitogen-activated protein kinase 8 interacting protein 1 (Mapk8ip1)	1.48	0.023
93	**DLX2**	distal-less homeobox 2 (Dlx2)	1.48	0.020
94	**ISLR2**	immunoglobulin superfamily containing leucine-rich repeat 2 (Islr2)	1.48	0.003
95	**TGFB2**	transforming growth factor, beta 2 (Tgfb2)	1.48	0.008
96	**LOC100045726**	PREDICTED: hypothetical protein LOC100045726 (LOC100045726)	1.48	0.009
97	**9130213B05RIK**	RIKEN cDNA 9130213B05 gene (9130213B05Rik)	1.48	0.041
98	**NUFIP1**	nuclear fragile X mental retardation protein interacting protein 1 (Nufip1)	1.47	0.022
99	**CYB5D2**	cytochrome b5 domain containing 2 (Cyb5d2)	1.47	0.005
100	**ACO1**	aconitase 1 (Aco1)	1.47	0.040

Table 2.S3 – Transcriptionally altered genes by microarray, WNV-good higher than WNV-Poor. Genes higher in WNV-good than in WNV-poor (top 100 genes by fold change and p value < 0.05)

	Pathway	p val	Altered genes
1	Primary immunodeficiency	6.3E-04	IGHG, TAP2, LCK, AIRE, IGH-VJ558
2	Cytokine-cytokine receptor interaction	9.3E-04	IFNAB, TNF, CCL2, TNFRSF12A, IL21R, IL11RA1, TNFRSF4, CXCL10, CCL6, LEP, TNFRSF1A, FAS, IL1A
3	Natural killer cell mediated cytotoxicity	2.6E-03	IFNAB, IGHG, CD244, TNF, ARAF, LCK, FAS, KLRA3,
4	Calcium signaling pathway	4.2E-03	IGHG, EDNRB, PDE1C, TACR1, CAMK2D, PLCD4, PLCD1, CHRNA7, CAMK2A, IGH-VJ558
5	Allograft rejection	5.4E-03	LOC100048770, IGHG, TNF, H2-T10, FAS, H2-DMA, IGH-VJ558
6	Graft-versus-host disease	5.4E-03	TNF, H2-T10, FAS, H2-DMA, IL1A, KLRA3
7	Apoptosis	7.1E-03	TNFRSF1A, IRAK3, TNF, NFKBIA, FAS, BIRC2, IL1A
8	Autoimmune thyroid disease	1.3E-02	IFNAB, LOC100048770, IGHG, H2-T10, FAS, H2-DMA, IGH-VJ558
9	B cell receptor signaling pathway	2.0E-02	LOC100048770, IGHG, IFITM1, NFKBIA, PIK3AP1, INPP5D, IGH-VJ558
10	Intestinal immune network for IgA production	2.1E-02	LOC100048770, IGHG, LOC100048841, TNFSF13B, H2-DMA, IGH-VJ558
11	Hematopoietic cell lineage	2.4E-02	LOC100048770, IGHG, TNF, ITGA1, IL11RA1, IL1A, IGH-VJ558
12	Asthma	2.6E-02	LOC100048770, IGHG, TNF, H2-DMA, IGH-VJ558
13	NOD-like receptor signaling pathway	3.3E-02	TNF, CCL2, ERBB2IP, NFKBIA, BIRC2
14	Type I diabetes mellitus	3.5E-02	TNF, H2-T10, FAS, H2-DMA, IL1A
15	Adipocytokine signaling pathway	4.2E-02	LEP, TNFRSF1A, TNF, NFKBIA, CPT1A

Table 2.S4. Pathway analysis of genes significantly higher in WNV-poor spatial memory performers compared to WNV-good at 25 days post-infection. KEGG pathway analysis using DAVID bioinformatics database functional annotation tool v.6.7. Analysis generated with list of genes having greater than 1.5 fold change and p value of less than 0.05 in WNV-poor vs. WNV-good analysis. Adjusted p-values determined by Benjamini false discovery rate.

	Pathway	p	Altered genes
1	Long-term potentiation	0.002	GRM5, GRIN2B, GRIN1, PPP3CA, PPP1CC, PPP1CB, PRKCB
2	Calcium signaling pathway	0.013	TRPC1, PHKB, PDE1A, CACNA1G, RYR2, PRKCB, CACNA1B
3	Axon guidance	0.014	EPHA5, SEMA6C, PLXNA4, ROCK2, ROBO1, SEMA3E, SLIT2
4	Wnt signaling pathway	0.027	TBL1XR1, CCND1, ROCK2, SIAH1B, SIAH1A, CUL1, PRKCB
5	Terpenoid backbone biosynthesis	0.030	LOC100040592, MVD, FDPS
6	MAPK signaling pathway	0.035	MAPT, CACNA1G, PLA2G6, FGF13, MAPK8IP1, TGFB2
7	Butanoate metabolism	0.036	LOC100040592, GAD1, PDHB, ALDH3A2
8	Glyoxylate and dicarboxylate metab.	0.039	GLYCTK, ACO1, AFMID
9	Steroid biosynthesis	0.043	TM7SF2, SQLE, SC4MOL
10	p53 signaling pathway	0.046	CCND1, SIAH1B, SIAH1A, CCNG2, ATM

Table 2.S5. Pathway analysis of genes significantly higher in WNV-good spatial memory performers compared to WNV-poor at 25 days post-infection. KEGG pathway analysis using DAVID bioinformatics database functional annotation tool v.6.7. Analysis generated with list of genes having greater than 1.5 fold change and p value of less than 0.05 in WNV-good vs. WNV-poor analysis. Adjusted p-values determined by Benjamini false discovery rate.

Group	Age	Sex	PMI	Cause of Death	Other findings / Comorbidities	DG	CA2/3	CA1	EC
WNV	46	f	15	WNV encephalitis	History of non-Hodgkin's lymphoma, bone-marrow transplant recipient	-	+++	-	-
	51	f	22	WNV encephalitis	S. aureus infection, history of rheumatoid arthritis, lupus, and immunosuppressive therapy	-	+++	-	-
	62	m	20	WNV encephalitis	History of cardiac, lung, and brain sarcoidosis, cardiomegaly, atherosclerosis, steroid treatment	-	+	-	+
	75	m	?	WNV encephalitis	History of mantle cell lymphoma, bone-marrow transplant recipient	-	-	-	-
	79	f	16	WNV encephalitis	Atherosclerosis, history of pyelonephritis, rheumatoid arthritis	-	-	-	-
Mean:	**62.6**		**18.3**						

Group	Age	Sex	PMI	Cause of Death	Other findings / Comorbidities	DG	CA2/3	CA1	EC
Control	47	f	21	Cardiac arrest	Emphysema, kidney atrophy, history of congestive heart failure, multiple small vessel embolisms	-	-	-	-
	56	f	15	Cardiogenic shock	Coronary artery disease, pericardial metastatic carcinoma, history of hepatitis C, transplant recipient	-	-	-	-
	57	m	4	Cardiac arrest	Atherosclerosis, history of prostate cancer, emphysema, hypertension	-	-	-	-
	60	m	17	Cardiac arrest	History of cardiac arrest, atherosclerosis, cardiomegaly, emphysematous changes	-	-	-	-
	60	f	12	Cardiac arrest	History of cerebral ischemic stroke (MCA), gram-negative sepsis	-	-	-	-
	65	m	17	PEA cardiac arrest	Bronchopneumonia, chronic obstructive pulmonary disease, history of myocardial infarction	-	-	-	-
	72	m	25	PEA cardiac arrest	Atherosclerosis, history of congestive heart failure, history of hypotension	-	-	-	-
	84	f	39	Undetermined	Renal disease, myocyte hypertrophy, pulmonary fibrosis, history of sepsis	-	-	-	-
Mean:	**62.6**		**18.8**						

Table 2.S6 – Human post-mortem tissue. Relevant information on human autopsy cases used in this study, including age, sex, post-mortem interval (PMI) in hours, cause of death, and other comorbidities noted. Abbreviations used: Pulseless electrical activity (PEA), Dentate Gyrus (DG), Entorhinal Cortex (EC). Scoring = negative (-), mild (+), moderate (++) or severe (+++) for West Nile virus antigen immunostaining.

CHAPTER 3 – Alterations to hippocampal and subventricular zone adult neurogenesis during West Nile virus encephalitis

Abstract

Cognitive sequelae have been reported to occur following the neuroinvasive infections of several neurotropic viruses including Japanese Encephalitis virus[152], St. Louis Encephalitis virus[153], acute sporadic encephalitis caused by Herpes Simplex[154], and more recently, West Nile virus[12,14,15]. West Nile Virus (WNV) is a mosquito-borne flavivirus capable of infecting and killing mature neurons and eliciting antiviral immune responses throughout the central nervous system (CNS). In the United States, WNV has been responsible for over 13,000 reported cases of encephalitis and meningitis since its emergence in 1999. Of interest, over 50% of patients who recover from WNV neuroinvasive disease (WNND) suffer cognitive sequelae, including confusion, depression, and memory impairments for a year or longer beyond the course of acute viral infection. Memory impairments and depression have both been linked to alterations in adult neurogenesis, suggesting WNV impacts on this process. Previous studies by our group, using a well-established murine model, have determined that chemoattractant molecules expressed by WNV-infected neurons are responsible for recruiting lymphocytes to promote viral clearance and survival[40]. Here we report that during WNND recovery, significantly fewer new granule cell neurons are born within the hippocampal dentate gyrus, as revealed by BrdU-labeling. And although neuronal progenitor cells (NPCs) are not direct targets of WNV infection, their homeostatic levels of proliferation, differentiation, and migration were significantly altered. Using immunohistochemistry and

flow cytometry coupled with *in vivo* BrdU labeling during acute WNV infection, we found NPCs within the subventricular (SVZ) and subgranular (SGZ) neurogenic zones generated fewer new neuroblasts, but greater numbers of astrocytes, an effect which slowly recovers over about 45 days. This effect was dependent upon Interleukin-1 receptor (IL-1R) signaling, which we have previously shown to be necessary for promotion of viral clearance by T lymphocytes[10]. Lastly, IL-1R deficient mice were resistant to the WNV-mediated impairment in spatial learning and memory observed in wild type mice (Vasek and Klein, chapter 2) via the Barnes maze task at 45 days post infection, suggesting that the alterations to neuronal progenitor cell homeostasis during adult neurogenesis may underlie long term cognitive consequences of WNND.

Introduction

West Nile Virus (WNV) has recently experienced resurgence in the United States. Both the number of total cases and the number of neuroinvasive cases more than quadrupled in 2012 compared to 2011[11]. In the acute stage of infection, patients suffering from WNV encephalitis or meningitis can experience confusion, fatigue, loss of motor control, memory loss, coma, and a mortality rate of about 8-10%[12]. Unfortunately, of the many patients who survive neuroinvasive WNV, about half experience long term cognitive sequelae including depression, memory impairments, and motor impairments for several months to years beyond the episode of symptomatic infection[14–16,97,126]. To date, there have been no published studies that investigate the mechanistic causes of long-term cognitive sequelae or the extent of damage and repair that occurs beyond the acute phase of WND.

Once WNV has entered the central nervous system, it preferentially infects and replicates within neurons and can cause apoptosis via caspase-3 induction[20,21]. A robust encephalitic response follows CNS WNV infection, in which T cells are crucial for viral clearance and survival[37,38]; however it is possible that this infiltration of leukocytes into the CNS may cause additional neuron damage. Likely, the specific brain regions which are variably infected by WNV might dictate the symptoms and sequelae experienced by patients in the short and long-term, respectively. The hippocampus, an area often infected in both human and murine WNV encephalitis[19,155], is essential for spatial and contextual memory formation. Inputs from the entorhinal cortex enter the hippocampus and relay through the dentate gyrus, CA3, and CA1[98]. Damage to hippocampal neurons or their synaptic connections could restrict proper spatial memory formation or memory recall.

Another component of hippocampal learning involves the process of adult neurogenesis, which occurs within the hippocampal dentate gyrus (DG) and the subventricular zone (SVZ)[156]. Within the DG, adult neural stem cells give rise to astrocytes and intermediate neuronal progenitors, the latter of which proliferate and differentiate into neuroblasts. These neuroblasts migrate into the granule cell layer of the DG, mature into granule cell neurons and integrate into the hippocampal circuit over the course of a few weeks[71,157]. Although the precise extent to which adult neurogenesis contributes to spatial learning is a field which needs further careful investigation, it is clear that voluntary running and environmental enrichment increase neurogenesis as well as performance in several spatial learning and memory tasks in rodents [158–160]. Furthermore, ablation of neurogenesis by X-ray irradiation leads to impaired spatial learning in the Barnes Maze[72]. The fact that many WNND patients experience memory impairments for

months to years beyond viral clearance suggests a chronic condition with either sustained damage or limited repair.

The inflammatory cytokine Interleukin 1 (IL-1), which has two main forms, IL-1α and IL-1β, has also been shown to impact on cognitive function in the context of neuroinflammation. While IL-1 is known to be a key player in orchestrating the CNS immune response, including onset of fever[161], it also plays a role in spatial learning and memory-related behavior[162]. Indeed, injection of IL-1β into the brain impairs spatial learning, contextual fear memory, and adult neurogenesis[163–165]. Of interest, IL-1R-deficient mice are slow to learn the Morris water maze task, display a deficit in long-term potentiation in the hippocampus, and exhibit longer freezing times during contextual fear memory testing[166,167]. Although several studies have investigated impacts of IL-1 on hippocampal-based learning and behavior, few have done so in a setting of physiological IL-1 induction, such as during CNS infection.

In this study we utilize a previously described murine model of WNND recovery replete with spatial memory impairments out to 50 days post-infection (Chapter 2). Utilizing a brdU pulse-chase experiment, we show that adult WNV-recovered mice experience a loss in newborn dentate granule cell neurons during the period of spatial learning and memory impairments. Using flow cytometry, we were able to show that this neuronal loss is due to a reduction in the proliferation/differentiation of neural progenitors along the neuronal lineage during the acute phase of WNV infection, which lasts out to at least 30 days post-infection. Interestingly, neuronal progenitors within the SVZ suffered a similar reduction in neuroblast proliferation during WNND, as well as an additional aberration in their migratory patterns. Wild type mice infected and recovered from WNV-

NS5-E218A infection displaying impaired spatial learning and memory were found to have upregulated transcripts relating to IL-1R signaling. Furthermore, IL-1R -/- mice did not experience the WNV-mediated alterations to neuronal progenitor cell proliferation and importantly, also did not show a WNV-mediated impairment to spatial learning and memory in the Barnes Maze task. This study highlights a potential pathway and mechanism underlying impairments to memory during WNND.

Results and Discussion

To better understand the cognitive sequelae experienced by many patients who have recovered from WNV encephalitis we established a murine model of WNV recovery to study cognitive impairments. Because footpad infection with wildtype WNV (WNV-NY) leads to variable levels of CNS infection and direct intracranial infection with WNV-NY virus is 100% lethal, we intracranially inoculated mice with 10^4 pfu of an attenuated mutant form of WNV (2'O methyltransferase-E218A)[9,168]. The mutant WNV-E218A does infect neurons when administered via this route, replicates within the CNS, and induces an antiviral encephalitic response, however over 90% of mice survive and recover from the encephalitis. Intracranial (i.c.) infection with WNV-E218A is capable of infecting all brain regions infected by WNV-NY including the hippocampus, cortex, striatum, cerebellum, and brainstem and capable of inducing neuronal apoptosis[9].

Because the process of adult neurogenesis contributes to hippocampal spatial learning and memory[71], we evaluated the generation of new neurons during WNV encephalitis and the recovery period. We administered BrdU during the peak of WNV encephalitis for a period of 4 days (days 3-7), and then allowed mice to recover for 52

days. WNV-recovered mice exhibited fewer BrdU-labeled neurons within the dentate gyrus granule cell layer than mock-infected controls (**Fig. 3.1**).

One possible explanation of fewer new neurons after the recovery period of WNV encephalitis is that neuroblasts are dying before reaching maturity. In agreement with previous studies, we confirmed that neural stem cells and intermediate neuronal progenitors were not permissive to WNV infection[128], and observed that less than 1% of doublecortin-expressing neuroblasts were infected in vivo in both the SVZ and SGZ (**Fig. 3.2**). Furthermore rates of neuroblast apoptosis during acute WNND were equivalent to mock-infected controls (data not shown). The few infected neuroblasts which were observed within the DG were located within the granule cell layer, suggesting that these may be late-stage neuroblasts as they are transitioning into immature neurons. Late-stage neuroblasts exhibit many of the same properties as neurons including, receptors, filament proteins, and cellular processes (e.g. axon formation and the beginning of dendrite formation), thus potentially explaining the ability of WNV to infect them.

Another explanation for reduced neurogenesis includes the alteration in the rate of neuronal progenitor cell proliferation. To test this, mock-infected versus WNV-NY-infected or WNV-E218A-infected mice were administered BrdU during the peak of encephalitis, followed by either immunohistochemical (**Fig. 3.3a**) or flow cytometric (**Fig. 3.3b**) evaluation of hippocampal neuronal progenitors, as described previously[149]. Infections with either wild type WNV (NY-99) via the peripheral footpad route (**Fig. 3.3a**), via the intracranial infection route, or attenuated WNV-NS5-E218A all led to fewer BrdU-labeled neuroblasts at 6-8 days post-infection (**Fig. 3.3b**). This reduction in neuroblast-genesis was assessed over the course of WNND recovery, at 6, 15, and 30 days post-infection

(after normalization to age-matched controls) and found that deficits persist until at least day 15 within the hippocampus and day 30 within the SVZ (**Fig. 3.3c**).

Alterations in the proliferation rates of neural progenitors could result in changes to the overall pool of stem cells over time. Using-GFP-expressing mice, we counted the numbers of Nestin and GFAP-double positive cells remaining within the hippocampal SGZ at 45 days post-infection, but found no differences in the numbers of neural stem cells expressed by mock and WNV-NS5-E218A recovered mice (data not shown).

To further investigate the potential for an alteration in cell fate / differentiation of early stage progenitors, we tested to see if fewer neuronal progenitors were produced in favor of more glial progenitors within the hippocampus of WNV-infected mice. To test this, mock-infected versus WNV-NY-infected or WNV-E218A-infected mice were administered BrdU during the peak of encephalitis followed by flow cytometric evaluation of hippocampal neuronal progenitors and astrocytes 48 hours later (**Fig. 3.4**). Infections with either wild type WNV (NY-99) or attenuated WNV-NS5-E218A led to more BrdU-labeled gfap-expressing astrocytes at 7 days post infection than mock-infected controls (**Fig. 3.4**).

The migration of neuroblasts to their proper targets remains an additional important component of functional adult neurogenesis[71]. Upon examining neuroblasts within the SVZ from WNV-infected mice, we additionally discovered an abberant migration pattern expressed by these cells, in that more DCX+ cells were found at distances greater than 30 microns from the walls of the lateral ventricle (**Fig. 3.5**). This phenomenon has previously been observed in striatal ischemic models[169], but has not been previously described in viral models of CNS infection.

Since adult neural stem cells within the DG can give rise to both the astrocyte and neuronal lineages in vivo[170], our results suggest that there is either a reduction in proliferation of neuronal progenitors in combination with an increase in proliferation of astrocyte progenitors, or there is a shift in the differentiation of neural stem cells, causing more daughter cells to enter the astrocyte lineage in favor of the neuronal lineage. The cytokines, Interleukin-1α (IL-1α) and Interleukin-1β (IL-1β), have been shown to induce neural stem and progenitor cells *in vitro* to favor the astrocyte rather than neuronal lineage[171]. Furthermore, two members of the IL-1 receptor (IL-1R) signaling pathway, Caspase-1, which cleaves and activates IL-1β, and IL-1α, were identified by a microarray screen in chapter 2 as being highly expressed in mice with sever spatial memory impairments during WNND. In additional cohorts of wild-type mice, we validated this microarray by quantitative PCR and found significant hippocampal upregulation of both genes specifically within the WNV-poor spatial memory performing mice compared to mock-infected controls (**Fig. 3.6**).

Next, we tested if the WNV-mediated reduction in neuroblast proliferation would occur in mice lacking IL-1 signaling utilizing IL-1R -/- mice. Mock-infected and WNV-NS5-E218A-infected IL-1R -/- mice were administered BrdU during the peak of encephalitis, followed by flow cytometric evaluation of hippocampal neuronal progenitors. In contrast to the reduction in neuroblast genesis observed in wild type animals, IL-1R -/- were resistant to changes in neuroblast proliferation rates (**Fig 3.7**).

If reductions to neurogenesis was underlying the spatial memory impairments exhibited by WNND recovering mice (**Fig 2.1a**), then it might be expected that IL-1R -/- mice recovering WNND may exhibit preservation of spatial learning and memory. Thus,

after i.c. infection with WNV-NS5-E218A, we allowed IL-1R -/- mice to recover for a month beyond viral clearance (46 days post infection) and tested their ability to spatially locate and remember the location of a target hole in a Barnes maze over the course of 10 trials held twice daily for 5 days. In contrast to wild type mice, IL-1R -/- mice recovering from WNND performed equally well on the Barnes Maze spatial learning task (**Fig. 3.8**).

One significant caveat to the experiments utilizing IL-1R -/- mice is that in other spatial learning tasks (e.g. morris water maze), IL-1R -/- mice have altered baseline spatial memory performance than wild type mice and it is possible that the same pathway(s) which becomes impaired during WNND recovery of wild type animals is already impaired in adult IL-1R -/- animals. Experiments with IL-1R pathway antagonists performed in wild type mice may be warranted to confirm the aforementioned results.

Taken together, our results show that during the acute phase of viral infection, the proliferation, migration, and differentiation fates of neural progenitor cells are altered during the recovery period of WNV encephalitis. Interestingly, mice deficient in IL-1R signaling are resistant to both the altered npc proliferation as well as spatial memory impairments which are observed in wild type WNND mice. The combinatorial effect of synapse loss (chapter 2) and reduced neurogenesis (chapter 3) is likely to seriously impact hippocampal spatial learning and memory long beyond the initial episode of infection.

Materials and methods

Animals

5-8 week-old male mice were used at the outset of all experiments. C57BL/6J mice were obtained from Jackson Laboratories. IL-1R -/- mice (> 10 generations backcrossed to C57Bl/6) were obtained from Jackson Laboratories. Nestin-GFP mice (> 10 generations backcrossed to C57Bl/6) were obtained from Dr. Gregory Enikolopov (Cold Spring Harbor Laboratories). All experimental protocols were performed in compliance with the Washington University School of Medicine Animal Safety Committee (protocol# 20140122).

Mouse models of WNV infection

Footpad: (WNV-NY99) The WNV strain 3000.0259 was isolated in New York in 2000 (Ebel et al., 2001) and passaged once in C6/36 *Aedes albopictus* cells to generate an insect cell–derived stock. 100 plaque forming units (pfu) of WNV-NY99 were delivered in 50 uL to the footpad of anaesthetized mice.

Intracranial: "WNV-NS5-E218A," which harbors a single point mutation in the 2'O-methyl-transferase gene, was obtained from Dr. Michael Diamond (Washington University) and passaged in vero cells as described previously[8]. Deeply anaesthetized mice were administered 10^4 pfu of WNV-NS5-E218A or 10 pfu of WNV-NY99 in 10 uL into the brain's third ventricle via a guided 29 gauge needle.

Stock titers of all viruses were determined by using BHK21 cells for viral plaque assay as previously described[103].

Antibodies

WNV (1:100 described previously[10]), GFAP (1:200 Invitrogen), Doublecortin (1:150 Cell Signaling), BrdU (1:50 for flow cytometry BD Biosciences), BrdU (1:200 for IHC Abcam) NeuN-biotin (1:100 Millipore), GFP (1:1000 Abcam),

Secondary antibodies conjugated to Alexa-488, Alexa-555, or Alexa-647 (Invitrogen) were used at 1:400 dilution.

Immunohistochemistry

Following perfusion with ice-cold PBS and 4% PFA, brains were immersion-fixed overnight in 4% PFA, followed by cryoprotection in 2 exchanges of 30% sucrose for 72 hours, then frozen in OCT (Fisher). 9μm-thick fixed-frozen coronal brain sections were washed with PBS and permeabilized with 0.1% Triton X-100 (Sigma-Aldrich), and nonspecific Ab was blocked with 5-10% normal goat serum (Santa Cruz Biotechnology) for 1 h at room temperature. Mouse on Mouse kit (MOM basic kit, Vector) was used per manufacturers protocol when detecting synaptophysin (mouse, DAKO) to reduce endogenous mouse Ab staining. After block, slides were exposed to primary Ab or isotype matched IgG overnight at 4°C, washed with 0.2% FSG in PBS and incubated with secondary Abs for 1 h at room temperature. Nuclei were counterstained with ToPro3 (Invitrogen) and coverslips were applied with vectashield (Vector). Immunofluorescence was analyzed using a Zeiss LSM 510 laser-scanning confocal microscope and accompanying software (Zeiss). Positive immunofluorescent signals were quantified using the public domain NIH Image analysis software, ImageJ.

TUNEL staining was performed using the TMR-red in situ cell death detection kit (Roche) as per manufacturer's instructions. C1qA staining was performed as previously described[147].

Flow cytometry

Cells were isolated from brains of WT mice at day 6, 15, or 30 days post-infection and stained with fluorescently conjugated antibodies to CD45, BrdU, and Doublecortin as previously described[149]. Data collection and analysis were performed with an LSRII flow cytometer using FlowJo software.

Real-time quantitative RT-PCR

cDNA was synthesized using random hexamers, oligodT15, and MultiScribe reverse transcriptase (Applied Biosystems). A single reverse transcription master mix was used to reverse transcribe all samples in order to minimize differences in reverse transcription efficiency. The following conditions were used for reverse transcription: 25°C for 10 min, 48°C for 30 min, and 95°C for 5 min.

Behavioral Testing

The Barnes Maze was used to assess for visual spatial memory. An elevated Barnes Maze (36" diameter, custom built) containing 19 empty holes and 1 target hole with a hidden escape chamber was used for testing (2" diameter holes were evenly spaced around the table, 2.5" from the edge). Visual cues were placed around the room and remained in the same location during the entire testing period. Mice were tested on the

Barnes Maze over the course of 5 consecutive days. Each mouse received two trials per day, spaced exactly 30 minutes apart. For each trial, the mouse was placed in the center of the maze in a covered start box for 10 seconds, and removal of the box signaled the start of a trial. Each mouse was given 3 minutes to explore the maze and find the target hole. Mice that did not enter the target hole within 3 minutes were gently guided into the hole. After each trial, the mouse remained in the target hole for exactly 1 minute, and then was returned to its home cage. The maze was decontaminated with 70% ethanol between each trial. The numbers of errors (nose pokes over non-target holes) and the latency to find the target hole (amount of time elapsed before nose poke over target hole) were measured. Behavior was recorded using a camera (Canon Powershot SD1100IS), and a blinded experimenter scored the trials.

Figures and Tables

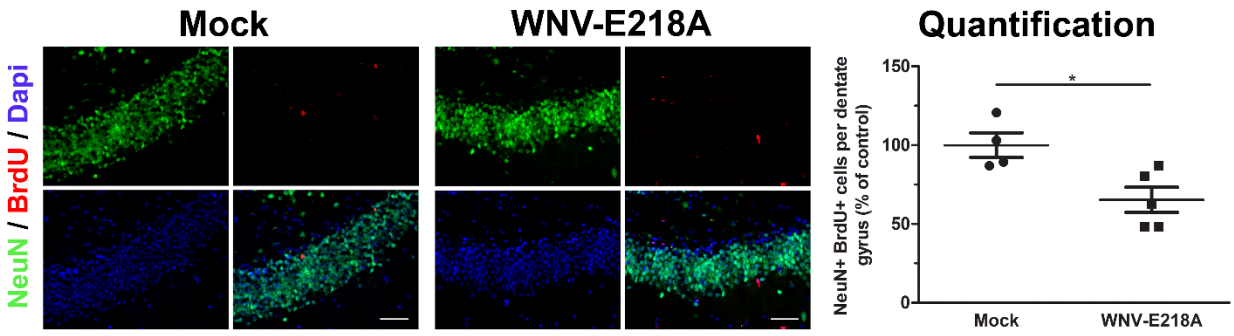

Fig 3.1. Fewer new neurons are born within the dentate gyrus during WNV-NS5-E218A recovery. Mice were given an I.P. BrdU injection (75 mg/kg) every 12 hours for 3.5 days (7 injections) beginning at day 4 pi, then we waited until 52 days post-infection to sacrifice mice for immunohistochemistry analysis. Cells born during the period of BrdU labeling are labeled with anti-BrdU (red) and neurons are labeled with NeuN (green), nuclei are labeled with Dapi (blue). Right: The number of BrdU+ NeuN+ cells per section of dentate gyrus were quantified and normalized to percent of mock-infected control. * $p < 0.05$ by student's t-test. > 4 sections per animal analyzed

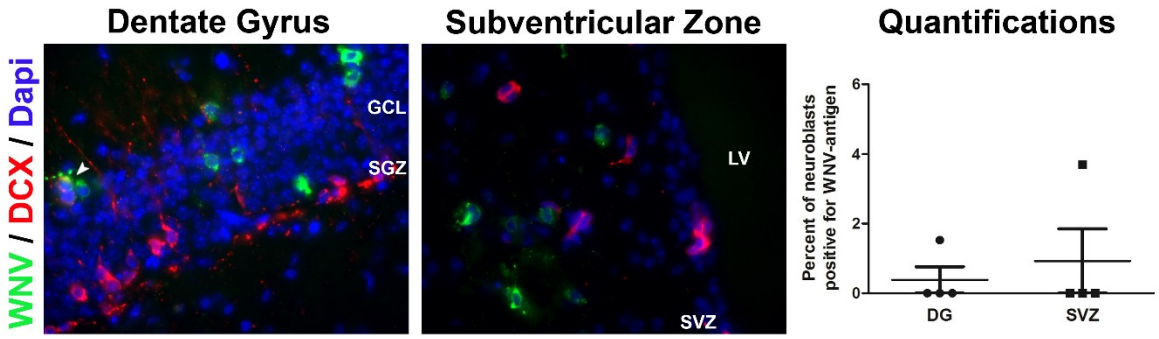

Fig 3.2 WNV Permissivity within Doublecortin-positive neuroblasts *in vivo*. 5 week old mice were infected via the footpad with 100 pfu of wild type WNV(NY99) and harvested for tissue collection on day 8 post infection. Immunohistochemistry is shown for West Nile antigen and the neuroblast marker, doublecortin (DCX) within the Dentate gyrus and Subventricular Zones (SVZ). Many WNV+ neurons can be seen within the granule cell layer (GCL) of the Dentate gyrus and the striatum neighboring the SVZ, however only 1 out of 4 animals showed any WNV and DCX-double positive cells (shown by white arrowhead, Left), resulting in a mean % of infection of less than 1% of total DCX+ cells. Within the Dentate gyrus, infected DCX+ cells were always located within the GCL – indicating that they are more mature neuroblasts or immature neurons.

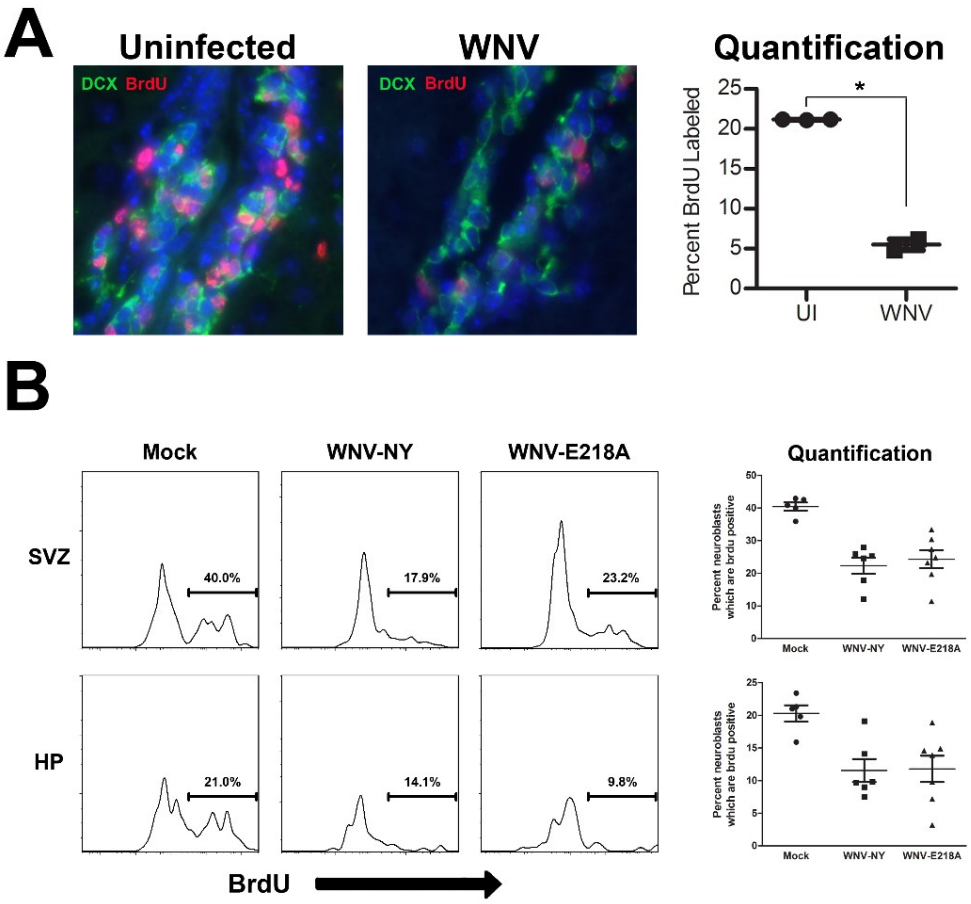

Fig 3.3 Deficits in adult neurogenesis during WNV infection.

Mice were given an i.p. BrdU injection (100 mg/kg) at 24 and 48 hours prior to harvest.

A) Immunohistochemistry shows fewer BrdU-labeled neuroblasts, marked by the marker, Doublecortin (DCX), within the SVZ at 8 days post-infection with WNV-NY via the footpad (100 pfu) compared to uninfected age-matched controls. B) The proliferation rates of neuroblasts were measured (% BrdU incorporation) within subventricular zone (SVZ) or hippocampus (HP) dissections from mice, and isolation of cells for flow cytometry. Shown are graphs of BrdU+ cells after gating on doublecortin+ cells at 6 days post intracranial infection with either wild type WNV-NY99, WNV-NS5-E218A, or saline (Mock). C) The proliferation rates of neuroblasts were measured by % of neuroblasts with BrdU incorporation using flow cytometry after gating on doublecortin+ cells at 6, 15, and 30 days post WNV-NS5-E218A or mock infection. All data in (C) normalized to age-matched mock-infected controls to compensate for age-related alterations in neurogenesis.

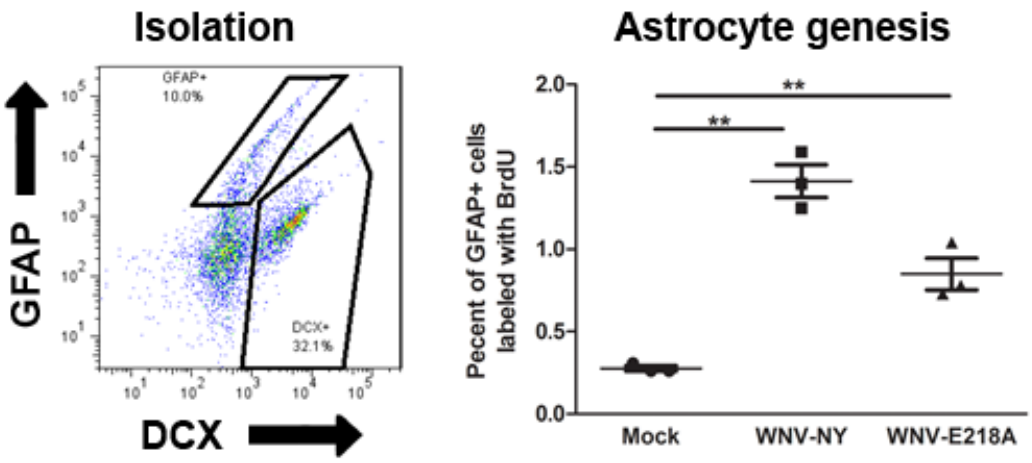

Fig 3.4. Greater numbers of BrdU-labeled astrocytes neurons are born within the hippocampus during acute WNV encephalitis. Mice were given an i.p. BrdU injection (100 mg/kg) at 24 and 48 hours prior to harvest on day 6 pi. Left: Isolation of GFAP+ astrocytes and DCX+ neuroblasts by flow cytometry. Right: Percentage of GFAP+ astrocytes labeled with BrdU at day 6 post intracranial WNV-NY or WNV-E218A infection. ** $p < 0.01$ by Two-tailed Student's T-test.

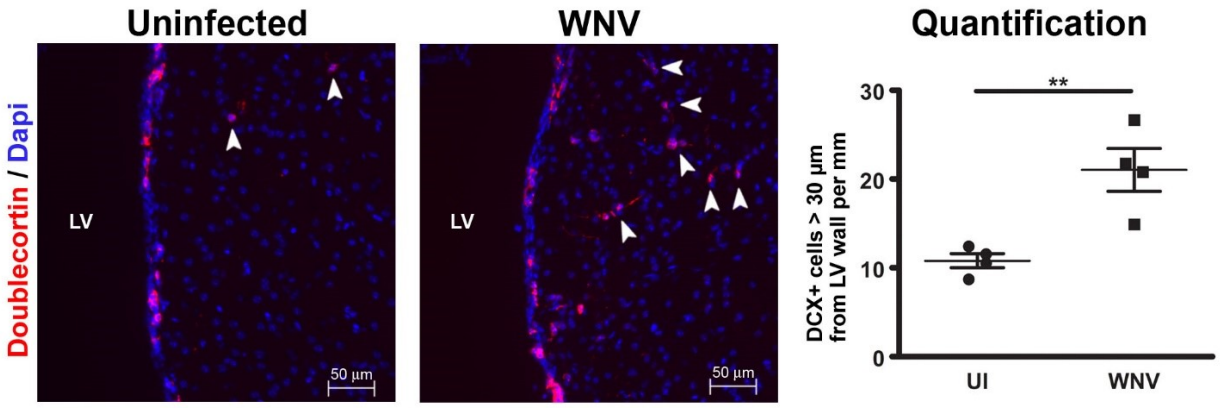

Fig 3.5 Aberrant migration of SVZ neuroblasts during WNV infection. Age and sex-matched uninfected mice or mice infected via the footpad with 100 pfu of WNV-NY (1999), were collected at 8 days post infection. Following immunohistochemichal staining for the neuroblast marker, Doublecortin (DCX), the number of DCX+ cells found greater than 30 microns (depicted by white arrowheads) from the lateral ventricle wall were calculated. ** $p < 0.01$ by Two-tailed Student's T-test.

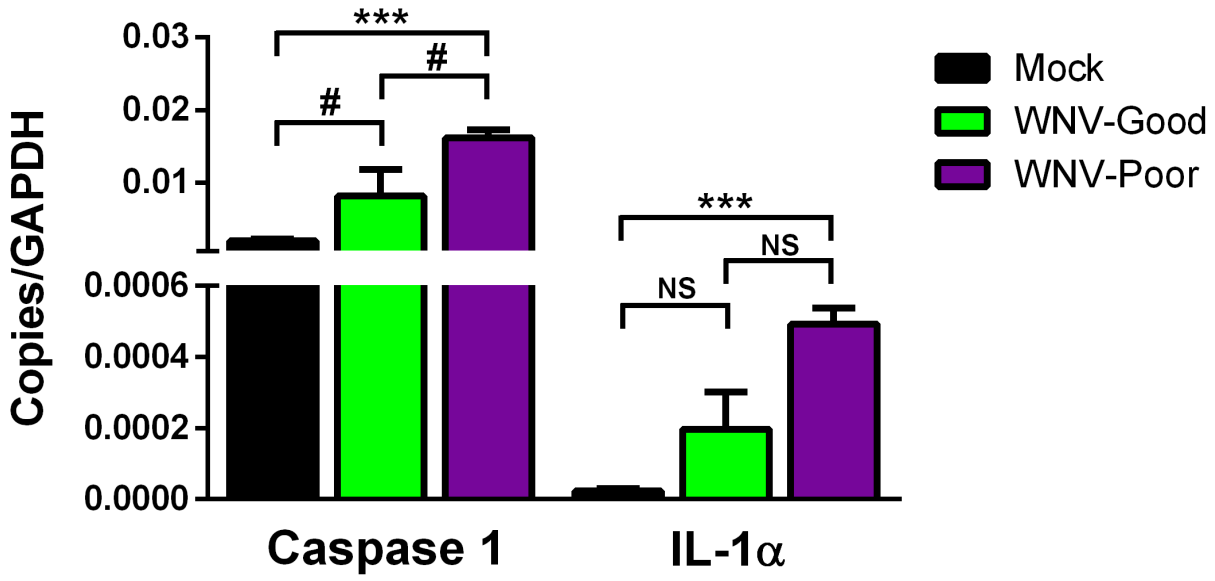

Fig 3.6 Gene transcripts in the IL-1R signaling pathway are altered specifically in WNV-NS5-E218A-infected poor spatial learning mice. RNA from hippocampi was collected at day 25 post-infection from Mock, and WNV-NS5-E218A infected, recovering mice which exhibited good or poor spatial memory on the Barnes Maze task. NS = not significant, # = trend towards significance ($0.10 > p > 0.05$), *** = $p < 0.001$ by Two-tailed Student's T-test.

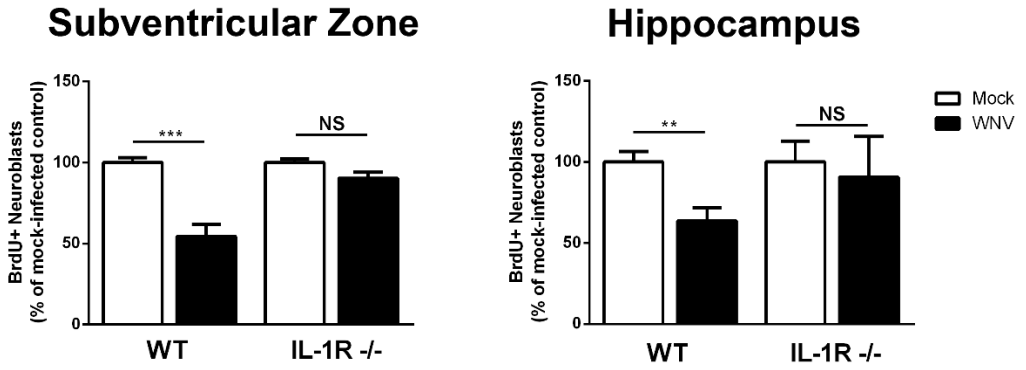

Fig 3.7 IL-1R -/- mice are resistant to WNV-mediated alterations to neuroblast proliferation. The proliferation rates of neuroblasts were measured (% BrdU incorporation) within subventricular zone or hippocampus following dissection and isolation of cells for flow cytometry. Shown are graphs of % of BrdU+ cells after gating on doublecortin+ cells at 6 days post intracranial infection with WNV-NS5-E218A, or saline (Mock) and normalization against genotype and age-matched mock-infected controls. ** $p < 0.01$, *** $p < 0.001$ by Two-tailed student's T-test.

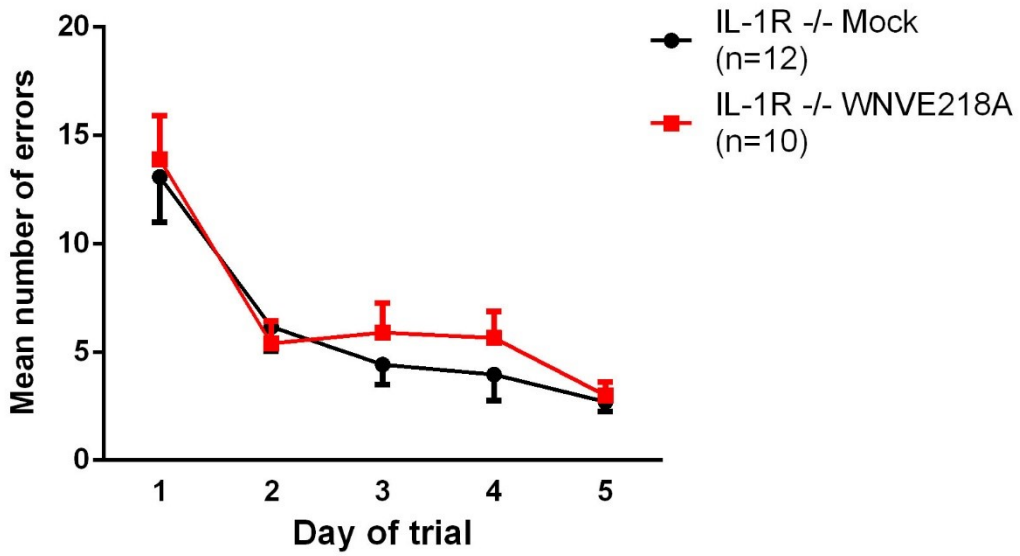

Fig 3.8 IL-1R -/- WNV-E218A-infected mice do not harbor significant differences in spatial learning and memory via the Barnes Maze behavior task. Mice were infected with 10^4 pfu of WNV-NS5-E218A at 8 weeks of age and allowed to recover for 45 days before the initiation of Barnes Maze testing. Number of errors (nose poke in non-target hole) committed before finding the target hole in the Barnes Maze were measured twice per day and averaged, with an inter-trial interval of 30 minutes, over the course of 5 days of testing. Statistics: not significant by repeated measures two-way ANOVA.

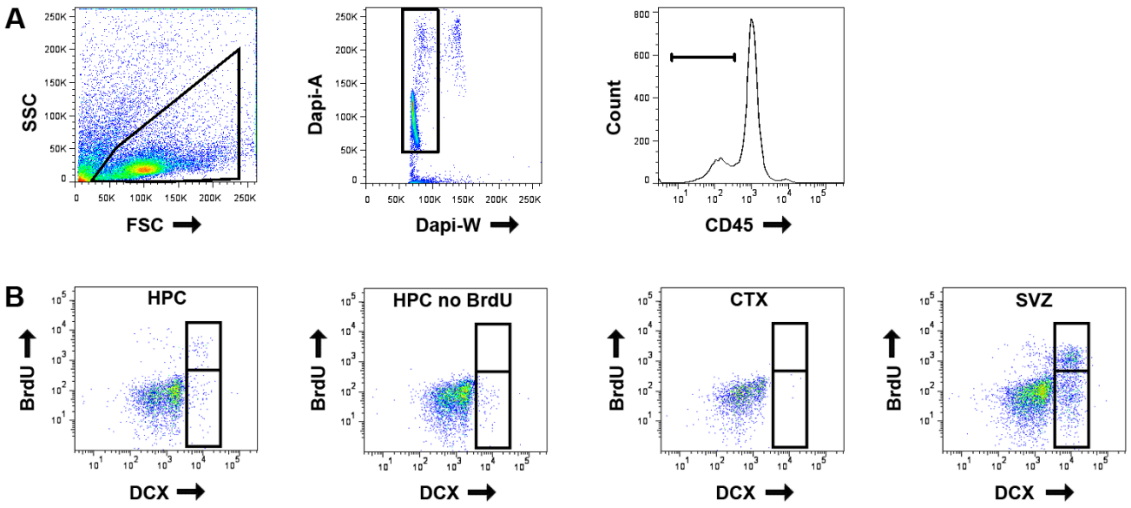

Fig 3.S1. Flow Cytometry gating strategy. A) Following isolation and staining with Dapi and antibodies to CD45, Doublecortin, and BrdU, doublets were excluded, and the CD45-negative population was utilized for further gates. B) Percentage of BrdU+ neuroblasts, through expression of the marker, DCX, was calculated and example plots shown from Hippocampus (HPC), Hippocampus from an animal which did not receive BrdU injection (HPC no BrdU), Cortex (CTX), and Subventricular Zone (SVZ).

CHAPTER 4 – Conclusions and Future Directions

Conclusions

Within the introduction, I discussed critical roles that molecular pathways utilized by the immune system in pathogen defense can also contribute to normal (healthy) CNS development. This idea formed the basis for the development and characterization of a murine WNND recovery model, in order to study how CNS inflammatory processes during WNND may contribute to the cognitive impairments experienced by WNND survivors – and specifically to spatial learning and memory, which is well-modeled by murine behavioral studies.

Two pathways have been highlighted in previous chapters of this thesis, the role of classical complement and microglia in synaptic maintenance through synaptic pruning, and the role of cytokines, especially Interleukin-1 signaling, in regulation of neuronal progenitor cell proliferation and fate. And although these pathways clearly represent pathways with effects on spatial learning and memory in these contexts, additional genes and pathways likely play important roles as well, as is suggested by the several hundred altered genes identified in our microarray experiment within chapter 2 (**Figure 2.2**).

In chapter 2 we investigated the role of microglia and classical complement-mediated synaptic pruning during WNND on cognitive function. Using a novel murine model to study memory impairments during recovery from WNND, we showed that mice exhibit spatial learning and memory deficits during recovery and robust microglial activation during the acute phase that persists for nearly two months post-WNV infection. Using electron and confocal microscopy, we demonstrate that these activated microglia

phagocytize synapses during the peak of WNV infection, leading to a significant loss of synapses in the hippocampus and entorhinal cortex. Using whole transcriptome array approaches we identified genes and pathways associated with poor spatial learning, including molecules involved in microglial- and complement-mediated phagocytosis of synapses. Consistent with these data, we observed upregulation of complement protein C1q within neurons and microglia and showed that CA3 synapse elimination is abolished in mice deficient in either microglia or complement C3. Moreover, we detected significantly reduced numbers of hippocampal CA3 synapses in post-mortem human specimens of WNV encephalitis compared with age- and sex-matched controls, highlighting the relevancy of our murine model for human infections with WNV.

This study was the first to show synapse elimination as a pathological feature of WNV encephalitis and to delineate mechanisms that underlie synapse elimination. While the classical complement pathway may, at first glance, represent an intriguing therapeutic target for WNND survivors, this avenue must be examined with caution, as many off-target effects, such as increased susceptibility to further infections could result. A more intriguing therapeutic target would include the identification of a component of this pathway specifically expressed by microglia, but absent within the periphery. Even in this case, the consequences of altering homeostatic synaptic pruning have not yet been studied.

In chapter 3 we showed that during the acute phase of viral infection, the proliferation, migration, and differentiation fates of neural progenitor cells are altered despite not being direct targets of WNV infection. Of interest, mice deficient in IL-1R

signaling were resistant to both the altered progenitor cell proliferation as well as spatial memory impairments which are observed in wild type WNND recovering mice.

Of interest, there are documented studies linking alterations in network excitability of the hippocampal circuit and resulting feedback from GABAergic interneurons to regulation of adult neurogenesis[172,173]. Furthermore, the specific synapses studied within chapter 2 were the axon terminals between the dentate gyrus and CA3 pyramidal neurons, some of which are derived from adult-born granule cell neurons of the dentate gyrus. The combinatorial effect of synapse loss, identified within chapter 2, and reduced neurogenesis, identified within chapter 3, is likely to seriously impact hippocampal spatial learning and memory long beyond the initial episode of infection.

Future Directions

Determine if the classical complement cascade prevents transsynaptic spread of neurotropic viruses

In Chapter 2, I discussed how in response to WNV infection, the classical complement cascade is upregulated, leading to the pruning of synapses by microglia. A speculative hypothesis is that this process has evolved as a way for virus-infected neurons to be recognized and disconnected from the local neural circuit in order to limit both transsynaptic viral spread, as is achieved by rabies virus and herpes simplex virus type 1, as well as any aberrant or excitotoxic signaling originating from the infected neuron. It would be interesting to test if in the absence of a functional complement cascade, for example in mice null for complement C3, if either WNV or a virus known to traffic transsynaptically, such as HSV-1 is able to spread more quickly. Though it would

be most compelling to show this effect *in vivo*, perhaps a simpler and easier to quantify system to use might include a hippocampal ex vivo slice preparation or with primary neurons plated in a campenot chamber in coculture with microglia as has been described[174]. In either setup, viral infection would be done (a GFP reporter particle would work best for in vitro studies) within specific neurons of a slice preparation or within one side of the campenot chamber, followed by measurements of viral spread to connecting neurons either in the presence of complement inhibitors or within microglia and neurons from complement deficient mice.

Determine if MHC Class I pathway contributes to disruptions in spatial learning and memory during WNV recovery

In Chapter 2 we performed a microarray experiment to search for candidate genes and pathways involved in spatial learning and memory defects in WNV-infected and recovering mice. One gene pathway which was identified in our screen, but have yet to follow-up with further experiments, is the MHC Class I pathway. This pathway is famously known for its role in the immune response in displaying non-self peptides at the cell surface for recognition by lymphocytes[52]. More recently, the MHC class I pathway has been shown to be instrumental in setting up neuronal connections and enhancing plasticity within the brain during development[55,56]. The following genes within the MHCI pathway were found to be altered specifically within poor spatial learning and memory WNV-infected and recovered mice: TAPBP, PSMB8, H2-DMA, H2-T10, HMHA1. Further investigation using transgenic and knockout mice might yield insights into how induction of this pathway during CNS infection may impact correlates of learning and memory.

Additional gene transcripts altered in WNV-poor learners with known effects on neurons and neural connections include, Sema6c and Sema3e[175], ROBO1, Sema3F[176]. These molecules represent additional targets which could be further investigated.

Determine if IL-1R antagonism in wild type mice rescues spatial learning and memory during WNV recovery

Since it is known that IL-1R -/- mice exhibit baseline (naïve animals) differences to both spatial learning and memory and neurogenesis, a better test to determine the role of IL-1R signaling is to do so in the absence of any developmental abnormalities, in wild type mice. To do so, IL-1RA (IL-1 receptor antagonist) could be administered peripherally (high dose) or via the lateral ventricle. The timing of this administration would have to be determined using pilot studies, since our group has previously reported that IL-1R signaling is crucial to proper T cell priming and viral clearance[10] – thus the therapy should probably begin at approximately 12-15 days post-infection, a point in time when virus is on the decline and T cells have already received priming. Mice would then be tested on the Barnes Maze spatial memory task at days 46-50 post-infection as has been previously described.

Determine if the WNV-mediated reduction in neurogenesis is due to direct infection, PRR recognition by NPCs, or a more global cytokine effect

Two experiments could be performed to address this question. First, the incubation of neurosphere-derived neuronal progenitors could be incubated with WNV *in vitro*, and pulsed with BrdU in the media. Rates of division would be measured in the setting of WNV

or PBS (control) conditions. The second experiment would involve injecting ultraviolet-killed WNV intracranially, and measuring rates of neuroblast proliferation as was done previously (Chapter 3). If UV-killed WNV induces similar deficits in neurogenesis, this would suggest a more global, pattern recognition receptor-mediated induction of cytokines which impacts on the process of adult neurogenesis. If UV-killed WNV fails to induce an alteration in proliferation, then the experiment is less conclusive and could indicate either a certain threshold of infection necessary to elicit the neurogenic alterations or that live, replicating virus is necessary for the response.

References

1. Labeaud, A. D., Bashir, F. & King, C. H. Measuring the burden of arboviral diseases: the spectrum of morbidity and mortality from four prevalent infections. *Popul. Health Metr.* **9,** 1 (2011).

2. Petersen, L. R. *et al.* Estimated cumulative incidence of West Nile virus infection in US adults, 1999-2010. *Epidemiol. Infect.* **141,** 591–5 (2013).

3. Hoffman, J. E. & Paschal, K. A. Functional outcomes of adult patients with West Nile virus admitted to a rehabilitation hospital. *J. Geriatr. Phys. Ther.* **36,** 55–62

4. Wu, M. D. *et al.* Adult murine hippocampal neurogenesis is inhibited by sustained IL-1β and not rescued by voluntary running. *Brain. Behav. Immun.* **26,** 292–300 (2012).

5. Kokovay, E. *et al.* Adult SVZ Lineage Cells Home to and Leave the Vascular Niche via Differential Responses to SDF1/CXCR4 Signaling. *Cell Stem Cell* **7,** 163–173 (2010).

6. Battista, D., Ferrari, C. C., Gage, F. H. & Pitossi, F. J. Neurogenic niche modulation by activated microglia: transforming growth factor beta increases neurogenesis in the adult dentate gyrus. *Eur. J. Neurosci.* **23,** 83–93 (2006).

7. Stevens, B. *et al.* The classical complement cascade mediates CNS synapse elimination. *Cell* **131,** 1164–78 (2007).

8. Daffis, S. *et al.* 2'-O methylation of the viral mRNA cap evades host restriction by IFIT family members. *Nature* **468,** 452–6 (2010).

9. Szretter, K. J. *et al.* 2'-O methylation of the viral mRNA cap by West Nile virus evades ifit1-dependent and -independent mechanisms of host restriction in vivo. *PLoS Pathog.* **8,** e1002698 (2012).

10. Durrant, D. M., Robinette, M. L. & Klein, R. S. IL-1R1 is required for dendritic cell-mediated T cell reactivation within the CNS during West Nile virus encephalitis. *J. Exp. Med.* **210,** 503–16 (2013).

11. ArboNET & Centers for Disease Control and Prevention. West Nile virus disease cases and deaths reported to CDC by year and clinical presentation, 1999-2014. 1–2 (2014). at <http://www.cdc.gov/westnile/resources/pdfs/data/1-wnv-disease-cases-by-year_1999-2014_06042015.pdf>

12. Sejvar, J. J. *et al.* Neurologic manifestations and outcome of West Nile virus infection. *JAMA* **290,** 511–5 (2003).

13. Staples, J. E., Shankar, M. B., Sejvar, J. J., Meltzer, M. I. & Fischer, M. Initial and long-term costs of patients hospitalized with West Nile virus disease. *Am. J. Trop. Med. Hyg.* **90,** 402–9 (2014).

14. Haaland, K. Y. *et al.* Mental status after West Nile virus infection. *Emerg. Infect. Dis.* **12,** 1260–2 (2006).

15. Klee, A. L. *et al.* Long-term prognosis for clinical West Nile virus infection. *Emerg. Infect. Dis.* **10,** 1405–11 (2004).

16. Carson, P. J. *et al.* Long-term clinical and neuropsychological outcomes of West Nile virus infection. *Clin. Infect. Dis.* **43,** 723–30 (2006).

17. Nolan, M. S., Hause, A. M. & Murray, K. O. Findings of long-term depression up to 8 years post infection from West Nile virus. *J. Clin. Psychol.* **68,** 801–8 (2012).

18. Watson, J. T. *et al.* Clinical characteristics and functional outcomes of West Nile Fever. *Ann. Intern. Med.* **141,** 360–5 (2004).

19. Armah, H. B. *et al.* Systemic distribution of West Nile virus infection: postmortem immunohistochemical study of six cases. *Brain Pathol.* **17,** 354–62 (2007).

20. Shrestha, B., Gottlieb, D. & Diamond, M. S. Infection and injury of neurons by West Nile encephalitis virus. *J. Virol.* **77,** 13203 (2003).

21. Samuel, M. a, Morrey, J. D. & Diamond, M. S. Caspase 3-dependent cell death of neurons contributes to the pathogenesis of West Nile virus encephalitis. *J. Virol.* **81,** 2614–23 (2007).

22. Johnston, L. J., Halliday, G. M. & King, N. J. Langerhans cells migrate to local lymph nodes following cutaneous infection with an arbovirus. *J. Invest. Dermatol.* **114,** 560–8 (2000).

23. Samuel, M. A. & Diamond, M. S. Alpha / Beta Interferon Protects against Lethal West Nile Virus Infection by Restricting Cellular Tropism and Enhancing Neuronal Survival. *Society* **79,** 13350–13361 (2005).

24. Klein, R. S. & Diamond, M. S. Immunological headgear: antiviral immune responses protect against neuroinvasive West Nile virus. *Trends Mol. Med.* **14,** 286–294 (2008).

25. Daniels, B. P. *et al.* Viral pathogen-associated molecular patterns regulate blood-brain barrier integrity via competing innate cytokine signals. *MBio* **5,** e01476–14 (2014).

26. Chai, Q., He, W. Q., Zhou, M., Lu, H. & Fu, Z. F. Enhancement of blood-brain barrier permeability and reduction of tight junction protein expression are modulated by chemokines/cytokines induced by rabies virus infection. *J. Virol.* **88,** 4698–710 (2014).

27. Roe, K. *et al.* West Nile virus-induced disruption of the blood-brain barrier in mice is characterized by the degradation of the junctional complex proteins and increase in multiple matrix metalloproteinases. *J. Gen. Virol.* **93,** 1193–203 (2012).

28. Samuel, M. A., Wang, H., Siddharthan, V., Morrey, J. D. & Diamond, M. S. Axonal transport mediates West Nile virus entry into the central nervous system and induces acute flaccid paralysis. *Proc. Natl. Acad. Sci. U. S. A.* **104,** 17140–5 (2007).

29. Wang, H., Siddharthan, V., Hall, J. O. & Morrey, J. D. West Nile virus preferentially transports along motor neuron axons after sciatic nerve injection of hamsters. *J. Neurovirol.* **15,** 293–9 (2009).

30. Carroll, M. V. & Sim, R. B. Complement in health and disease. *Adv. Drug Deliv. Rev.* **63,** 965–975 (2011).

31. Leslie, J. D. & Mayor, R. Complement in animal development: unexpected roles of a highly conserved pathway. *Semin. Immunol.* **25,** 39–46 (2013).

32. Liszewski, M. K., Farries, T. C., Lublin, D. M., Rooney, I. A. & Atkinson, J. P. Control of the complement system. *Adv. Immunol.* **61,** 201–83 (1996).

33. Bhakdi, S. & Tranum-Jensen, J. Complement lysis: a hole is a hole. *Immunol. Today* **12,** 318–20; discussion 321 (1991).

34. Mehlhop, E. & Diamond, M. S. Protective immune responses against West Nile virus are primed by distinct complement activation pathways. *J. Exp. Med.* **203,** 1371–81 (2006).

35. Mehlhop, E. *et al.* Complement activation is required for induction of a protective antibody response against West Nile virus infection. *J. Virol.* **79,** 7466–77 (2005).

36. Avirutnan, P. *et al.* Antagonism of the complement component C4 by flavivirus nonstructural protein NS1. *J. Exp. Med.* **207,** 793–806 (2010).

37. Shrestha, B. & Diamond, M. S. Role of CD8+ T Cells in Control of West Nile Virus Infection. *J. Virol.* **78,** 8312–8321 (2004).

38. Sitati, E. M. & Diamond, M. S. CD4+ T-cell responses are required for clearance of West Nile virus from the central nervous system. *J. Virol.* **80,** 12060–9 (2006).

39. Diamond, M. S., Shrestha, B., Marri, A., Mahan, D. & Engle, M. B cells and antibody play critical roles in the immediate defense of disseminated infection by West Nile encephalitis virus. *J. Virol.* **77,** 2578–86 (2003).

40. Klein, R. S. *et al.* Neuronal CXCL10 directs CD8+ T-cell recruitment and control of West Nile virus encephalitis. *J. Virol.* **79,** 11457 (2005).

41. Shrestha, B., Zhang, B., Purtha, W. E., Klein, R. S. & Diamond, M. S. Tumor necrosis factor alpha protects against lethal West Nile virus infection by promoting trafficking of mononuclear leukocytes into the central nervous system. *J. Virol.* **82,** 8956–64 (2008).

42. Durrant, D. M., Daniels, B. P. & Klein, R. S. IL-1R1 signaling regulates CXCL12-mediated T cell localization and fate within the central nervous system during West Nile Virus encephalitis. *J. Immunol.* **193,** 4095–106 (2014).

43. Mccandless, E. E., Zhang, B., Diamond, M. S. & Klein, R. S. CXCR4 antagonism increases T cell trafficking in the central nervous system and improves survival from West Nile virus encephalitis. *Proc. Natl. Acad. Sci* (2008).

44. Glass, W. G. *et al.* Chemokine receptor CCR5 promotes leukocyte trafficking to the brain and survival in West Nile virus infection. *J. Exp. Med* **202,** 1087–1098 (2005).

45. Ransohoff, R. M. & Perry, V. H. Microglial physiology: unique stimuli, specialized responses. *Annu. Rev. Immunol.* **27,** 119–45 (2009).

46. Aravalli, R. N., Hu, S., Rowen, T. N., Palmquist, J. M. & Lokensgard, J. R. Cutting edge: TLR2-mediated proinflammatory cytokine and chemokine production by microglial cells in response to herpes simplex virus. *J. Immunol.* **175,** 4189–93 (2005).

47. Colton, C. a. Heterogeneity of microglial activation in the innate immune response in the brain. *J. Neuroimmune Pharmacol.* **4,** 399–418 (2009).

48. Ghoshal, A. *et al.* Proinflammatory mediators released by activated microglia induces neuronal death in Japanese encephalitis. *Glia* **55,** 483–96 (2007).

49. Jessell, T. M. Neuronal specification in the spinal cord: inductive signals and transcriptional codes. *Nat. Rev. Genet.* **1,** 20–9 (2000).

50. Bailey, C. H. & Kandel, E. R. Synaptic remodeling, synaptic growth and the storage of long-term memory in Aplysia. *Prog. Brain Res.* **169,** 179–98 (2008).

51. Gorer, P. A., Lyman, S. & Snell, G. D. Studies on the Genetic and Antigenic Basis of Tumour Transplantation. Linkage between a Histocompatibility Gene and 'Fused' in Mice. *Proc. R. Soc. B Biol. Sci.* **135,** 499–505 (1948).

52. Zinkernagel, R. M. & Doherty, P. C. Restriction of in vitro T cell-mediated cytotoxicity in lymphocytic choriomeningitis within a syngeneic or semiallogeneic system. *Nature* **248,** 701–2 (1974).

53. Liu, Y., King, N., Kesson, A., Blanden, R. V. & Müllbacher, A. Flavivirus infection up-regulates the expression of class I and class II major histocompatibility antigens on and enhances T cell recognition of astrocytes in vitro. *J. Neuroimmunol.* **21,** 157–168 (1989).

54. Corriveau, R. a, Huh, G. S. & Shatz, C. J. Regulation of class I MHC gene expression in the developing and mature CNS by neural activity. *Neuron* **21,** 505–520 (1998).

55. Huh, G. S. Functional Requirement for Class I MHC in CNS Development and Plasticity. *Science (80-.).* **290,** 2155–2159 (2000).

56. Syken, J., Grandpre, T., Kanold, P. O. & Shatz, C. J. PirB restricts ocular-dominance plasticity in visual cortex. *Science* **313,** 1795–800 (2006).

57. Xu, H. *et al.* The immune protein CD3zeta is required for normal development of neural circuits in the retina. *Neuron* **65,** 503–15 (2010).

58. Bordet, J. J. B. . Les Leucocytes et les Propriétés Actives du Sérum chez les Vaccinés. *Ann Inst Pateur* **9,** 81487–4 (1895).

59. Schafer, D. P. *et al.* Microglia sculpt postnatal neural circuits in an activity and complement-dependent manner. *Neuron* **74,** 691–705 (2012).

60. Eikelenboom, P. & Stam, F. C. Immunoglobulins and complement factors in senile plaques. An immunoperoxidase study. *Acta Neuropathol.* **57,** 239–42 (1982).

61. Afagh, A., Cummings, B. J., Cribbs, D. H., Cotman, C. W. & Tenner, A. J. Localization and cell association of C1q in Alzheimer's disease brain. *Exp. Neurol.* **138,** 22–32 (1996).

62. Michailidou, I. *et al.* Complement C1q-C3 associated synaptic changes in multiple sclerosis hippocampus. *Ann. Neurol.* **77,** 1007–1026 (2015).

63. Bjartmar, L. *et al.* Neuronal pentraxins mediate synaptic refinement in the developing visual system. *J. Neurosci.* **26,** 6269–81 (2006).

64. Mccandless, E. E. CXCL12 limits inflammation by localizing mononuclear infiltrates to the perivascular space during experimental autoimmune encephalomyelitis. (2006).

65. Cruz-Orengo, L. *et al.* CXCR7 influences leukocyte entry into the CNS parenchyma by controlling abluminal CXCL12 abundance during autoimmunity. *J. Exp. Med.* **208,** 327–339 (2011).

66. Klein, R. S. *et al.* SDF-1 alpha induces chemotaxis and enhances Sonic hedgehog-induced proliferation of cerebellar granule cells. *Development* **128,** 1971–81 (2001).

67. Sánchez-Alcañiz, J. A. *et al.* Cxcr7 controls neuronal migration by regulating chemokine responsiveness. *Neuron* **69,** 77–90 (2011).

68. Deng, W., Aimone, J. B. & Gage, F. H. New neurons and new memories: how does adult hippocampal neurogenesis affect learning and memory? *Nat. Rev. Neurosci.* **11,** 339–50 (2010).

69. Bonaguidi, M. a, Song, J., Ming, G.-L. & Song, H. A unifying hypothesis on mammalian neural stem cell properties in the adult hippocampus. *Curr. Opin. Neurobiol.* 1–8 (2012). doi:10.1016/j.conb.2012.03.013

70. Aguirre, A. & Gallo, V. Postnatal neurogenesis and gliogenesis in the olfactory bulb from NG2-expressing progenitors of the subventricular zone. *J. Neurosci.* **24,** 10530–41 (2004).

71. Zhao, C., Deng, W. & Gage, F. H. Mechanisms and functional implications of adult neurogenesis. *Cell* **132,** 645–60 (2008).

72. Raber, J., Rola, R., LeFevour, A. & Morhardt, D. Radiation-induced cognitive impairments are associated with changes in indicators of hippocampal neurogenesis. *Radiat. …* **162,** 39–47 (2004).

73. Winocur, G., Wojtowicz, J. M., Sekeres, M., Snyder, J. S. & Wang, S. Inhibition of neurogenesis interferes with hippocampus-dependent memory function. *Hippocampus* **16,** 296–304 (2006).

74. Deng, W., Aimone, J. B. & Gage, F. H. New neurons and new memories: how does adult hippocampal neurogenesis affect learning and memory? *Nat. Rev. Neurosci.* **11,** 339–50 (2010).

75. Gonzalez-Perez, O. *et al.* Immunological regulation of neurogenic niches in the adult brain. *Neuroscience* (2012). doi:10.1016/j.neuroscience.2012.08.053

76. Robertson, F. A Microscopic Demonstration of the Normal and Pathological Histology of Mesoglia Cells. *Br. J. Psychiatry* **46,** 724–724 (1900).

77. Rosenthal, S. Experimentelle Studien über amöboide Umwandlung der Neuroglia. *Nissl-Alzheimer Histol. Histopathol. Arb* **6,** 89–160 (1913).

78. Ginhoux, F. *et al.* Fate mapping analysis reveals that adult microglia derive from primitive macrophages. *Science* **330,** 841–5 (2010).

79. Shimojo, M., Nakajima, K., Takei, N., Hamanoue, M. & Kohsaka, S. Production of basic fibroblast growth factor in cultured rat brain microglia. *Neurosci. Lett.* **123,** 229–31 (1991).

80. Cunningham, C. L., Martínez-Cerdeño, V. & Noctor, S. C. Microglia regulate the number of neural precursor cells in the developing cerebral cortex. *J. Neurosci.* **33,** 4216–33 (2013).

81. Frade, J. M. & Barde, Y.-A. Microglia-Derived Nerve Growth Factor Causes Cell Death in the Developing Retina. *Neuron* **20,** 35–41 (1998).

82. Bessis, A., Béchade, C., Bernard, D. & Roumier, A. Microglial control of neuronal death and synaptic properties. *Glia* **55,** 233–8 (2007).

83. Wakselman, S. *et al.* Developmental neuronal death in hippocampus requires the microglial CD11b integrin and DAP12 immunoreceptor. *J. Neurosci.* **28,** 8138–43 (2008).

84. Paloneva, J. *et al.* Loss-of-function mutations in TYROBP (DAP12) result in a presenile dementia with bone cysts. *Nat. Genet.* **25,** 357–361 (2000).

85. Roumier, A. *et al.* Impaired synaptic function in the microglial KARAP/DAP12-deficient mouse. *J. Neurosci.* **24,** 11421–8 (2004).

86. Paolicelli, R., Bolasco, G., Pagani, F. & Maggi, L. Synaptic pruning by microglia is necessary for normal brain development. *Science (80-.).* **1456,** 10–13 (2011).

87. Parkhurst, C. N. *et al.* Microglia promote learning-dependent synapse formation through brain-derived neurotrophic factor. *Cell* **155,** 1596–609 (2013).

88. Wake, H., Moorhouse, A. J., Jinno, S., Kohsaka, S. & Nabekura, J. Resting microglia directly monitor the functional state of synapses in vivo and determine the fate of ischemic terminals. *J. Neurosci.* **29,** 3974–80 (2009).

89. Rogers, J. T. *et al.* CX3CR1 deficiency leads to impairment of hippocampal cognitive function and synaptic plasticity. *J. Neurosci.* **31,** 16241–50 (2011).

90. Petersen, L. R., Brault, A. C. & Nasci, R. S. West Nile virus: review of the literature. *JAMA* **310,** 308–15 (2013).

91. Omalu, B. I., Shakir, A. A., Wang, G., Lipkin, W. I. & Wiley, C. A. Fatal fulminant pan-meningo-polioencephalitis due to West Nile virus. *Brain Pathol.* **13,** 465–72 (2003).

92. Samuel, M. a & Diamond, M. S. Pathogenesis of West Nile Virus infection: a balance between virulence, innate and adaptive immunity, and viral evasion. *J. Virol.* **80,** 9349–60 (2006).

93. Clarke, P. *et al.* Death receptor-mediated apoptotic signaling is activated in the brain following infection with West Nile virus in the absence of a peripheral immune response. *J. Virol.* **88,** 1080–9 (2014).

94. Kleinschmidt-DeMasters, B. K. *et al.* Naturally acquired West Nile virus encephalomyelitis in transplant recipients: clinical, laboratory, diagnostic, and neuropathological features. *Arch. Neurol.* **61,** 1210–20 (2004).

95. Davis, L. E. *et al.* West Nile virus neuroinvasive disease. *Ann. Neurol.* **60,** 286–300 (2006).

96. Sejvar, J. J. *et al.* Neurocognitive and functional outcomes in persons recovering from West Nile virus illness. *J. Neuropsychol.* **2,** 477–99 (2008).

97. Sadek, J. *et al.* Persistent neuropsychological impairment associated with West Nile virus infection. *J. Clin. Exp. Neuropsychol.* **32,** 81–87 (2010).

98. Jarrard, L. E. On the role of the hippocampus in learning and memory in the rat. *Behav. Neural Biol.* **60,** 9–26 (1993).

99. Hu, X. *et al.* Microglial and macrophage polarization-new prospects for brain repair. *Nat. Rev. Neurol.* (2014). doi:10.1038/nrneurol.2014.207

100. Cartier, N., Lewis, C.-A., Zhang, R. & Rossi, F. M. V. The role of microglia in human disease: therapeutic tool or target? *Acta Neuropathol.* **128,** 363–80 (2014).

101. Paolicelli, R. C. *et al.* Synaptic pruning by microglia is necessary for normal brain development. *Science* **333,** 1456–8 (2011).

102. Chu, Y. *et al.* Enhanced synaptic connectivity and epilepsy in C1q knockout mice. *Proc. Natl. Acad. Sci. U. S. A.* **107,** 7975–80 (2010).

103. Engle, M. J. & Diamond, M. S. Antibody prophylaxis and therapy against West Nile virus infection in wild-type and immunodeficient mice. *J. Virol.* **77,** 12941–9 (2003).

104. Oliphant, T. *et al.* Development of a humanized monoclonal antibody with therapeutic potential against West Nile virus. *Nat. Med.* **11,** 522–30 (2005).

105. Smeraski, C. a, Siddharthan, V. & Morrey, J. D. Treatment of spatial memory impairment in hamsters infected with West Nile virus using a humanized monoclonal antibody MGAWN1. *Antiviral Res.* **91,** 43–9 (2011).

106. Habjan, M. *et al.* Sequestration by IFIT1 impairs translation of 2'O-unmethylated capped RNA. *PLoS Pathog.* **9,** e1003663 (2013).

107. Appler, K. K. *et al.* Persistence of West Nile virus in the central nervous system and periphery of mice. *PLoS One* **5,** e10649 (2010).

108. Barnes, C. Memory deficits associated with senescence: a neurophysiological and behavioral study in the rat. *J. Comp. Physiol. Psychol.* **93,** 74–104 (1979).

109. Hickman, S. E. *et al.* The microglial sensome revealed by direct RNA sequencing. *Nat. Neurosci.* **16,** 1896–905 (2013).

110. Stewart, B. S., Demarest, V. L., Wong, S. J., Green, S. & Bernard, K. A. Persistence of virus-specific immune responses in the central nervous system of mice after West Nile virus infection. *BMC Immunol.* **12,** 6 (2011).

111. Browne, T. C. *et al.* IFN-γ Production by amyloid β-specific Th1 cells promotes microglial activation and increases plaque burden in a mouse model of Alzheimer's disease. *J. Immunol.* **190,** 2241–51 (2013).

112. Mutnal, M. B., Hu, S., Little, M. R. & Lokensgard, J. R. Memory T cells persisting in the brain following MCMV infection induce long-term microglial activation via interferon-γ. *J. Neurovirol.* **17,** 424–37 (2011).

113. Prajeeth, C. K. *et al.* Effector molecules released by Th1 but not Th17 cells drive an M1 response in microglia. *Brain. Behav. Immun.* **37,** 248–59 (2014).

114. Song, X., Tanaka, S., Cox, D. & Lee, S. C. Fcgamma receptor signaling in primary human microglia: differential roles of PI-3K and Ras/ERK MAPK pathways in phagocytosis and chemokine induction. *J. Leukoc. Biol.* **75,** 1147–55 (2004).

115. Quan, Y., Möller, T. & Weinstein, J. R. Regulation of Fcgamma receptors and immunoglobulin G-mediated phagocytosis in mouse microglia. *Neurosci. Lett.* **464,** 29–33 (2009).

116. Takahashi, K., Rochford, C. D. P. & Neumann, H. Clearance of apoptotic neurons without inflammation by microglial triggering receptor expressed on myeloid cells-2. *J. Exp. Med.* **201,** 647–57 (2005).

117. Ueyama, T. *et al.* Superoxide production at phagosomal cup/phagosome through beta I protein kinase C during Fc gamma R-mediated phagocytosis in microglia. *J. Immunol.* **173,** 4582–9 (2004).

118. Caliezi, C. *et al.* C1-Esterase Inhibitor: An Anti-Inflammatory Agent and Its Potential Use in the Treatment of Diseases Other Than Hereditary Angioedema. *Pharmacol. Rev.* **52,** 91–112 (2000).

119. Molina, H. *et al.* Distinct receptor and regulatory properties of recombinant mouse complement receptor 1 (CR1) and Crry, the two genetic homologues of human CR1. *J. Exp. Med.* **175,** 121–9 (1992).

120. Berg, A. *et al.* Reduced removal of synaptic terminals from axotomized spinal motoneurons in the absence of complement C3. *Exp. Neurol.* **237,** 8–17 (2012).

121. Nithianantharajah, J. *et al.* Synaptic scaffold evolution generated components of vertebrate cognitive complexity. *Nat. Neurosci.* **16,** 16–24 (2013).

122. Purgert, C. A. *et al.* Intracellular mGluR5 can mediate synaptic plasticity in the hippocampus. *J. Neurosci.* **34,** 4589–98 (2014).

123. Chen, P. E. *et al.* Behavioral deficits and subregion-specific suppression of LTP in mice expressing a population of mutant NMDA receptors throughout the hippocampus. *Learn. Mem.* **16,** 635–44 (2009).

124. Clarke, P., Leser, J. S., Bowen, R. A. & Tyler, K. L. Virus-induced transcriptional changes in the brain include the differential expression of genes associated with interferon, apoptosis, interleukin 17 receptor A, and glutamate signaling as well as flavivirus-specific upregulation of tRNA synthetases. *MBio* **5,** e00902–14 (2014).

125. Wang, Y. *et al.* IL-34 is a tissue-restricted ligand of CSF1R required for the development of Langerhans cells and microglia. *Nat. Immunol.* **13,** 753–60 (2012).

126. Sejvar, J. J. The long-term outcomes of human West Nile virus infection. *Clin. Infect. Dis.* **44,** 1617–24 (2007).

127. Guarner, J. *et al.* Clinicopathologic study and laboratory diagnosis of 23 cases with West Nile virus encephalomyelitis. *Hum. Pathol.* **35,** 983–990 (2004).

128. Shrestha, B., Gottlieb, D. & Diamond, M. S. Infection and Injury of Neurons by West Nile Encephalitis Virus. *Society* **77,** 13203–13213 (2003).

129. Ebenbichler, C. F. *et al.* Human immunodeficiency virus type 1 activates the classical pathway of complement by direct C1 binding through specific sites in the transmembrane glycoprotein gp41. *J. Exp. Med.* **174,** 1417–24 (1991).

130. Veerhuis, R. *et al.* Cytokines associated with amyloid plaques in Alzheimer's disease brain stimulate human glial and neuronal cell cultures to secrete early complement proteins, but not C1-inhibitor. *Exp. Neurol.* **160,** 289–99 (1999).

131. Nawrocka-Kunecka, A., Papierz, W. & Liberski, P. P. Complement factors C1q and C3b in brains with Creutzfeldt-Jakob disease. *Pol. J. Pathol.* **56,** 127–9 (2005).

132. Olson, E. E. & McKeon, R. J. Characterization of cellular and neurological damage following unilateral hypoxia/ischemia. *J. Neurol. Sci.* **227,** 7–19 (2004).

133. Boivin, N., Sergerie, Y., Rivest, S. & Boivin, G. Effect of pretreatment with toll-like receptor agonists in a mouse model of herpes simplex virus type 1 encephalitis. *J. Infect. Dis.* **198,** 664–72 (2008).

134. Lehmann, S. M. *et al.* Extracellularly delivered single-stranded viral RNA causes neurodegeneration dependent on TLR7. *J. Immunol.* **189,** 1448–58 (2012).

135. Jiang, R. *et al.* Roles of TLR3 and RIG-I in mediating the inflammatory response in mouse microglia following Japanese encephalitis virus infection. *J. Immunol. Res.* **2014,** 787023 (2014).

136. Faissner, S. *et al.* Cytoplasmic HIV-RNA in monocytes determines microglial activation and neuronal cell death in HIV-associated neurodegeneration. *Exp. Neurol.* **261,** 685–97 (2014).

137. Fuhrmann, M. *et al.* Microglial Cx3cr1 knockout prevents neuron loss in a mouse model of Alzheimer's disease. *Nat. Neurosci.* **13,** 411–3 (2010).

138. Pei, Z. *et al.* MAC1 mediates LPS-induced production of superoxide by microglia: the role of pattern recognition receptors in dopaminergic neurotoxicity. *Glia* **55,** 1362–73 (2007).

139. Aguzzi, A., Barres, B. A. & Bennett, M. L. Microglia: scapegoat, saboteur, or something else? *Science* **339,** 156–61 (2013).

140. Graeber, M. B. Changing Face of Microglia. *Science (80-.).* **330,** 783–788 (2010).

141. Walsh, J. G., Muruve, D. A. & Power, C. Inflammasomes in the CNS. *Nat. Rev. Neurosci.* **15,** 84–97 (2014).

142. Chen, Z. *et al.* Microglial displacement of inhibitory synapses provides neuroprotection in the adult brain. *Nat. Commun.* **5,** 4486 (2014).

143. Ugolini, G. Rabies virus as a transneuronal tracer of neuronal connections. *Adv. Virus Res.* **79,** 165–202 (2011).

144. Openshaw, H. & Ellis, W. G. Herpes simplex virus infection of motor neurons: hypoglossal model. *Infect. Immun.* **42,** 409–13 (1983).

145. Friedman, H. M., Cohen, G. H., Eisenberg, R. J., Seidel, C. A. & Cines, D. B. Glycoprotein C of herpes simplex virus 1 acts as a receptor for the C3b complement component on infected cells. *Nature* **309,** 633–5

146. Ebel, G. D. *et al.* Partial genetic characterization of West Nile virus strains, New York State, 2000. *Emerg. Infect. Dis.* **7,** 650–3

147. Stephan, A. H. *et al.* A dramatic increase of C1q protein in the CNS during normal aging. *J. Neurosci.* **33,** 13460–74 (2013).

148. Bialas, A. R. & Stevens, B. TGF-β signaling regulates neuronal C1q expression and developmental synaptic refinement. *Nat. Neurosci.* **16,** 1773–82 (2013).

149. Sun, T., Vasek, M. J. & Klein, R. S. Congenitally acquired persistent lymphocytic choriomeningitis viral infection reduces neuronal progenitor pools in the adult hippocampus and subventricular zone. *PLoS One* **9,** e96442 (2014).

150. Storey, J. D. & Tibshirani, R. Statistical significance for genomewide studies. *Proc. Natl. Acad. Sci. U. S. A.* **100,** 9440–5 (2003).

151. Huang, D. W., Sherman, B. T. & Lempicki, R. A. Systematic and integrative analysis of large gene lists using DAVID bioinformatics resources. *Nat. Protoc.* **4,** 44–57 (2009).

152. Monnet, F. P. Behavioural disturbances following Japanese B encephalitis. *Eur. Psychiatry* **18,** 269–73 (2003).

153. Greve, K. W. *et al.* The neurobehavioural consequences of St. Louis encephalitis infection. *Brain Inj.* **16,** 917–927 (2002).

154. Hokkanen, L. & Launes, J. Cognitive outcome in acute sporadic encephalitis. *Neuropsychol. Rev.* **10,** 151–67 (2000).

155. Eldadah, A. & Nathanson, N. Pathogenesis of west nile virus encephalitis in mice and rats. *Am. J. Epidemiol.* **88,** 776–790 (1967).

156. Ming, G.-L. & Song, H. Adult neurogenesis in the Mammalian brain: significant answers and significant questions. *Neuron* **70,** 687–702 (2011).

157. Toni, N. *et al.* Neurons born in the adult dentate gyrus form functional synapses with target cells. *Nat. Neurosci.* **11,** 901–7 (2008).

158. Kee, N., Teixeira, C. M., Wang, A. H. & Frankland, P. W. Preferential incorporation of adult-generated granule cells into spatial memory networks in the dentate gyrus. *Nat. Neurosci.* **10,** 355–62 (2007).

159. Tashiro, A., Makino, H. & Gage, F. H. Experience-specific functional modification of the dentate gyrus through adult neurogenesis: a critical period during an immature stage. *J. Neurosci.* **27,** 3252–9 (2007).

160. Bruel-Jungerman, E., Laroche, S. & Rampon, C. New neurons in the dentate gyrus are involved in the expression of enhanced long-term memory following environmental enrichment. *Eur. J. Neurosci.* **21,** 513–21 (2005).

161. Duff, G. W. & Durum, S. K. Fever and immunoregulation: hyperthermia, interleukins 1 and 2, and T-cell proliferation. *Yale J. Biol. Med.* **55,** 437–42

162. Rothwell, N. J. Functions and mechanisms of interleukin 1 in the brain. *Trends Pharmacol. Sci.* **12,** 430–6 (1991).

163. Oitzl, M. S., van Oers, H., Schöbitz, B. & de Kloet, E. R. Interleukin-1 beta, but not interleukin-6, impairs spatial navigation learning. *Brain Res.* **613,** 160–3 (1993).

164. Goshen, I. *et al.* A dual role for interleukin-1 in hippocampal-dependent memory processes. *Psychoneuroendocrinology* **32,** 1106–15 (2007).

165. Ben Menachem-Zidon, O. *et al.* Intrahippocampal transplantation of transgenic neural precursor cells overexpressing interleukin-1 receptor antagonist blocks chronic isolation-induced impairment in memory and neurogenesis. *Neuropsychopharmacology* **33,** 2251–62 (2008).

166. Koo, J. W. & Duman, R. S. Interleukin-1 receptor null mutant mice show decreased anxiety-like behavior and enhanced fear memory. *Neurosci. Lett.* **456,** 39–43 (2009).

167. Avital, A. *et al.* Impaired interleukin-1 signaling is associated with deficits in hippocampal memory processes and neural plasticity. *Hippocampus* **13,** 826–34 (2003).

168. Daffis, S. *et al.* 2'-O methylation of the viral mRNA cap evades host restriction by IFIT family members. *Nature* **468,** 452–6 (2010).

169. Kojima, T. *et al.* Subventricular zone-derived neural progenitor cells migrate along a blood vessel scaffold toward the post-stroke striatum. *Stem Cells* **28,** 545–54 (2010).

170. Ma, D. K., Bonaguidi, M. a, Ming, G.-L. & Song, H. Adult neural stem cells in the mammalian central nervous system. *Cell Res.* **19,** 672–82 (2009).

171. Green, H. F. *et al.* A role for interleukin-1β in determining the lineage fate of embryonic rat hippocampal neural precursor cells. *Mol. Cell. Neurosci.* **49,** 311–21 (2012).

172. Ge, S. *et al.* GABA regulates synaptic integration of newly generated neurons in the adult brain. *Nature* **439,** 589–93 (2006).

173. Jang, M.-H. *et al.* Secreted frizzled-related protein 3 regulates activity-dependent adult hippocampal neurogenesis. *Cell Stem Cell* **12,** 215–23 (2013).

174. Bahrini, I., Song, J., Diez, D. & Hanayama, R. Neuronal exosomes facilitate synaptic pruning by up-regulating complement factors in microglia. *Sci. Rep.* **5,** 7989 (2015).

175. Yoshida, Y., Han, B., Mendelsohn, M. & Jessell, T. M. PlexinA1 signaling directs the segregation of proprioceptive sensory axons in the developing spinal cord. *Neuron* **52,** 775–88 (2006).

176. Capone, G., Pagoni, M., Delfino, A. P. & Kanduc, D. Evidence for a vast peptide overlap between West Nile virus and human proteomes. *J. Basic Microbiol.* **53,** 800–7 (2013).